UNITED STATES AUTOMOTIVE MATERIALS PARTNERSHIP LLC

Validation Of Material Models For Automotive Carbon Fiber Composite Structures Via Physical And Crash Testing (VMM Composites Project)

U.S. Department of Energy (DoE)

Final Closeout Technical Report

Cooperative Agreement DE-EE0005661

Project Duration: June 1, 2012 - July 31, 2017

DOE VTO Staff: Felix Wu
DOE-NETL Staff: Aaron Yocum

September 27, 2017

This report does not contain any protected data.

Co-Principal Investigators:
Omar Faruque *(Ford Motor Co)* and Anthony Coppola *(General Motors)*

United States Automotive Materials Partnership LLC
1000 Town Center Building, Suite 300
Southfield, MI 48075
USAMP DUNS Number: 826406808

CO-AUTHORS:

Co-Principal Investigators:
Omar Faruque *(Ford Motor Co)* and Anthony Coppola *(General Motors)*

Task Leaders:
Derek Board,
Martin Jones
Yijung Chen
(Ford Motor Company)

James Truskin
Jian Tao
(FCA US LLC)

Technical Project Manager/Administrator:
Manish Mehta
(M-Tech International LLC)

Acknowledgement
This program is supported by the U.S. Department of Energy under Cooperative Agreement Number DE-EE0005661 awarded to the United States Automotive Materials Partnership (USAMP). Neither the USAMP, members of USAMP, or United States Government nor any agency thereof, nor any of their employees, makes any warranty, express or implied, or assumes any legal liability or responsibility for the accuracy, completeness, or usefulness of any information, apparatus, product, or process disclosed, or represents that its use would not infringe privately owned rights. Reference herein to any specific commercial product, process, or service by trade name, trademark, manufacturer, or otherwise does not necessarily constitute or imply its endorsement, recommendation, or favoring by the United States Government or any agency thereof. The views and opinions of authors expressed herein do not necessarily state or reflect those of the United States Government or any agency thereof.

Contents

List of Acronyms

ACC	Automotive Composites Consortium
ACCE	Advanced Composites Conference and Exhibition
CAE	Computer-Aided Engineering
CAI	Compression After Impact
CC	Crush Can
CF	Carbon Fiber
CFTF	Carbon Fiber Technology Facility (at ORNL)
CORA	CORrelation and Analysis Metric
CSP	Continental Structural Plastics, Inc.
DOE	U.S. Department of Energy
FBCC	Front Bumper (FB) and Crush Can (CC) System
FBG	Fiber Bragg Grating
FEA	Finite Element Analysis
IIHS	Insurance Institute for Highway Safety
LCCF	Low Cost Carbon Fiber
MPS	Material and Process System
NCAP	New Car Assessment Program
NWU	Northwestern University
OEM	USCAR Owner/Member Original Equipment Manufacturer
ORNL	Oak Ridge National Laboratory
PM	Project Management
PMP	Program Management Plan
QI	Quasi-Isotropic
RUC	Representative Unit Cell
SC	Steering Committee
SMC	Sheet Molding Compound
SOPO	Statement of Project Objectives
TBC	Triaxially Braided Composite
UM	University of Michigan
USAMP	United States Automotive Materials Partnership, LLC
USCAR	United States Council for Automotive Research, LLC
VMM	Validation of Material Models for Automotive Carbon-Fiber Composite Structures Via Physical and Crash Testing
WSU	Wayne State University

Executive Summary

As automotive fuel economy requirements increase, the push for reducing overall vehicle weight will likely include the consideration of materials that have not previously been part of mainstream vehicle design and manufacturing, including carbon fiber composites. Vehicle manufacturers currently rely on computer-aided engineering (CAE) methods as part of the design and development process, so going forward, the ability to accurately and predictably model carbon fiber composites will be necessary. If composites are to be used for structural components, this need applies to both, crash and quasi-static modeling.

This final report covers a five-year, $6.89M, 50% cost-shared research project between Department of Energy (DOE) and the US Advanced Materials Partnership (USAMP) under Cooperative Agreement DE-EE-0005661 known as “Validation of Material Models for Automotive Carbon Fiber Composite Structures Via Physical and Crash Testing (VMM).” The objective of the VMM Composites Project was to validate and assess the ability of physics-based material models to predict crash performance of automotive primary load-carrying carbon fiber composite structures. Simulation material models that were evaluated included micro-mechanics based meso-scale models developed by the University of Michigan (UM) and micro-plane models by Northwestern University (NWU) under previous collaborations with the DOE and Automotive Composites Consortium/USAMP, as well as five commercial crash codes: LS-DYNA, RADIOSS, VPS/PAM-CRASH, Abaqus, and GENOA-MCQ. CAE predictions obtained from seven organizations were compared with experimental results from quasi-static testing and dynamic crash testing of a thermoset carbon fiber composite front-bumper and crush-can (FBCC) system gathered under multiple loading conditions. This FBCC design was developed to demonstrate progressive crush, virtual simulation, tooling, fabrication, assembly, non-destructive evaluation and crash testing advances in order to assess the correlation of the predicted results to the physical tests. The FBCC was developed to meet a goal of 30-35% mass reduction while aiming for equivalent energy absorption as a steel component for which baseline experimental results were obtained from testing in the same crash modes. The project also evaluated crash performance of thermoplastic composite structures fabricated from commercial prepreg materials and low cost carbon fiber sourced from Oak Ridge National Laboratory.

The VMM Project determined that no set of predictions from a CAE supplier were found to be universally accurate among all the six crash modes evaluated. In general, crash modes that were most dependent on the properties of the prepreg were more accurate than those that were dependent on the behavior of the joints. The project found that current CAE modeling methods or best practices for carbon fiber composites have not achieved standardization, and accuracy of CAE is highly reliant on the experience of its users. Coupon tests alone are not sufficient to develop an accurate material model, but it is necessary to bridge the gap between the coupon data and performance of the actual structure with a series of subcomponent level tests. Much of the unreliability of the predictions can be attributed to shortcomings in our ability to mathematically link the effects of manufacturing and material variability into the material models. This is a subject of ongoing research in the industry.

The final report is organized by key technical tasks to describe how the validation project developed, modeled and compared crash data obtained on the composite FBCC to the multiple sets of CAE predictions. Highlights of the report include a discussion of the quantitative comparison between predictions and experimental data, as well as an in-depth discussion of remaining technological gaps that exist in the industry, which are intended to spur innovations and improvements in CAE technology.

1.0 Introduction

1.1 Project Objectives and Technical Approach

The Validation of Material Models (VMM) Project sought to assess the predictive capability of micromechanics-based computational crash models using finite-element analysis (FEA) tools for carbon fiber composites for automotive applications. The overall goal of VMM was to increase the adoption of carbon fiber composite materials in automotive components such as FBCCs through improved confidence in our ability to use these predictive tools for design and engineering of the system, and thereby to meet progressive crush and safety requirements via vehicle lightweighting solutions. It was not the project's objective to directly compare performance of steel versus composite FBCCs, but rather to focus on the prediction of composite failure by progressive crush. Production-feasibility was a secondary objective, hence, composite material systems and manufacturing processes for the FBCC were selected by the USAMP team based on technology maturity and suitability for application in mass-produced automotive systems to ensure relevance of the results in meeting future federal Corporate Average Fuel Economy (CAFÉ) targets.

The technical approach to execution of the program is summarized as a validation process flow diagram in Figure 1, where physical tests are shown in blue boxes, CAE predictive modeling in green and validation/correlation activity in red. Nineteen technical milestones were defined by the team at the beginning of the VMM Project to track progress on tasks with several Go/No-Go gate reviews. More detail on milestone accomplishments is provided in each individual task report.

The project team was comprised of USAMP-member automotive company researchers, academic researchers, selected automotive design/engineering service suppliers, composite manufacturers, material suppliers, test laboratories, and crash test vendors. Key technical service providers were selected per USAMP's competitive bid guidelines. In addition to a Program Management task (Task 1) involving the establishment of project support, contract monitoring infrastructure, team management and reporting systems, the VMM Project was conducted across six phases or tasks as outlined in the technical approach below, each of which are described in further detail in the respective sections of the report.

The first technical phase (Task 2) was concerned with the definition of realistic crash performance targets in terms of peak loads and crash energy absorption, which would help drive the design of an equivalent composite FBCC. A baseline steel FBCC design from a production vehicle was selected as the target by establishing the accuracy and reproducibility of the dynamic models for a steel structure. The corresponding predictive analysis of the steel FBCC system were performed in four high-speed and two low-speed load cases, using PAM-CRASH, LS-DYNA, RADIOSS, and Abaqus. Concurrently, physical crash testing of the steel FBCC was conducted to establish both, the physical targets and the modeling targets for the composite FBCC.

The second phase (Task 3) involved designing the composite FBCC, of which an integral part was selecting a carbon fiber composite material and process system (MPS). The FBCC design was developed using ESI's VPS finite-element analysis software (formerly PAM-CRASH code) and its suite of manufacturing analysis tools with a goal of 30-35% mass reduction set by the USAMP OEM team, aiming for equivalent energy absorption as the steel component. The MPS team molded plaques to test both, unidirectional and woven fabrics, using prepreg materials and compression molding, and investigated other high-volume processing methods that are less common for carbon fiber or automotive production, such as pultrusion. Material testing was an essential part of this task, requiring standard tensile, compression, and shear testing, as well as fracture toughness measurements for use in modeling. The two academic material models also required microscopic geometric analysis and size effect testing. The material and process systems selected influenced the FBCC design, and vice versa, requiring several iterations.

Since the crush cans carry most of the crash loads, a number of crush can designs were evaluated for mass efficiency over the variety of high- and low-velocity load cases being considered. The project scope also included designing the bumper beam, joint configurations and assembly methodologies that were production-feasible. For this, additional intermediate parts were fabricated from the down-selected composite material for testing and to aid in calibration/tuning of the CAE crash codes and material models. As the USAMP team froze the FBCC design and engaged in tooling reviews at the end of this phase, the detailed predictive analysis of the entire system were performed, so as to estimate the crash testing requirements based on the boundary conditions specific to the composite FBCC and packaging constraints.

The next phase (Task 4), involved the complete tooling, fabrication and assembly step of the thermoset composite FBCC. This was conducted in collaboration with an automotive supplier that had experience in high-volume production, and specifically included molding of the crush cans and bumper beam, as well as their trimming, assembly and adhesive joining using semi-automated production equipment. Due to availability of Low Cost Carbon Fiber (LCCF) in experimental quantities from the Oak Ridge National Laboratory (ORNL), the VMM Project also conducted limited processing and molding trials with thermoplastic composite systems, in order to deliver an alternate material system for further design and performance evaluation. This effort achieved partial success, as prepreg material yield was too low to permit extensive molding trials.

In Task 5, the assembled composite FBCC was crash tested using the same set of high- and low-speed load cases as were used for the steel FBCC. This involved the testing of at least thirty composite FBCC assemblies, with several repeat tests in order to obtain a good statistical understanding of the pattern of progressive crush and crash performance of the composite FBCC.

Ongoing throughout Tasks 2-5, was Task 6, comprised of an investigation of non-destructive evaluation (NDE) methods and structural health monitoring of complex carbon fiber composite structures. While NDE and structural health monitoring are common in aerospace, the requirements in automotive engineering include much higher production volumes. These NDE systems must be more robust, as the opportunity for required routine maintenance is far less in automotive systems. Several intermediate demonstrations of NDE methods were held to improve the team's understanding of composite material and bonded joint quality achievable, and also applied to validate the selected fabrication methods and joint materials.

The final phase (Task 7) of the VMM Project involved the comparison and correlation of all virtual CAE data with experimental crash test data, and to perform analyses for any short comings in the technologies involved. The predictive analysis reported herein included analysis of the results of the commercial CAE models and the two academic models, and comparing each to the other, relative to the results of the crash testing of the composite FBCC, with variances assigned to potential gaps in CAE technology. Detailed numerical analysis of what aspects of the models best fit the physical crash results was performed, to assess the broader CAE industry capability in application of FEA-based crash and material modeling, as well as to guide future development.

Through this systematic technical approach, the USAMP VMM Project has established best practices in crash modeling of composite structures, strengthened the CAE capabilities of vendors, and thereby advanced the application of carbon fiber composites, so as to enhance their readiness for greatly reducing weight in primary automotive structures.

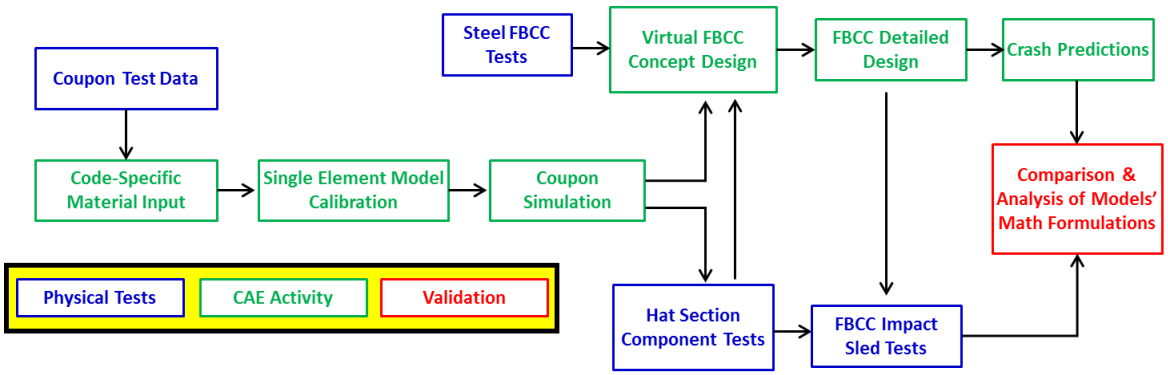

Figure 1. Material model validation process work flow for the VMM Project.

The remainder of this report follows the DOE-prescribed format to summarize the comparison of the actual accomplishments to the goals and objectives of the VMM Project, based on achievements towards milestones in each task. To this end, the document highlights comparisons of CAE predictions to the experimental results obtained in each crash mode, as well as focuses on analysis of the technological gaps identified by the VMM team in the modeling and manufacturing approaches that may have led to inaccuracies in the simulations. Majority of the early task results from this program were previously documented in detailed quarterly technical and annual reports, and most recently also summarized in presentations delivered at the 2016 Society of Plastics Engineers (SPE) Automotive Composites Conference and Exhibition (ACCE). The reader is encouraged to refer to those publications listed as References for more information.

1.2 Selection of Composite Material Models for Validation

Material models considered included existing constitutive models in commercial codes, as well as academic models developed in previous projects jointly sponsored by the Automotive Composites Consortium (ACC, a division of USAMP) and the US Department of Energy (DOE). Academic models considered included micro-mechanics based meso-scale Representative Unit Cell (RUC) models developed by the UM[1] and micro-plane models developed by NWU[2]. Finite-element analysis models implemented in five commercial software suites for computer-aided engineering analysis (CAE) evaluated by the VMM project included:

- VPS (formerly called PAM-CRASH) from ESI Group
- LS-DYNA from Livermore Software Technology Corporation
- RADIOSS from Altair Engineering
- Abaqus from Dassault Systèmes
- GENOA-MCQ from AlphaStar Corporation

Developer organizations for above five codes were invited by the USAMP VMM team to participate and/or support respective CAE design vendors/users, however, one developer chose not to allocate resources to support the CAE effort. The details of material models used in each commercial code are provided in the Task 3 section.

---

[1] Song S, Waas AM, Shahwan KW, et al., Braided textile composites under compressive loads: Modeling the response, strength and degradation, Composites Science and Technology, 67(15-16), 3059-3070, 2007.

[2] Cusatis, G., Beghini, A., Bazant, Z.P, "Spectral Stiffness Microplane Model for Quasibrittle Composite Laminates – Part 1: Theory," Journal of Applied Mechanics, 75, 021009-1-6, 2008.

Predictions were obtained in each listed software from at least one modeling team comprised of either the original code developer/vendor, and/or engineering design/analysis service vendors serving the automotive industry. In addition, two separate sets of predictions were obtained from separate modeling teams (code developer and product designer) in two of the codes – the choice of material model was left to the discretion and experience of each vendor. Modelers were given all material property datasets generated from coupon testing, as well as component tests on an intermediate hat-section made using the same thermoset composite materials and compression-molding manufacturing method. All composite predictions were generated 'blind' – i.e., CAE analysts did not have access to the actual crash test results to ensure they delivered true "predictions" based on material and CAD data, using best practices. The results and discussion of performance by these individual crash codes and CAE vendors are anonymized in this report (see sections on Tasks 5 and 7) to ensure that the focus is on evaluating the accuracy of the CAE industry rather than on conducting a head-to-head competition amongst market leaders or to recommend the best software. CAE predictions obtained were compared with experimental results from quasi-static testing and dynamic crash testing of the thermoset FBCC system.

2.0 Experimental and Analytical Testing of Steel Baseline FBCC

The principal objectives of Task 2 were to build a sled system/fixture, to physically crash baseline steel FBCCs for six crash modes of various impact velocities, obtain objective and useful data to be used to identify key metrics in designing a crashworthy carbon fiber composite FBCC. Task 2 began in the second quarter of FY 2012 with identifying and selecting Wayne State University (WSU) as the primary vendor for crash data per six established load cases, and ESI North America Inc. for performing the corresponding CAE predictions and analysis and it was completed in second quarter FY 2015. USAMP received a complete and thorough report from WSU detailing the test protocols and findings for Task 2.

2.1 Summary of Objectives and Milestones

- Design and fabricate a sled fixture to test steel FBCCs under several loading modes.
- Create a repeatable test methodology including setup, boundary conditions, data acquisition, data post processing.
- Conduct crash tests for all six load cases.
- Provide CAE predictions of steel tests.
- Analytically compare CAE predictions to steel tests.

Milestones for Task 2:

Milestone	Title	Description	Metrics	Status
M1	Crash Test Fixtures for Steel FBCC	Mass, Initial and Boundary conditions of the sled, as well as outputs such as loads and accelerations will be defined to drive fixture design. Require design and fabrication of at least two different FBCC test fixtures (for low and high speed tests, plus angular).	Design, fabricate and validate fixtures for 6 load cases: Full-frontal, 40% Offset, 30 deg angular; Center-pole; Low speed centered and low speed quarter. For each case, a viable test must be conducted with no additional welding or fastening modifications to the fixtures.	Completed

M2	Steel FBCC Predictions Complete	An FBCC from a current vehicle will be identified, and the CAD, including front end packaging, made available to the project team. The CAE analysis of the steel FBCC will be performed in stages for all load cases using 4 commercially-available crash codes: PAM-CRASH, LS-DYNA, RADIOSS, Abaqus.	Report including CAE models, assessment of CAE model integrity (e.g., CAE best practices used, experimentally-determined material properties, energy error < 5%), analyses and predictions of selected responses for 6 load cases in 4 commercial crash codes, including FBCC assembly and physical test variability study for gages and materials. OEM-approved correlation metric used to quantify a goodness-of-fit of the CAE predictions to the physical test performance. Report with crash test results and comparison to CAE predictions for 6 load cases.	Completed
M3	Steel FBCC Crash Testing and Targets for Composite FBCC Design Complete	The steel FBCC will be physically crash tested for each of the load cases. Sufficient crash test repetitions will be done to establish reproducibility, and determine part-to-part variability. Test results will be used to establish critical response targets for the design of the composite FBCC.	Targets established for composite FBCC design. Data analysis completed. Test protocols completed in sufficient detail to perform future composite FBCC testing.	Completed

2.2 Key Accomplishments and Results

2.2.1 Sled Fixture and Test Setup

A secondary sled and associated fixtures were built to conduct both high- and low-speed crash testing of a steel FBCC (Figure 2). The method employed was a sled on sled setup, which lends for the FBCC to decelerate during energy absorption. Protocols for camera coverage, instrumentation, data acquisition and general test setup were created for each crash mode. Instrumentation was set up for redundant measures, meaning the accelerometers could be integrated to measure displacement to coincide with the high-speed cameras. The sled accelerometers could also be multiplied by sled mass to calculate impact load which also measured using load cells on the impact load wall.

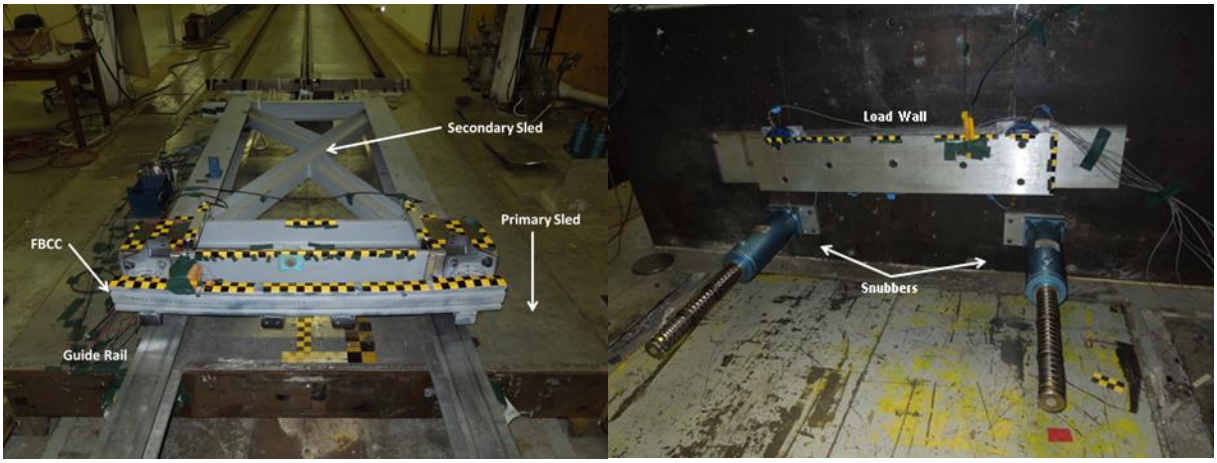

Figure 2. Front view of the crash test setup. Photos show the primary and secondary sled (left), and load wall and snubbers (right). Notice the FBCC is fixed to the secondary sled and the guide rail. The small blue box to the left is the data acquisition system. In this case, the load wall is instrumented with load cells.

The six crash modes conducted are full frontal, 40% frontal offset, center pole, 30 degree angular, low-speed center and low-speed quarter as shown below in Figure 3.

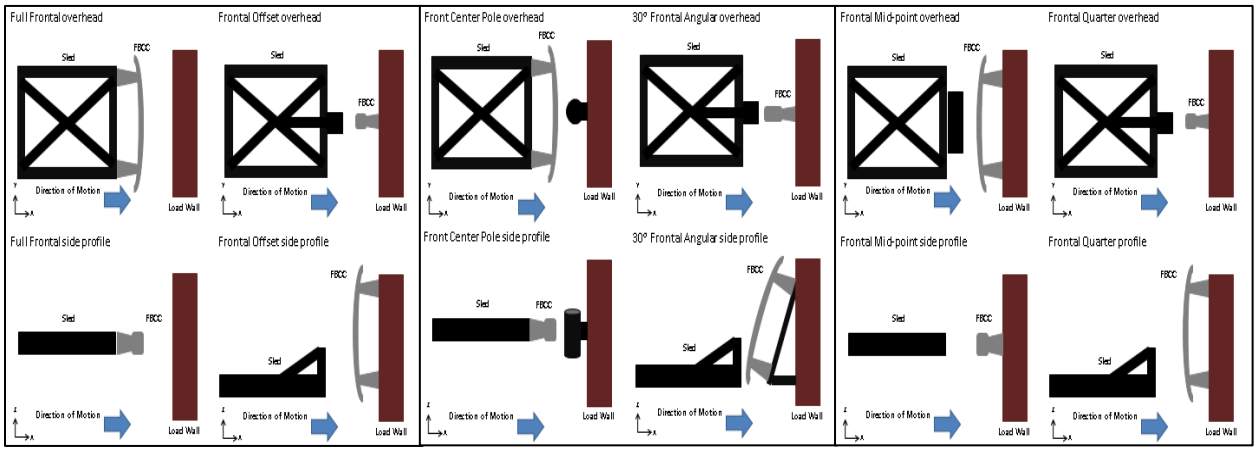

Figure 3. Test setup for all six crash modes.

2.2.2 Testing and Test Results

Before all load cases, practice tests were run to verify velocity and boundary conditions. As some of the test modes chosen for this project were anachronistic from the federal and public domain of test conditions, the original speeds designated were decreased for test integrity. For instance, the pole and angular test impact velocities were decreased by more than half. Additionally, these regulatory and public domain tests are based on full-vehicle tests, and these subcomponents are not designed for these modes.

Results from tests indicated that forces measured directly from the load cells were equivalent to Newton's Second Law of sled mass multiplied by acceleration. Results of displacement measured directly from high-speed film were equivalent to double integration of the sled accelerations. For frontal tests, progressive crushing of the crush can was observed and represented the greatest energy absorption.

Results from the steel FBCC testing are presented in Table 1. These results were provided to ESI as boundary conditions for all models (VPS/PAM-CRASH, LS-DYNA, RADIOSS, Abaqus). Note the small standard deviation relative to the mean for all load cases. This indicates exceptionally low coefficient of variability demonstrating a robust test setup with excellent repeatability.

Table 1. Results of Baseline Steel FBCC Crash Tests

Crash Mode	Mass (kg)	Impact Velocity (m/s) (S.D.)	Energy (KJ) (S.D)
Full Frontal	302.87	15.63 (0.15)	35.92 (1.75)
Frontal Offset	321.34	11.87 (0.17)	18.93 (0.67)
Frontal Pole	306.00	6.42 (0.04)	6.00 (0.14)
Frontal Angular	321.34	9.07 (0.08)	12.72 (0.22)
Low Speed Midpoint	302.30	4.48 (0.14)	12.76 (0.26)
Low Speed Quarter	326.40	4.23 (0.12)	2.14 (0.16)

2.2.3 Correlation of Steel Tests to Simulations

Previous methods to compare test data to CAE predictions relied on a level of subjectivity. In order to determine a best practice to objectively assess the simulations (VPS/PAM-CRASH, LS-DYNA, RADIOSS, Abaqus), the team determined to use the ISO/TR 16250: Road vehicles – Objective rating metrics for dynamic systems[3]. The standard has also been commonly called CORA. The ISO/TR Standard 16250 (that has been proposed) gives a score from 0 to 1 on how well the two signals correlate. The proposal constitutes two primary drivers: the first, the corridor method where the signals are compared using constant width or sigma based widths to arrive at a 1, 0<rating<1, or 0 and having a weight factor of 40%. The second driver is the cross-correlation method that looks at the differences between the two signals with respect to phase shift, amplitude and slope. Each of these carries a weight of 20%. Typically, this is carried out in Matlab comparing only one time history from a test to one time history of the simulation using the same metric.

Based on a USAMP decision, the findings from this correlation study do not identify the individual codes. In Figure 4, an example of force-time history curves showing the both the average of all tests (dark blue), all of the tests (light blue) and the simulation (red) is provided. Centered in a table is the calculated ISO score for each code. For the sake of brevity, only one mode and one

[3] *[1] C. Gehre, H. Gades, and P. Wenicke, "Objective Rating Of Signals Using Test And Simulation Responses", . Proc. Int. Tech. Conf. Enhanced Safety Vehicles, 2009.*

metric is shown (six crash modes with three metrics each).

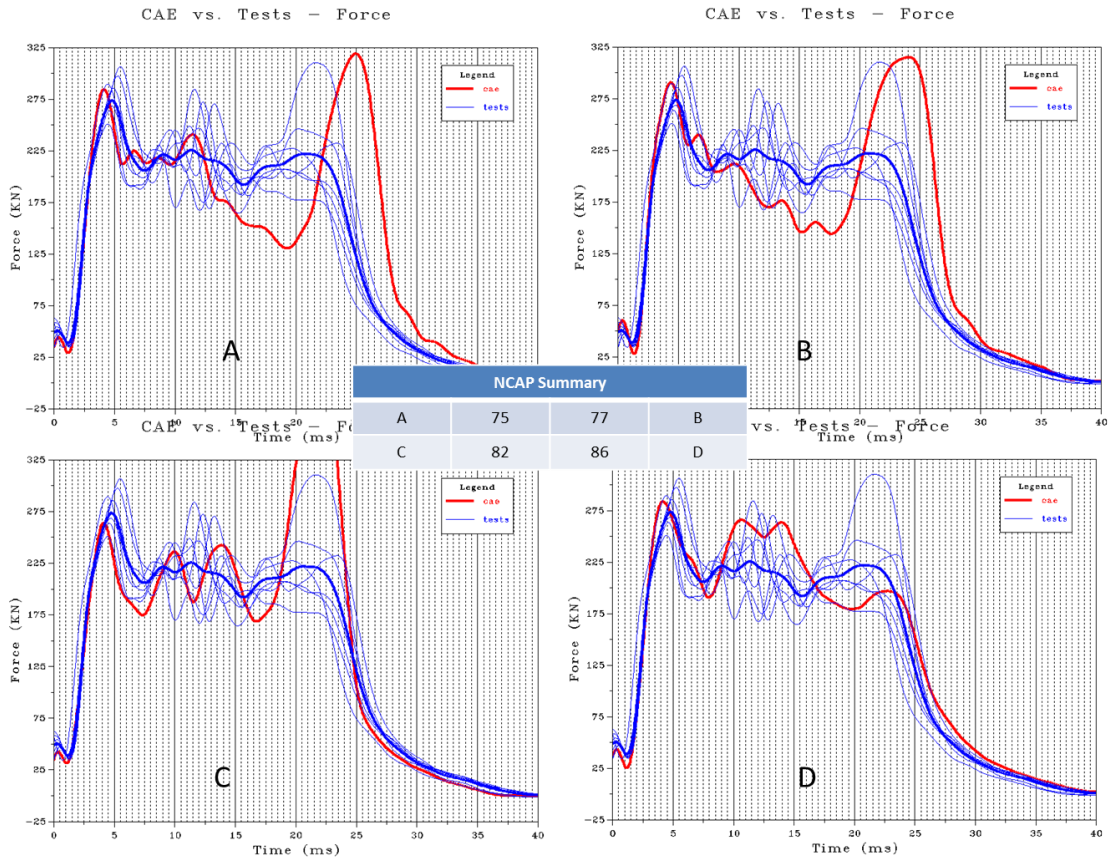

Figure 4. Sample of force-time history comparisons of physical tests, average of those tests and the simulation and the corresponding CORA scores for each crash code. Red= prediction, Bold blue= average crash data, Light blue= individual crash data.

Upon completion of the correlation analysis for the steel tests and simulations, no one code stood out as superior and all codes for all test modes scored 0.70 or greater. However, several correlations scored over 0.80. The sliding scale of the rating is graded as follows in Table 2 (from ISO/TR 16250:2013(E)):

Table 2. Ratings used for the goodness of fit between CAE and crash test data.

Rank r	Grade	Rating R	Description
1	Excellent	R >0,94	The characteristics of the reference signal are captured almost perfectly.
2	Good	0,80< R ≤0,94	The characteristics of the reference signals are captured pretty good, but there are noticeable differences between both signals.
3	Fair	0,58< R ≤0,80	The characteristics of the reference signal are basically captured, but there are significant differences between both signals.
4	Poor	R ≤0,58	There is almost no correlation between both signals.

Figure 5 illustrates the results for each code under each loading condition. For the full frontal mode, there is a wide range in the correlations while in the offset mode, there is very little variation.

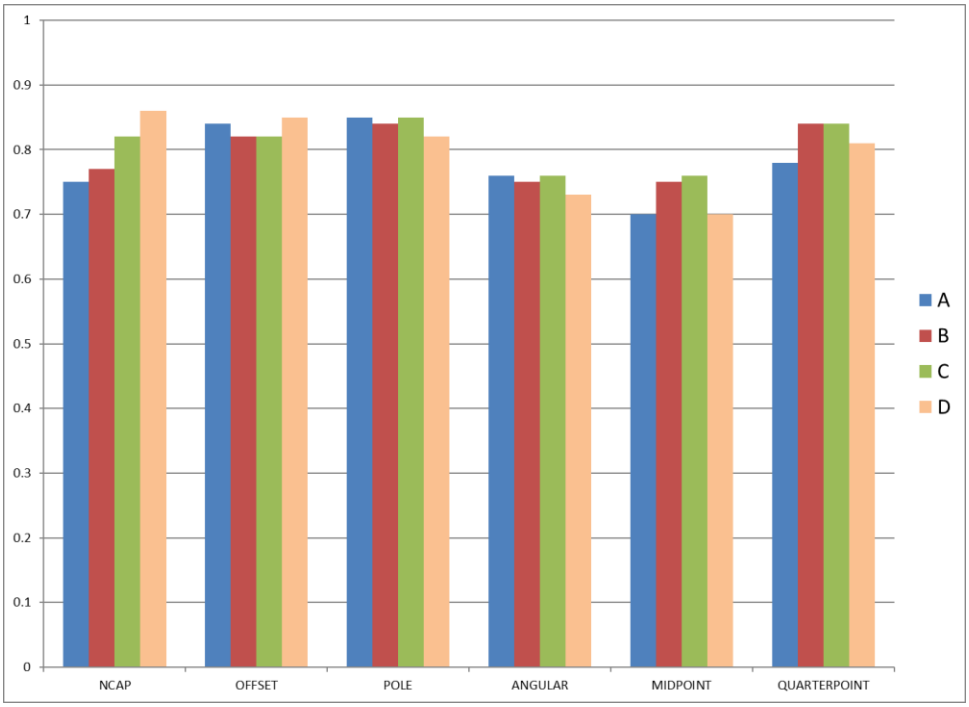

Figure 5. CORA results for all crash modes using each crash modeling code. The four individual codes have been left unidentified – i.e., VPS/PAM-CRASH, LS-DYNA, RADIOSS, and Abaqus.

2.3 Task Conclusions and Technological Gaps Identified

A successful series of multiple load conditions were carried out using steel FBCCs in order to develop a proper test procedure that included the test setup, instrumentation, data acquisition, post-processing analysis and dissemination of data in a concise manner in order to replicate the tests with the carbon fiber FBCCs. Based on the low coefficient of variation for all crash modes, the procedure was deemed exceptional and repeatable, producing valuable boundary conditions to provide ESI for simulations.

ESI provided simulations for all crash modes using the four commercial codes. Upon the USAMP's objectively rating the time history data obtained from the physical tests to the simulations, there was no single consistently superior crash code. The results of each mode were provided to ESI but the codes were left unidentified to maintain the scientific integrity of the process, since the project objective is to evaluate how well CAE codes can predict carbon fiber performance in crash.

3.0 Design of Composite FBCC

3.1 Material and Process Selection

In Task 3, the main requirement was the ability to design and produce a composite FBCC from commercially available materials that fit within the design space of the benchmarked steel system. A secondary criterion for material and process selection was the ability to scale the production method to large volumes. With these restrictions in mind, the team developed a design with five separate compression molded components that could be adhesively joined. In addition, the requirement to use the same design space as for the steel FBCC resulted in challenging geometries to mold with continuous fiber alone. A co-molding method was developed with continuous fiber prepreg and SMC. The prepreg formed the primary structural features while the SMC formed the complex geometric features.

The SMC chosen was Mitsubishi Rayon Pyrofil CVS1016-2BK. This material was chosen for its commercial availability and compatibility with the epoxy prepreg. This SMC contained 53% fiber by weight with a fiber length of 1 inch. The resin was an epoxy acrylate. Per the manufacturer, the tensile strength was 150 MPa, the modulus was 33 GPa, and the glass transition temperature was 130° C. The prepreg was composed of 2x2 twill woven Toray standard modulus carbon fiber (CF) with Cytec MTM 54FRB epoxy resin. The fabric was 343 gsm with 42% resin weight. Fully consolidated parts were confirmed digestion in H_2SO_4 + H_2O_2 to contain 58% fiber by volume. This resin was chosen for its relatively fast curing time of 15 minutes at 140° C and ability to be demolded while still hot because of the high glass transition temperature generated during cure. Note that faster curing prepregs are now available on the market that were not available during the early stages of execution of this project. Use of these prepregs would significantly increase production rate of the parts.

3.1.1 Coupon Testing for Material Property and Layup Selection

Coupon testing of the prepreg-based materials was primarily used for generating the material cards for the simulated crash predictions in each crash code. However, the team performed additional testing to compare several layups and material choices. The list of material test data required for each stage of validation is shown in Figure 6 below.

It is important to note that the goal of this testing was not to fully optimize the material selection, and further testing in the future could result in improved material selection. Coupon testing was performed on four different layups: unidirectional (uni) fiber oriented $[0]_{4s}$, uni oriented $[0/90]_{2s}$, woven fiber (woven) oriented $[0/90]_{2s}$, and woven oriented quasi-isotropically $[0/45/-45/90]_s$. Plaques were molded using compression molding in a 610 x 610 mm tool. Testing results were used for developing material cards for the models, as well as for comparing the layups for the design of the FBCC. Tension tests followed ASTM D3039, compression followed ASTM D3410, shear followed ASTM D7078, and flexure followed ASTM D7264. Results from the tests are shown in Figure 7. In general, unidirectional fibers showed higher strength and modulus than woven fibers, but with lower elongation. Woven QI showed by far the best shear performance, due to the inclusion of ±45° fibers. Ultimately, the woven QI layup was chosen for its relatively high elongation, good shear performance, and good performance in the closed-hat section testing discussed later.

Extensive USAMP discussions with NWU, UM, and ESI - the selected design/CAE source - resulted in a consolidated list of 15 critical tests to characterize material properties for all commercial and ACC simulation codes. These tests, completed at Delsen Labs, Glendale, CA,

included tensile, compression, shear, and flexural testing, as well as cyclic tension, inter-laminar fracture toughness [G_{1c} (Double Cantilever Beam) and G_{2c} a(End Notch Flex)] at 3 thicknesses, notched tension at 3 sizes, and micrography analysis of the geometry of the woven samples. The fracture toughness (also referred to as Size Effect tests) were completed by Northwestern University.

In order to obtain material properties for the firsts stage of CAE modeling and virtual analysis of concepts, 250 mm x 450 mm plaques were compression molded in a variety of configurations, including:

Unidirectional CF/epoxy pre-preg
- $(0)_8$
- $(0/90)_{2s}$
- $(0/45/-45/90)_s$ (QI)

Woven CF/epoxy pre-preg, 2x2 twill
- $(0/90)_{2s}$
- $(0/45/-45/90)_s$ (QI)

All of these tests are quite standard in the industry, except for the fracture toughness and cyclic tension tests which were required for the damage calibration in the Microplane, RUC and *MAT131 PAM-CRASH material models. Further details of the cyclic tension test formulation and material test results can be found in the FY2014 Annual Report.

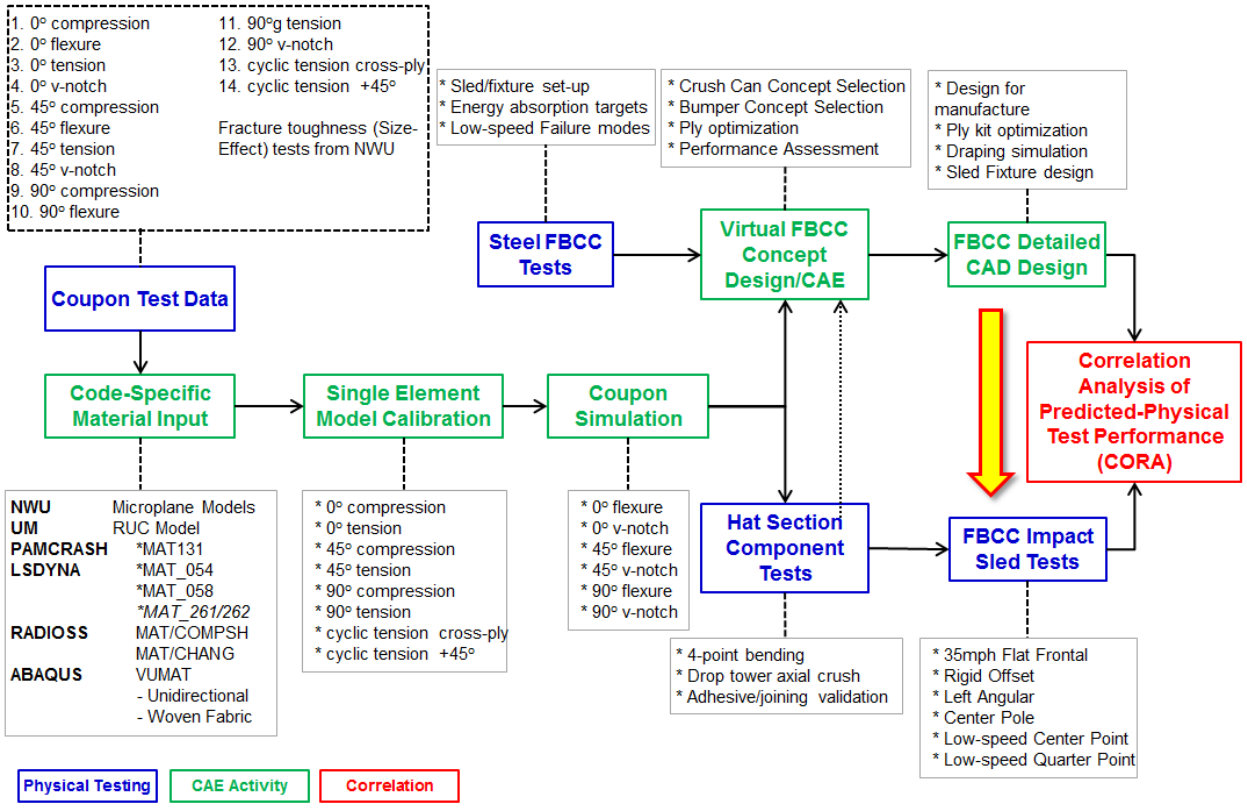

Figure 6. Graphical flow-chart to identify the validation work-flow processes for carbon fiber composite material crash models. The figure shows the interaction of testing, design, and analysis activities for the virtual design of the carbon fiber FBCC.

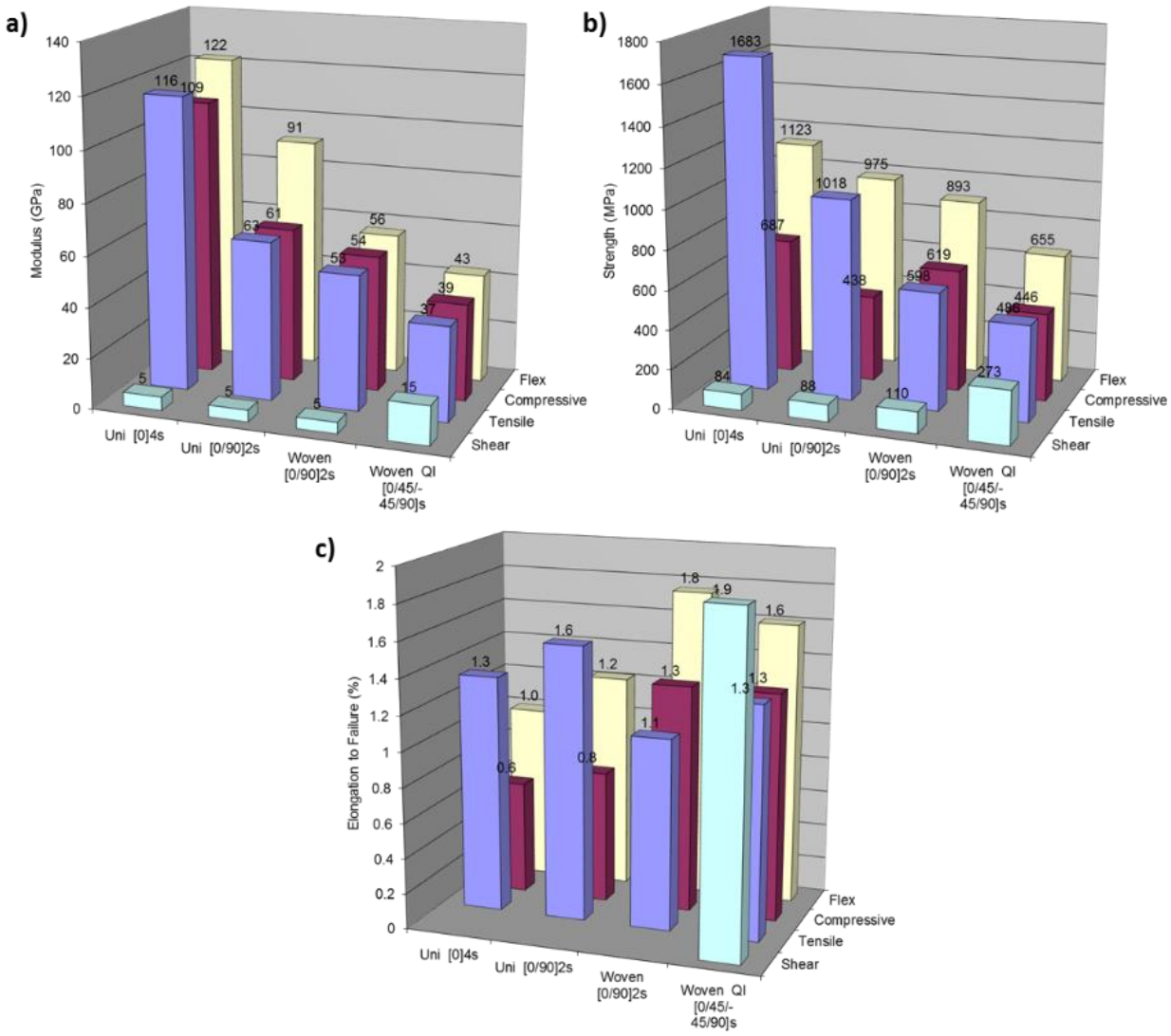

Figure 7. Monotonic coupon testing results for the prepreg in various layup configurations, including a) modulus, b) strength, and c) strain to failure.

3.1.2 Adhesive Selection for Joining Thermoset Composites

Similar to coupon testing for prepreg material selection, coupon testing on the adhesive was conducted to compare several options. Three adhesives from Dow Automotive were evaluated for use in joining the thermoset FBCC system, each with distinct mechanical capabilities:

- DOW BETAFORCE® 2850S, a 2-component polyurethane (PU) adhesive, with lap shear for metal substrates of less than 11 MPa and elongation of approximately 115%
- DOW BETAMATE® 73326/73327, a 2-component epoxy adhesive, with lap shear of approximately 10 MPa and elongation of approximately 13%
- DOW BETASEAL® X2500 Plus, a 2-component polyurethane (PU) adhesive, with lap shear less than 5 MPa and elongation of approximately 150%.

The BETASEAL adhesive had the highest elongation, with relatively low strength, while the

BETAMATE adhesive had very high strength and relatively low elongation. The BETAFORCE adhesive was in the middle of these other systems in terms of performance. Three types of mechanical tests were used to evaluate the performance of these adhesives, including lap shear (ASTM D1002), cleavage peel (ASTM 3807), and impact peel (modified) (ISO 11343). Two different substrates were evaluated, both composed of the same woven-carbon-fiber/epoxy prepreg used in the FBCC. The first substrate type used an 8-layer cross-ply layup, while the second substrate types used an 11-layer quasi-isotropic layup [0/90/45/-45/0/90/0/-45/45/90/0].

The results from the testing are shown in Table 3 and Table 4 for the cross-ply and quasi-isotropic layups, respectively. Based on these tests, the BETAFORCE adhesive showed the most promise due to its superior performance in cleavage peel and impact peel. The impact peel performance was deemed to be the most important because of its similarity to the failure mode expected during crash tests of the FBCC.

Table 3. Results of the adhesive testing on the thermoset system for the cross-ply configuration. (CF=cohesive failure of adhesive; FT=fiber tear (cohesive failure) of substrate; AF=adhesive failure).

	BETAMATE™ 73326M/27M	BETAFORCE™ 2850L	BETASEAL™ X2500 Plus
Chemistry	Epoxy	Polyurethane	Polyurethane
Lap Shear (MPa)	6.74 ± 0.19 100% CF	2.19 ± 1.53 100% CF	2.09 ± 0.10 100% CF
Cleavage Peel Max Load (N) Peel (N·m)	52.0 ±18.7 0.88 ± 0.12 100% CF	131 ± 13.3 2.70 ± 0.56 100% CF	58.3 ± 12.9 1.05± 0.35 100% CF
Impact Peel (N/mm)	3.06 100% CF	30.3 90% CF 10% FT	11.2 35% CF 65% FT

Table 4. Results of the adhesive testing on the thermoset system for the quasi-isotropic configuration. (CF=cohesive failure of adhesive; FT=fiber tear (cohesive failure) of substrate; AF=adhesive failure).

	BETAMATE™ 73326M/27M	BETAFORCE™ 2850L	BETASEAL™ X2500 Plus
Chemistry	Epoxy	Polyurethane	Polyurethane
Lap Shear (MPa)	7.21 ± 1.17 100% CF	5.46 ±0.27 100% CF	1.38 ± 0.10 20% CF 80% AF
Cleavage Peel Max Load (N) Peel (N·m)	70.3 ±18.7 1.13 ± 0.29 100% CF	167 ± 36 3.17 ± 0.21 85% CF 15% FT	105 ± 12.3 2.07 ± 0.09 100% CF
Impact Peel (N/mm)	5.05 100% CF	24.8 15% CF 85% FT	19.0 65% CF 35% FT

3.2 Material Model Finite Element Validation

Following the material tests, the data had to be synthesized into a material model for validation of its accuracy compared to physical tests. The team followed a process commonly referred to in industry as “the building block approach”, where confidence is built up starting from a single element, to a coupon, to a component, prior to application on a large system.

The process to characterize the carbon fiber material for each code followed a similar procedure. The properties extracted from the Delsen material tests were input into the material card, and the stress-strain for a single finite element was first calculated for three different load conditions: axial, transverse and shear loads, as indicated in Figure 8. Additional code-dependent calibrations were performed for cross-ply and 45^{o} cyclic tension for the PAM-CRASH *MAT131. In general, a very good level of correlation was observed for ACC and commercial codes, with a good characterization of slope and failure limit achieved, as indicated by a sample of the results shown in Figure 9.

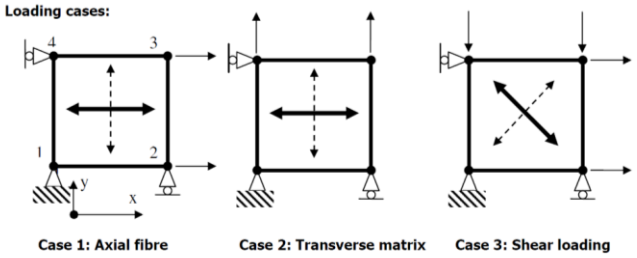

Figure 8. Single finite element loadcase set-up.

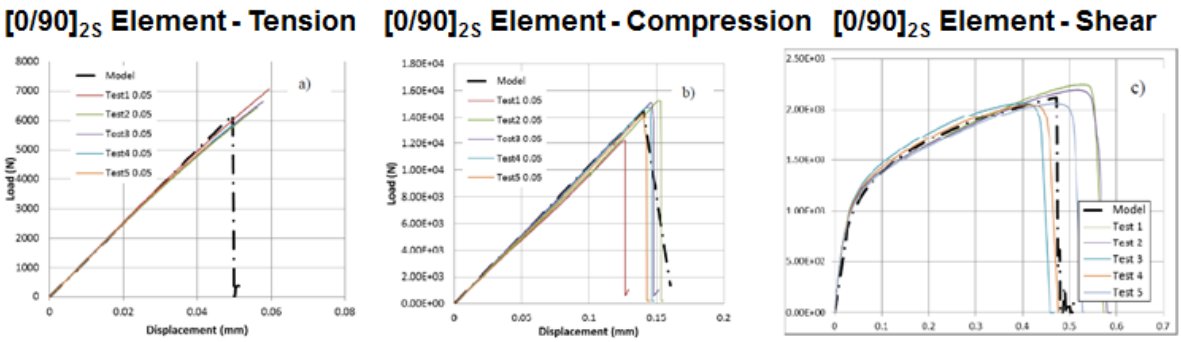

Figure 9. Sample indication of single element calibration stress-strain behavior for axial, transverse and shear load cases

Following the single element calibration, the characterization was applied to a coupon model, representing the physically tested coupon for the 0^{o}, 45^{o} and 90^{o} Flexure and V-notch tests.

A component model was later developed primarily to validate the adhesive and rivet joints along the flanges of the crush can, and ensure the design and manufacturing parameters of the adhesive were able to withstand the high loads of the crush can in axial crush and bending. These specimens also served to further validate the material model assumptions and finite element characterization.

In total, twelve different material models were used to characterize a common FBCC structure and provide performance predictions. Three different ACC-developed codes were used to characterize the crush can only and provide performance predictions to correlate to component tests of the same crush can, without the bumper system. The full list of evaluated material models is shown in Table 5. In some cases, these materials were also applied to the beam, although often

a different material was used for the SMC ribs in the beam. This is not captured in this table, as the SMC material was an assumed value from the vendor, and did not undergo the same rigorous characterization and testing as the continuous carbon fiber woven material.

Table 5. Material Models used to characterize the CF FBCC system.

Crush Can Material Definition Summary		
Vendor	**Code**	**Material Model**
Northwestern University	**ES3 MARS**	**Spectral Stiffness Microplane Model (SSMM)[4]**
	ABAQUS	**VUMAT - Microplane Triad Model (MTM)[5]**
University of Michigan	**ABAQUS**	**VUMAT - Representative Unit Cell (RUC)**
ESI	**VPS (PAM-CRASH)**	***MAT131**
		Pineda / Waas Material model was implemented into VPS at the conclusion of the project to industrialize the work done by USAMP in co-development of this formulation with the University of Michigan.
LSTC **Pratt & Miller**	**LS-DYNA**	***MAT_054**
		***MAT_058**
		****MAT_262/262*** ***Not applied in this project due to cost/time constraints, but recommended by LSTC for future composite modeling***
	Pratt & Miller	***MAT_054**
		***MAT_058**
Altair Engineering **Pratt & Miller**	**RADIOSS**	**MAT/LAW25(COMPSH)**
		MAT/LAW15(CHANG)
	Pratt & Miller	**MAT/LAW 25(CRASURV)**
InDepth Engineering Solutions, Inc.	**ABAQUS**	**VUMAT - Woven and Unidirectional**
AlphaStar	**GENOA**	**Multi-Scale Model MCQ in LS-DYNA**

[4] M Salviato, SE Ashari, G Cusatis, "Spectral Stiffness Micro-plane Model for Damage and Fracture of Textile Composites," Composite Structures 137, 170-184.

[5] K Kirane, M Salviato, ZP Bažant, "Microplane-Triad Model for Elastic and Fracturing Behavior of Woven Composites,", Journal of Applied Mechanics 83 (4), 041006.

3.3 Design Concept Development

At the start of the project, while the material selection and testing was not yet finalized, the Design team was solicited for ideas and concepts on how to execute a carbon fiber FBCC design. After the ideation period and brainstorming sessions were completed, eleven design concepts were proposed by the team for concept prioritization and preliminary design development.

A critical enabler to thrift designs and ensure they had a strong chance of success was the functional requirements table developed to understand the primary function of each piece of the design in each of the six impact load cases as shown in Table 6.

Table 6. Composite FBCC Functional Requirements for each loadcase.

COMPOSITE FBCC FUNCTIONAL REQUIREMENTS						
	Offset 40mph	**Full Frontal 35mph**	**30° Angular 30mph**	**Center Pole 20mph**	**Ctr Pendulum 5mph**	**Qtr Pendulum 5mph**
Crush Can	Absrobs Energy	Absrobs Energy	Absrobs Energy	Absrobs Energy?	Provides support (to Beam)	Absorbs Energy
	Progressive Crush (Frt-Back)	Progressive Crush (Frt-Back)	Progressive Crush (Frt-Back)	Provides Stiffness for Beam	Shows Damage (if damaged)	Shows Damage (if damaged)
	Unstruck Side - TBD				Absorbs Energy	
Bumper Beam	Distributes Energy (to cans)	Absorbs Energy *	Distributes Energy (to cans)	Remains in tact (no split)	Distributes Energy (to cans)	Absorbs Energy
	Absorbs Energy *		Absorbs Energy	Distributes Energy (to cans)	Absorbs Energy	
NOTES:	* If Crush Can runs to front of Bumper Beam, Bumper Beam eanergy absorption is reduced (replaced by can)					
	- EA Foam is not included in the scope of this project					

3.3.1 Crush Can Design

While it is well understood that the primary function of the crush cans is to absorb energy, the project ran through twelve iterations of crush can profile to maximize the energy absorption at the minimal weight. Figure 10 shows the profiles evaluated included single cell tubes, as well as tubes with integrated ribs, which were shown to very effectively increase the strength and energy absorption of the crush can.

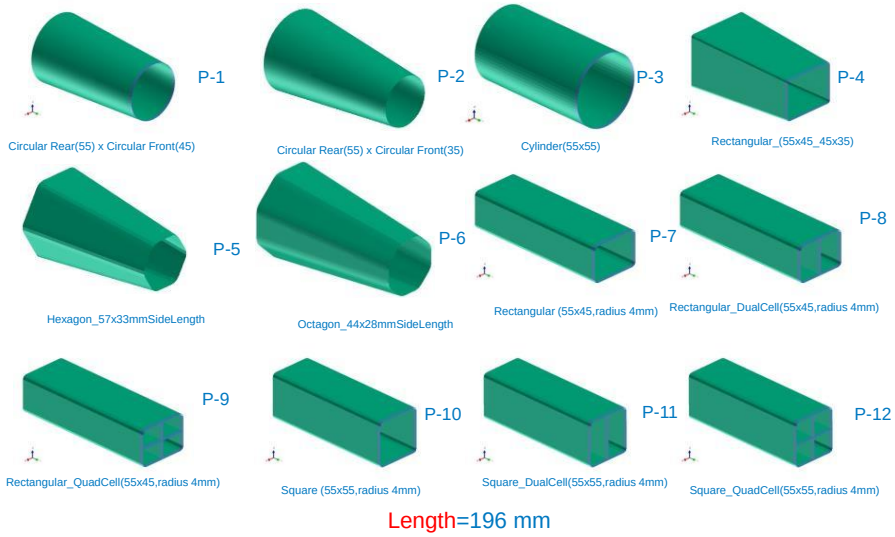

Figure 10. Crush Can profiles considered to determine efficient energy absorbing section for different crush modes.

Several different iterations of ply lay-up were completed to understand the effect of different ply angles, as well as outer ply orientations on the crush behavior of the tube.

The recommended compression molding process from the Materials and Process team drove the Design team to adapt a two-piece design, as the required length of the crush can would drive excessive draw for a single-piece molding, and the risk of significant fiber misalignment existed if there was some kind of “sock” preform used to fill the die cavity. This eliminated the ability to efficiently include internal stiffeners, so a tapered two-piece clamshell tube was selected as the leading design candidate, as it showed the highest energy absorption efficiency with a stable axial crush mode from the tapered design, which initiated crush at the tip of the can.

While the composite industry has frequently used composite tubes for energy absorption in a radial peel “crush” mode, this was not deemed the most suitable for this application where the load condition was not always linear, and the crush can had to handle off-axis moments and loads. So the crush can collapse mode and supporting geometry was adjusted to provide higher initial strength to off-axis loading. In addition, the NDE team also preferred flat surfaces along the can of at least 16mm in width, as this facilitated NDE inspection of the can. Based on the radius of the existing design a ten-sided - or dodecagonal - profile was developed and optimized for the carbon fiber crush can.

The primary engineering challenge of the compression two-piece design was ensuring a robust bond could be created between the two pieces. The development of a joining strategy for crush cans to the bumper beam, and validation of the riv-bonded joining system, using high strength structural adhesive from Dow Chemical coupled with steel structural rivets to act as peel-stoppers, was a key accomplishment of the Joining team. This approach allowed the focus of the project to remain on the validation of the carbon fiber material models, and thereby to avoid diverging time and efforts into detailed characterization of adhesive material and validation of the adhesive model. Consequently, virtual analysis was able to proceed with a verified assumption of a “rigid” connection between the bond flanges.

3.3.2 Bumper Beam Design

The structural concept for the bumper beam was developed as a single-piece design to help reduce tooling costs and part weight. The C-Section is commonly used in steel applications as is an efficient profile for transferring load to each crush can. However it was found in early analysis of the bumper that additional reinforcements would be required to stabilize the section and improve the load transfer. The addition of chopped carbon fiber SMC ribs that could be co-molded into the C-Section provided a good balance of performance and cost, and could be tailored to meet specific local stiffness needs, as shown in Figure 11.

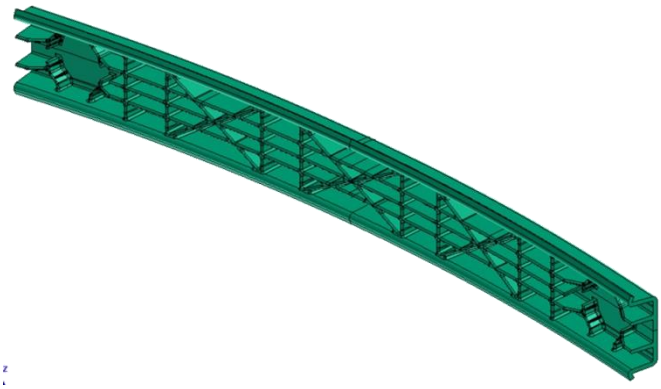

Figure 11. Final Bumper Beam design, showing rear of beam and co-molded SMC chopped carbon fiber ribs and pockets for crush cans.

Furthermore, the ability mold in features and pockets into the beam meant that the SMC ribs could be used to create a pocket – shown in Figure 12 – to locate the crush cans and imbed them into the Bumper Beam structure. Stand-offs were molded into the side-walls of the pockets to maintain a repeatable bond gap and help control adhesive squeeze out. Adhesive was the only fastening mechanism used to hold the cans in place. This novel design concept to join the carbon fiber crush cans to a carbon fiber bumper beam was awarded a US Patent[6] in early 2017 for the innovative joining strategy.

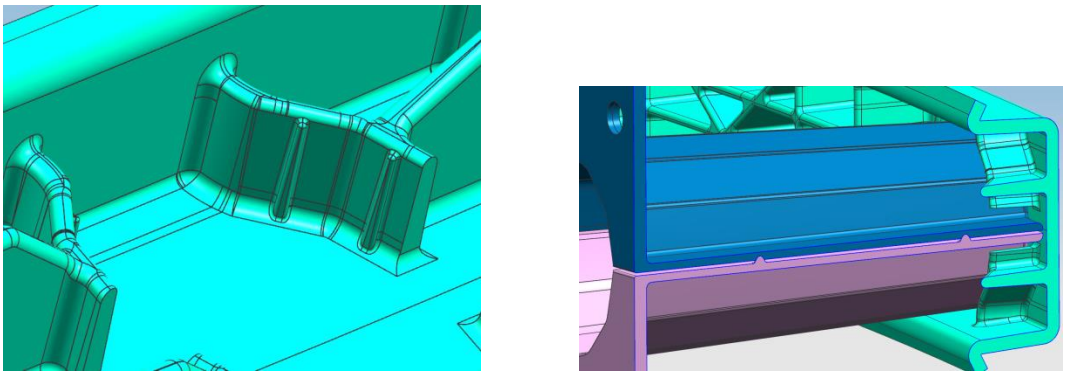

Figure 12. Molded-in SMC receiver pocket with stand-off beads to maintain bond thickness and control squeeze-out for crush can attachment.

3.3.3 Final Carbon Fiber FBCC Design and Crash Performance Summary

The virtual design of the composite FBCC released for tooling had a system weight save of 45% over the steel baseline design, the majority of which came from the crush can, as well as application of intelligent design to leverage the benefits of composites and allowed the integration of additional attachment brackets into the compression molded bumper and crush can parts. The final composite FBCC design was able to reduce the number of parts in the steel FBCC assembly from 9 parts to 5 parts. Figure 13 shows the final composite FBCC design concept for which CAD files were generated to enable tooling development under Task 4. The run-off areas, which facilitate forming and manufacturability of the parts, are also shown, and are machined off after molding to meet the final design geometry.

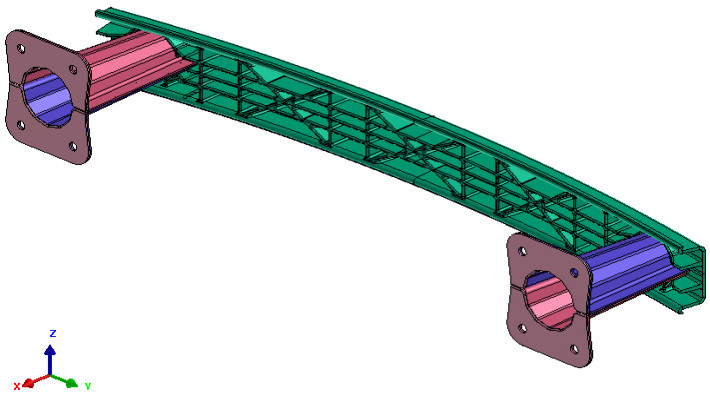

Figure 13. Composite FBCC system released for tooling development.

[6] *US Patent 9,598,033 B1 "Design of the Thermoset Composite Front Bumper Beam and Crush Can (FBCC) System."*

The carbon fiber bumper beam is molded as a 5.62mm thick C-Channel, made from 24 layers of woven carbon fiber material in a $[0/45/-45/90/0/45/-45/-45/90/0/45/-45/90]_s$ lay-up with chopped random fiber SMC ribs for local stiffness and to create a conical “pocket” feature into which the crush cans are inserted and bonded in place.

The crush can is designed with 2.8mm thickness out of 12 layers of unidirectional, continuous carbon fiber with a symmetrical [0/45/-45/0/45/0]s lay-up, which was shown to provide the most stable crush mode for the different angles of load input.

Performance predictions were completed and submitted for each of the impact load case events in Q3 2016. In the case of the RUC-based meso-scale and micro-plane codes developed by our academic partners, only the crush can itself is assessed for the rigid flat frontal and angular impact load conditions. The full FBCC system (crush cans and bumpers) were assessed using the commercial codes. Table 7 shows the performance summary (in terms of energy absorbed, which is the primary function of the crush can and a key correlation metric) for the different analyses and software code material formulations. The energy targets listed in the table were derived from the steel FBCC as part of Task 2, following the baseline steel FBCC crash testing assessment. The 17.5 kJ energy absorption (per crush can) predicted by PAM-CRASH is within 10% of the 37.8 kJ absorbed by baseline steel FBCC in a system-level crash test, and matches the energy absorbed by the steel FBCC predicted in the same software. It was therefore agreed by the team that this 35 kJ level of energy absorption would be acceptable to release the design for tooling.

While the system demonstrated adequate performance for most of the load cases, the design was not able to meet the center pole intrusion requirements, as the beam did not exhibit sufficient strength or elasticity, and simulations showed cracking early in the event. While a design solution was developed to mitigate the cracking and meet the performance objectives, it required an additional C-Channel piece to be joined at the back of the beam. This locally increased the stiffness of the section, but incurred additional part weight and fabrication costs. Hence, the project team made a tradeoff to proceed without the part, as it was agreed much could be learned if a similar failure mode was achieved in the physical tests, and the prediction could still be accurate.

The resultant mass of the design for the FBCC is presented in Table 8 with a projected savings of 45% over the steel baseline (based on CAE calculations). Further mass saving would be possible with further iteration of the bumper beam ribbing pattern and topology, which accounts for 1.9 kg or 32% of the total weight of the system. Additionally, the selection of compression molding and riv-bonded flanges for the crush can design adds additional weight and cost from the flanges and their required joining mechanism. This could be mitigated with an alternative manufacturing system, such as filament winding or pultrusion. These are recommended for future investigations of optimal crush can geometries to maximize weight savings and reduce material utilization, if the manufacturing processes can substantiate high volume and high quality production with repeatable component properties.

Table 7. Performance summary of composite FBCC predicted in different analysis codes. These predictions were refined later based on changes to boundary conditions.

Code	Event	EA Target	Energy Absorption Prediction	Stroke Prediction
PAM-CRASH *MAT131 Multi-Layered Orthotropic	Flat Frontal	~18.9kJ (per can)	17.5kJ	162mm
	Angular	~13.4kJ	13.0kJ	165mm
NU Microplane Model	Flat Frontal	~18.9kJ (per can)	13.5 / 13.3kJ Spectral Stiffness Microplane Model / Microplane Triad Model	190 / 204mm
	Angular	~13.4kJ	13.3-12.7kJ Spectral Stiffness Microplane Model / Microplane Triad Model	204mm
UM RC Model	Flat Frontal	~18.9kJ (per can)	12.8 / 12.6kJ S3R Shell Element SC6R Solid Element	165 / 195mm
	Angular	~13.4kJ	11.0 / 10.0 S3R Shell Element SC6R Solid Element	140 / 242mm

Table 8. Steel and composite FBCC mass summary.

Component	Total Mass (kG)
STEEL	
Steel Bumper	5.3
Steel Crush-Cans	1.8
Front Bracket	0.9
4 Additional Bumper Attachments	0.3
Rear Bracket	2.7
2 Additional Rear Bracket Attachments	0.3
Total Mass	**11.3**
Total Mass Without Additional Attachments	**10.7**
COMPOSITE	
Bumper 24 Layers	2.8
Crush-Cans 12 Layers	1.0
SMC Ribs in Bumper (7-5 mm Thick)	1.9
SMC Rear (~ 3 mm Thick)	0.2
Total Mass	**5.85**
Mass Savings Over Steel	**48.2%**
Mass Savings Without Additional Attachments on Steel	**45.5%**

3.3.4 Mesh Sensitivity Study

Early in the development and prior to concept convergence, a sensitivity study was also conducted to validate the mesh size and its effect on predictions for the crush can performance.

A conical crush can impacted by a flat mass of 150 kg at 35 miles per hour (mph) was considered for the purpose, as shown in Figure 14. The simple geometry allowed the investigation of a greater range of mesh sizes. Simulations were run with a 2-, 3- and 4- mm mesh for the NWU micro-plane models. As can be noted from Figures 15 (a) and (b), both micro-plane models results were

basically independent of the mesh size. This is an inherent feature of both the NWU and UM micro-plane models, where the crack band modeling approach employed in these material definitions de-sensitizes the models to mesh size changes. In the case of the approach employed by UM, the damage parameter is calculated based on a function of the mesh size. A small difference in dissipated energy, always below 3%, was noted, and it can be ascribed to the effect of element erosion required by the analysis codes to solve and run the simulations.

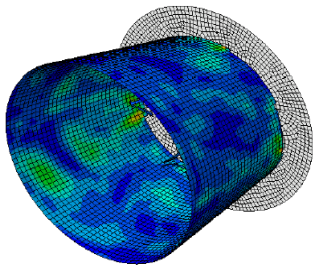

Figure 14. Conical crush can geometry for mesh sensitivity study.

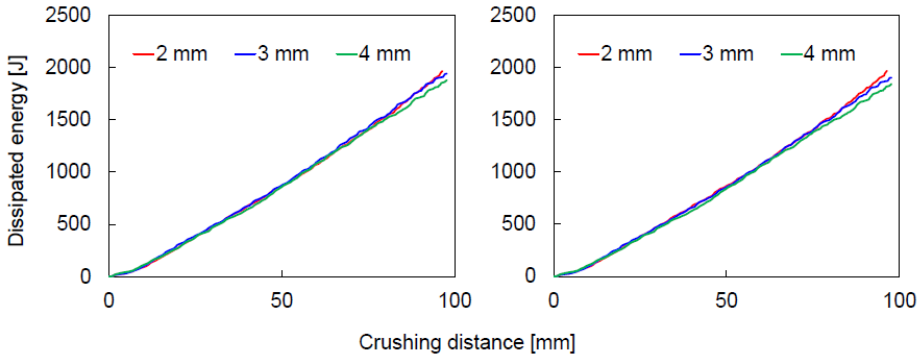

Figure 15. Predicted energy dissipated for various mesh sizes. (a) Spectral stiffness micro-plane model and (b) Micro-plane triad model.

The UM provided an assessment of the crush can design with both Shell and Solid element models in ABAQUS to make the prediction with the RUC material model. In general, the solid model exhibited *softer* behavior than the shell model, with lower energy absorption numbers despite a higher stroke. Important learnings and recommendations are expected once these results are compared to a physical test. Images of the solid model are shown in Figure 16 for reference, which also shows the solid elements used to model the rivet in the bond flange.

In the final phase of the project, ESI was able to implement the ACC-developed UM Waas-Pineda meso-scale RUC material into its latest version of its VPS software, released June 2017 to the broader industry. The new model resolves mesh-dependency of composite FEA crash simulations and provides a stable result. This was a significant achievement that facilitated the transfer of developmental academic codes into a commercial application, and it will foster further development and refinement of the model as it becomes more widely distributed and exercised over a broader range of composite structures, ply configurations and loading conditions.

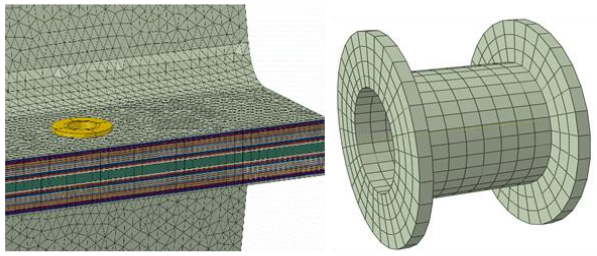

Figure 16. SC6R solid element models used to validate RUC model predictions.

3.4 Task Conclusions

In this task, the team designed a carbon Fiber FBCC system to withstand the loading requirements of six different high and low speed impact events, with equivalent performance to a production steel FBCC system design. The final design showed a 45% weight reduction over the baseline steel design, and was able to be implemented in a high-volume compression molded production process. The design was also applicable to a thermoset material, which is covered further in Task 4. Section 8 of this report includes a detailed discussion of the technological gaps and remaining challenges identified by the VMM Project that warrant future investigation.

4.0 FBCC Manufacture and Assembly Processes

4.1 Task Objectives

In Task 4, the MPS team worked closely with the NDE team, and a subcontracted supplier group (organized by Continental Structural Plastics, CSP) comprised of Detroit area suppliers providing tooling, molding and machining, as well as with Dow Automotive to leverage adhesive joining capabilities. The USAMP-supplier team pursued the following task objectives:

- Material and process selection for the thermoset FBCC design. This objective was completed and is reported in conjunction with Task 3: “Design of Composite FBCC.”
- Manufacture of the thermoset FBCC assemblies for crash testing and NDE evaluation. This included manufacturing the tooling and fixtures required for molding, trimming, and joining of the parts.
- Manufacture crush cans composed of alternative materials for comparison to the thermoset design. This included evaluation of a thermoplastic matrix and the ORNL low-cost carbon fibers.
- Identification of gaps in technology associated with the objectives listed above.

Specific milestones for this task are as follows.

M10	Manufacture Tooling	Tooling will be designed and fabricated for the selected design and MPS.	Completed
M11	Molding Process Development	Development of fabrication process for crush cans and bumper beams as well as joining methodology.	Completed
M12	Composite FBCC Assembly Delivered for Crash Testing	FBCC assemblies will be fabricated and delivered for crash testing, including set up parts and final display parts.	Completed

4.2 Summary of FBCC Materials and Manufacturing Process

As described in section 3.1, three material systems were used for fabrication of thermoset FBCC components.

1. A woven carbon fiber/epoxy prepreg used for the primary structural features of the FBCC (shown blue in Figure 17); it is composed of 2 x 2 twill-woven Toray standard modulus carbon fiber with Cytec MTM 54FRB epoxy resin.
2. A carbon-fiber SMC (shown orange in Figure 17); it is Mitsubishi Rayon Pyrofil CVS1016-2BK with 53% fiber by weight with a fiber length of 1 in.
3. A glass-fiber SMC, Continental Structural Plastics 834 SMC (shown orange for the crush can rear flanges in Figure 17). The switch from carbon fiber to glass fiber in this area resolved a processing issue as the flange was splitting after demolding.

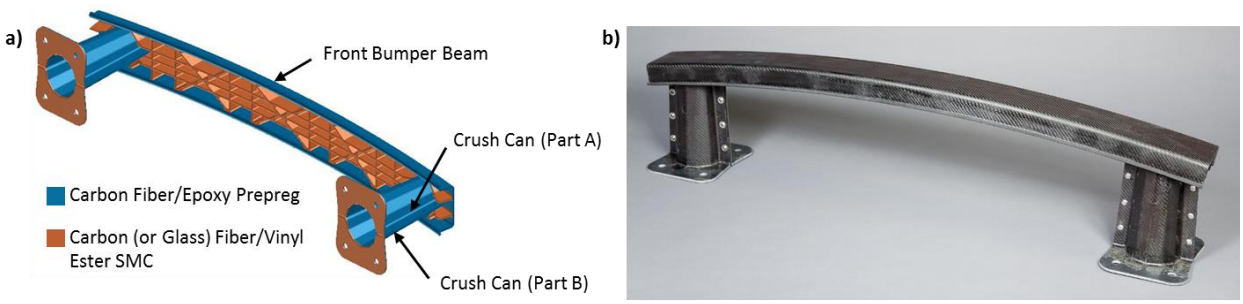

Figure 17. The designed and assembled FBCC ready for crash testing: (a) CAD image of the FBCC system and materials used, and (b) Photograph of an assembled FBCC for crash testing.

4.3 Manufacturing Considerations for the FBCC

The key criteria for the above material and process selection was to source commercial materials with the ability to scale the production method to large volumes. Additional requirements for the program included the ability to produce an FBCC that fit within the design space of the benchmarked steel system and the use of carbon fibers as the reinforcement. With these restrictions in mind, the team developed a design with five separate compression molded components that could be adhesively joined. In addition, the requirement to use the same design space as for the steel FBCC resulted in challenging geometries to mold with continuous fiber alone. A co-molding method was developed with continuous fiber prepreg and SMC. The prepreg formed the primary structural features while the SMC formed the complex geometric features.

The FBCC design resulting from Task 3 was an assembled sub-system for crash energy management, comprised of five parts, including the bumper beam and the right- and left- hand side crush cans, which are each composed of halves as one “A” and one “B” part (Figure 17). The crush cans were designed as two halves of a tapered cylinder that are assembled and joined using flanges. The bumper beam is swept and incorporates ribs for additional strength and stiffness. The components of the FBCC are joined using adhesive bonding. In addition, rivets are used on the crush can flanges to improve bonding and act as peels stoppers. The FBCC is mounted to the vehicle using four bolt holes in the large flanges on the vehicle side of the crush cans. In a frontal crash, the crush cans are the main energy absorbers, and do so by progressive crush failure of the composite. By design, crush starts at the impacted-end of the crush can and progresses towards the vehicle-end. Energy is absorbed through many delaminations, micro-cracks, fiber fractures, and other damages that are generated during this dynamic loading event.

The FBCC was designed in Task 3 for equivalent energy absorption as the steel design, established from the steel baseline crash testing, with a mass reduction goal of 30-35%. Iterative virtual design of the FBCC was performed in VPS/PAM-CRASH based on material models developed using coupon test data, as well as drop tower and four-point bend tests conducted on a composite hat-section manufactured using the same materials as the FBCC. These hat-section tests were used to tune the material models used in the virtual design, and later assembled into hat-section crush tube samples by bonding a flat sheet to cover the channel.

The CAD details for the FBCC components were finalized for tooling release for compression molding using two-part tools made of aluminum. A total of three molds were required, including one for the bumper-beam, one for part “A” of the crush-can and one for part “B”. All components were comprised of a combination of sheet molding compound (SMC) and continuous-fiber prepreg, co-molded and co-cured in a cycle time of under 15 minutes. This approach allowed for the use of the high performance prepreg in the main structural portions of the FBCC and the use of SMC to form complex structural features. The prepreg plies were precision-cut using an

automated cutting table, while the SMC was cut to shape by hand, and the quantity was verified by mass measurements. Prior to molding, the prepreg was manually preformed into rough 3D, then preformed to shape using dedicated forming tools, and stored in a freezer on a buck until it was time to mold. During molding, the parts were placed in the hot mold, cured, and removed from the press. Following molding, the parts were trimmed to final dimensions using CNC milling. Parts were then joined using adhesive bonding and rivets.

4.4 Manufacturability Evaluation for a Simple Structure

After the material selections were made in 2013 using plaque molding and testing (described under Task 3), more detailed material/layup and model validation studies were conducted during 2014 by testing an “intermediate” structure. The intent of this testing was to evaluate a structure that was more complex than a flat plaque, used available tooling, and contained features similar to the final FBCC. The closed-hat section shown in Figure 18 was chosen for its similar geometries to those found in both, the crush can and bumper beam, and the use of an adhesive bond for joining the two parts, similar to the crush can. Drop tower impact testing and four-point bend testing were used to compare layups. Three layups were compared, including “Woven 0/90” with $[0/90/0/90/0/90_{1/2}]_s$, “Woven QI” with $[0/90/45/-45/0/90_{1/2}]_s$, and “Uni/Woven QI Mix” $[0/0/0/90/45/90_{1/2}]_s$. In the Uni/Woven Mixed layup, layers 1, 2, 5, 10, and 11 were unidirectional fiber, while the rest were woven. Both, cross-ply and quasi-isotropic layups were evaluated with the BETAFORCE 2850S adhesive.

Figure 19 shows images of the closed-hat section after a drop tower test. Results summarizing the testing are shown in Table 9. All tests were run from approximately the same height and with the same impact mass. Crush distance varied significantly from test to test with no significant differences apparent between the three layup. Plateau load was constant for each layup but varied from one layup to the next with QI woven showing the highest plateau load. However, large-scale delamination was observed in the samples. In the cross-ply sample, the delamination was primarily within the plate and therefore was not attributed to the adhesive. In contrast, in the quasi-isotropic sample the delamination was at the interface with the adhesive. The difference can be attributed to the difference in delamination resistance between the two layups. In both cases, however, no catastrophic failures occurred during this testing.
Figure 20 shows an image of the four-point bend testing and the test results. Counter to the results from impact testing, the addition of unidirectional fibers improve the four-point bend strength of the closed-hat section. However, since the impact test is more similar to the loads experienced in the crash test and with input from the design/CAE team, the VMM team ultimately selected to use all woven material in a QI arrangement.

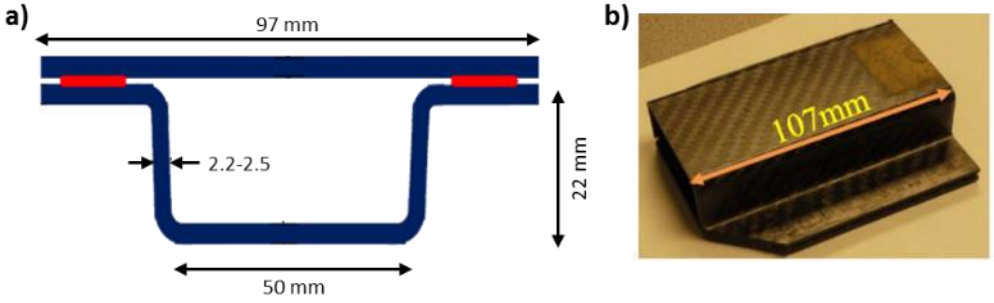

Figure 18. Composite hat section crush tubes. (a) Schematic of the geometry of the tube sample. (b) Photograph of the sample.

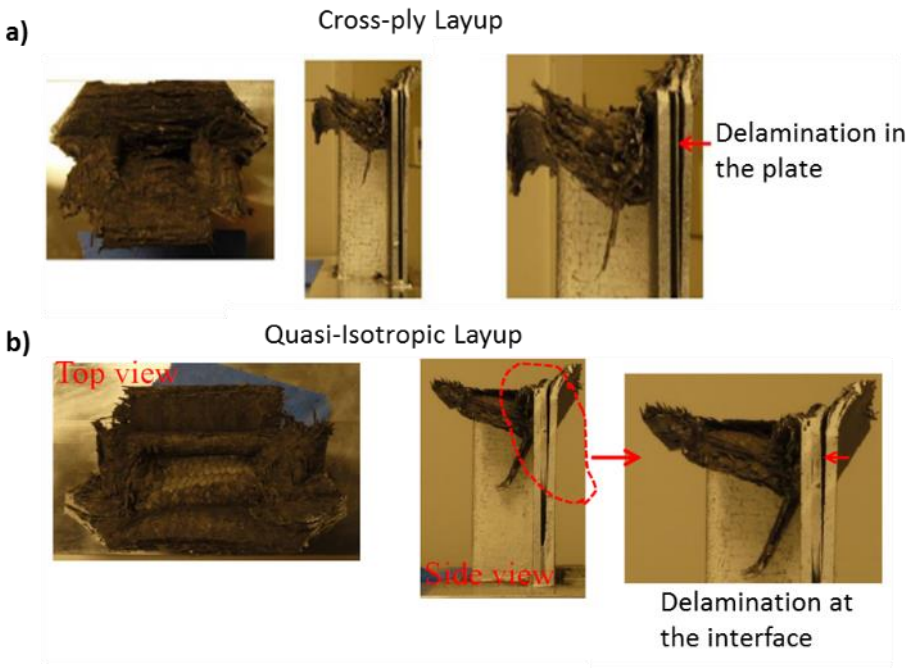

Figure 19. Images of the samples after testing for a) the cross-ply composite layup and b) the quasi-isotropic layup.

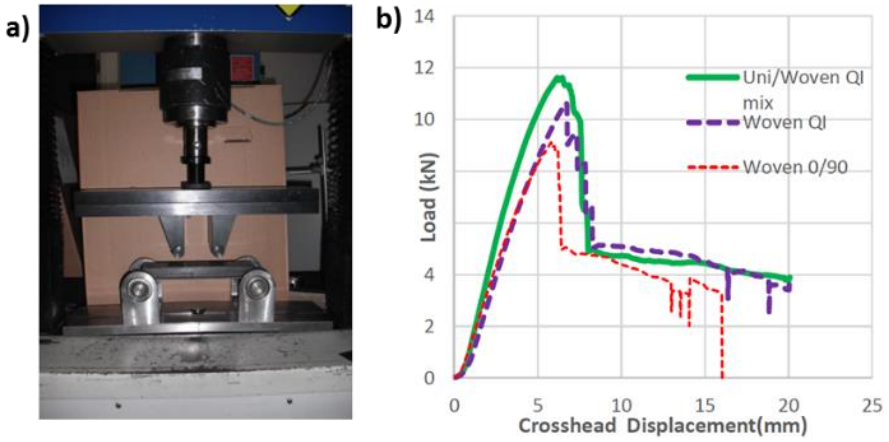

Figure 20. Four-point bend testing of the closed-hat section showing a) an image of the test and b) the test results.

Table 9. Summary of results for the three layup in the drop tower test. The structures were impacted with a 74.5 kg mass dropped from the indicated height.

	QI Woven		0/90 Woven		Uni/Woven QI Mix	
Drop Height [m]	0.98	0.98	1.00	1.00	0.97	1.00
Crush Distance [mm]	18.2	15.5	16.2	17.7	20.1	16.3
Plateau Load [kN]	41	41	-	36	35	35

4.5 Draping Analysis for Preform Design and Ply Cutting

Simulation tools were used to predict the draping of the prepreg kit during the preforming process. Siemens-Fibersim software was used initially to develop a 2D preform pattern for a single ply and help determine its drapability. A similar analysis was then performed in PAM-FORM, followed by a more detailed multi-ply analysis. Figure 21 shows the simulation of the preforming process for the crush can half using a simple rectangular ply design. This rectangular design was unable to conform to the complex geometry of the crush can half without significant wrinkling, particularly around the edges of the ply. Figure 22 shows a modified ply shape that was developed. Simulation results confirmed that this improved design was better able to conform to the geometry during preforming without wrinkles. PAM-FORM was then used to consider the full stack-up of the plies. Figure 23 shows the simulation of the bumper beam preforming process. Symmetry conditions were used to significantly simplify the model by allowing only a small portion of the beam to be simulated. A clamp was added to the top edge of tool to provide tension in the plies during the preforming process. This clamp was on the outside of the beam. Results showed that when this clamp was small, the plies would slip out from the clamp during the tool closing and significant wrinkling occurred. Figure 24 shows the results for a longer clamp design. Tension was retained throughout the process by using this larger clamp, resulting in no wrinkling. Similar modeling was performed for the crush can half, yielding analogous results. Draping analysis was found to be a valuable tool to workout potential preforming issues before finalizing the tool and ply-shape designs.

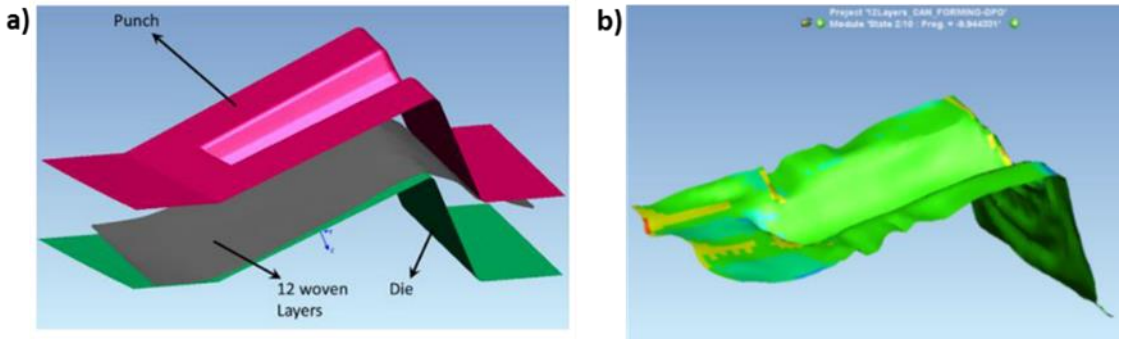

Figure 21. Fibersim and PAM-FORM were used to help predict draping of the kit during preforming by considering a single ply. (a) The setup of the model with a rectangular ply; (b) Wrinkling of the ply after preforming.

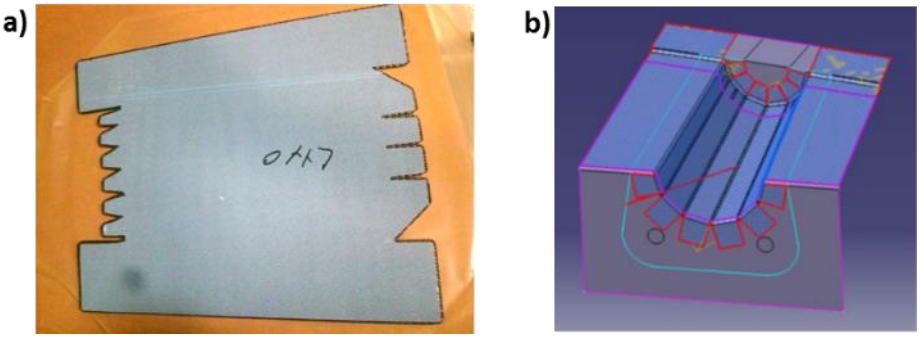

Figure 22. Based on the predictions showing wrinkling when the kit was rectangular, a modified ply design was developed. (a) The kitted prepreg prior to preforming cut to the modified ply design. (b) The kit preformed, showing no wrinkling.

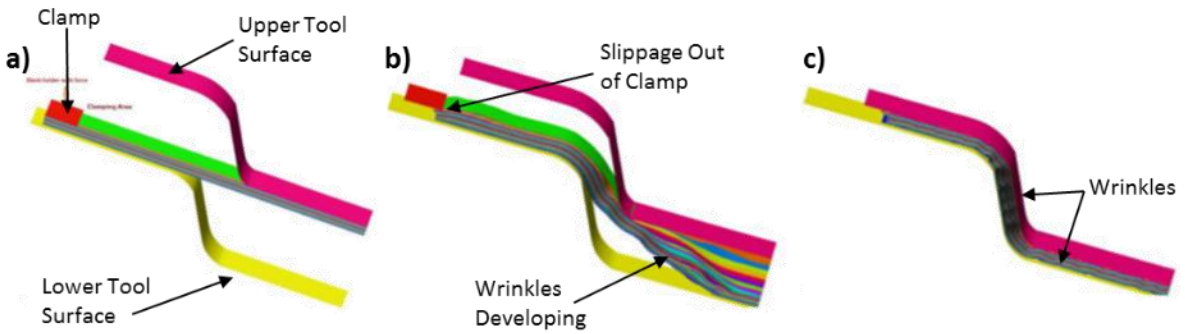

Figure 23. PAM-FORM model of the preforming process for a stack of plies. The section modeled represents the prepreg being deformed in the beam preforming tool. (a) The setup of the model, showing the tool surfaces, the clamp, and the plies. (b) The prepreg during deformation as the tool is closed- Note that the prepreg slips out of the small clamp. (c) The prepreg after the tool is fully closed, showing significant wrinkling.

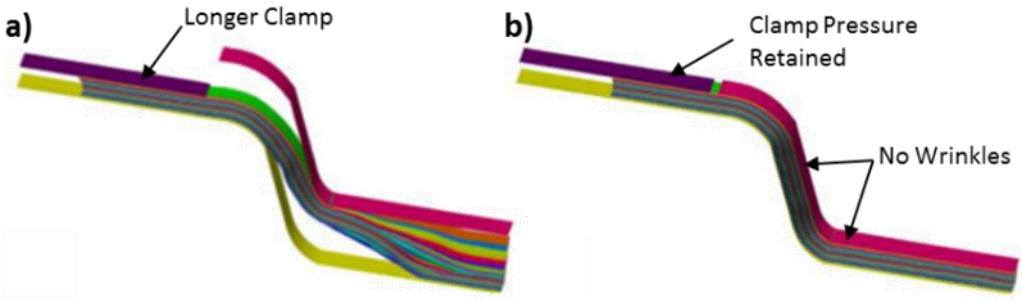

Figure 24. PAM-FORM model of the preforming process for a stack of plies with a larger clamp design. (a) The tool closing- Note that the larger clamp retained pressure on the prepreg throughout the process. (b) The tool fully closed, showing no wrinkling of the prepreg.

Prepreg plies were cut to the designated shapes determined by the draping analysis using an automated cutting table. Each ply was cut from the roll in a single layer, then stacked by hand to form the “ply-kit”. Kits were preformed using dedicated tooling shown for the crush can half and the bumper beam. Two sets of tooling for the crush can halves were required, one for half “A” and one for half “B”. Preform tooling was designed to deform the kit from a flat stack into the final shape of the part. Spring loaded draw bars (analogous to the “clamps” from simulation) applied light pressure to the prepreg edges as the ply stacks were being preformed, preventing wrinkling. The preformed prepreg was stored on a buck to maintain shape in a freezer until molding. Preforming was necessary as a separate step prior to molding to ensure that the plies deformed as intended and were easy to drop into the hot mold to be cured.

4.6 Component Tooling, Molding and Trimming

Once the prepreg plies were cut, kitted, and preformed, the FBCC components were formed using compression molding. Photographs of the tooling for the crush cans are shown in Figure 25. Two tools were required for molding the crush cans, one for half “A” and one for half “B”, which were mirror images of each other. Photographs of tooling for the bumper beam are shown in Figure 26. These tools were designed with 100 mm runoffs around the parts and used a shear edge to prevent resin flow out of the mold cavity. A gasket around the perimeter of the tool allowed for air to be removed during mold closing to prevent air entrapment in the tool. Spacers were designed to be adjustable to fine-tune the closed gap within the tooling.

Components were molded using a combination of sheet molding compound (SMC) and continuous-fiber prepreg, co-molded and co-cured. The main crush can structure was composed of 12 layers of woven carbon fiber prepreg with a $[0/45/-45/0/45/0]_s$ stacking sequence. The nominal target thickness was 2.8 mm. The flanges were molded from SMC inserted into the mold in the appropriate locations. For the crush cans, glass fiber SMC was used instead of carbon fiber SMC, because of its better flow characteristics. The extreme tilt of the tool prevented sufficient pressure on the SMC to give appropriate flow of the carbon fiber charge. The main beam structure was composed of 24 layers of the same prepreg with a $[0/45/-45/90/0/45/-45/90/0/45/-45/90]_s$ stacking sequence. The nominal target thickness was 5.6 mm. The ribs in the bumper beam were formed from the carbon fiber SMC.

Preforms were removed from the freezer and allowed to reach room temperature prior to molding. Leaving the outer layers of wax paper on the preforms during warm-up prevented moisture from forming directly on the preforms. The top mold was heated to 143° C and the bottom to 137° C. The difference in temperature prevented binding of the shear edges by allowing the top mold to expand slightly more than the bottom. During molding, the preformed prepreg was first dropped into the mold cavity. Excessive resin run-off was controlled by extending the prepreg exposure time to temperature in the mold (“pre-gel”) prior to application of pressure and localized use of SMC at the shear edges of the molds. The pre-gel time was approximately 2 minutes, but was adjusted regularly as needed. After the pre-gel step, a mass-measured quantity of SMC was the placed onto the prepreg in the proscribed location. The mold was then closed and the part cured for 10 minutes for the crush can and 15 minutes for the bumper beam under a compressive load over 250-450 tons.

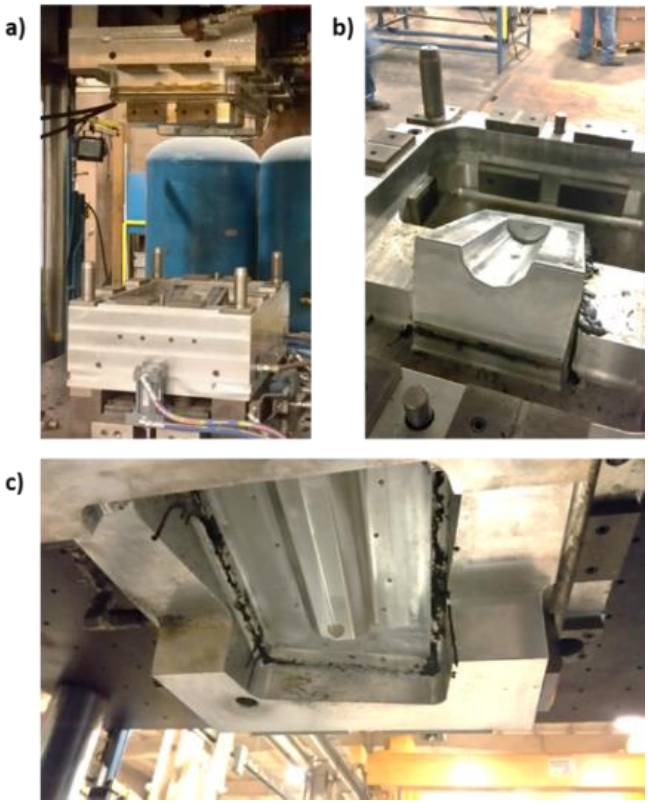

Figure 25. Photographs of the crush-can mold. A and B molds were mirror images of each other. a) The mold shown in the open state in the press. b) The lower half of the mold. c) The upper half of the mold.

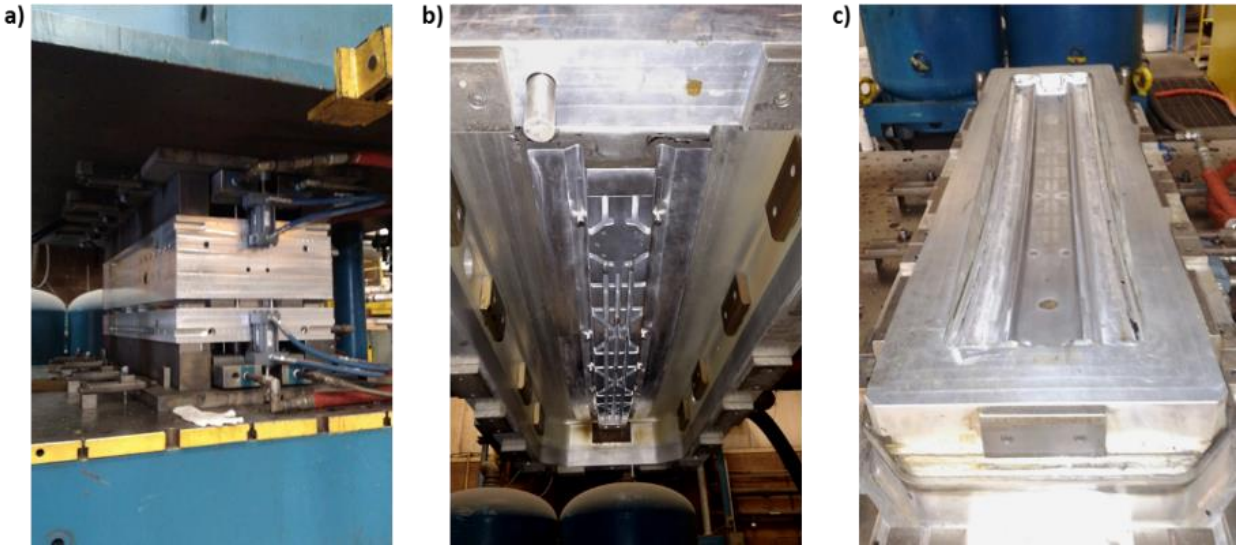

Figure 26. Photographs of the bumper beam mold. a) The mold shown in the closed state in the press. b) The upper half of the mold. c) The lower half of the mold.

Following molding, the parts were trimmed to final dimensions using CNC milling. Figure 27 shows CAD images of the parts before and after trimming. A five-axis mill was used for crush cans and a three-axis for the beams. Custom fixtures were designed to accurately hold the complex parts in place during trimming. During trimming of the crush cans, holes were drilled into the side flanges for rivets used as part of the joining process.

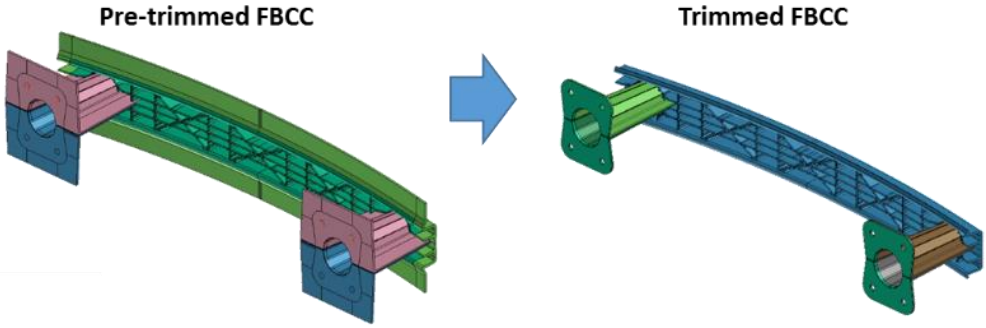

Figure 27. CAD image of the FBCC before and after trimming. Each component was trimmed separately prior to assembly.

4.7 Joining and Assembly of FBCC Components

After trimming, the parts were assembled into FBCCs at Dow Automotive using adhesive bonding and riveting. Each FBCC is composed of one bumper beam and two crush can sub-assemblies (each can is comprised of two molded halves). The objective of developing a joining procedure for the FBCC was to provide structurally strong interfaces within a fast cycle time applicable for full-scale production. The parts were primed with Dow BETASEAL 43532, then bonded with BETAFORCE 2850L, per selection process described in section 3.1.2. The following joining procedure was used:

1. Machine rivet holes during trimming of the molded parts.
2. Joining the crush can halves per the primer and adhesive application procedure developed by Dow.

3. Join the assembled crush cans to the bumper beam using a procedure recommended by CSP. For this step, a custom pneumatically operated bonding fixture (known as Bel-Kur press) was used (Figure 28) to accurately locate the FBCC parts and provide repeatable pressure during adhesive cure.

While this assembly procedure did successfully achieve geometrically-accurate and repeatable joining of the components, it is considered too slow for full scale production. Future improvements and optimizations recommended by USAMP to the joining procedure would include selection of a faster curing adhesive or use of higher temperature to speed up cure of the adhesive at each stage.

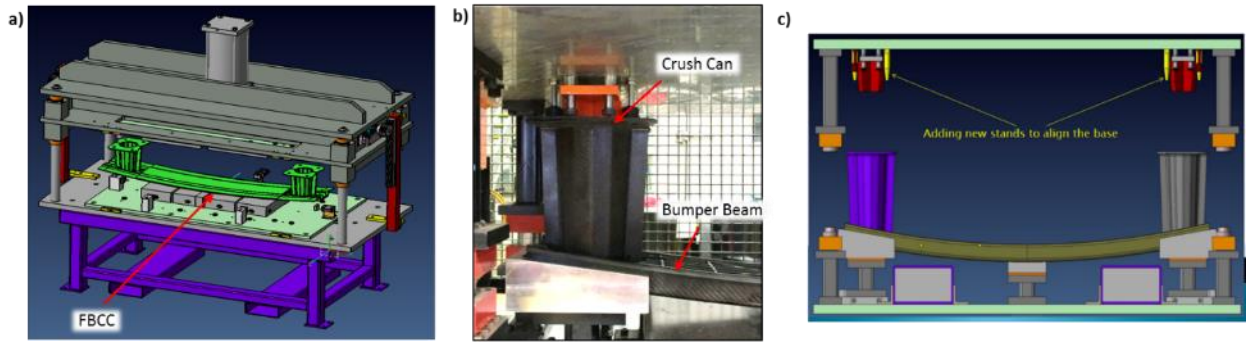

Figure 28. Schematic of the fixture used to join the assembled crush can and bumper beam. (a) Schematic of the press and fixture showing the location of the FBCC. (b) A zoomed-in photograph of the actual FBCC components in the press. (c) Pins were added to the fixture to ensure the holes for mounting the FBCC to the crash test sled were properly aligned.

4.8 Reduced Material Properties Compared to Flat Plaques

During early crash testing trials, it appeared that the crush cans were not absorbing the energy that was predicted during the design stage. To explore the cause, the MPS team conducted mechanical testing on coupons cut from the facets on molded crush cans (Figure 29). One molded crush can assembly (two halves) was obtained to cut tensile and compression specimens. Six tensile specimens and eight compression specimens were tested at Ford Research Labs. NDE was conducted on the specimens prior to testing to ensure that no damage, such as delaminations or excessive voids, was present in the crush cans.

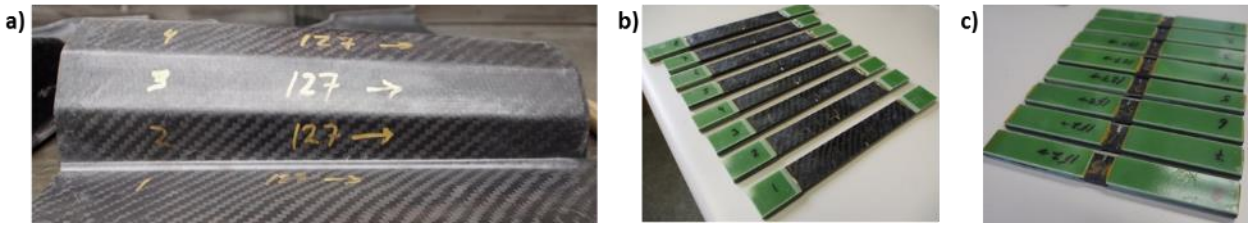

Figure 29. Coupons cut from the flat facets of the crush can for mechanical testing. (a) The crush can with the upper and lower flanges removed and future coupons labelled. (b) Tensile coupons. (c) Compression coupons

The specimens were cut on a wet-saw with diamond-coated circular blade. Widths for each specimen varied, dictated by the narrowest section and removal of any remaining radii. Facets selected were mixed to test all sides of both crush cans in tension and compression. After abrading the surface of the tab bonding area of the specimen and wiping with acetone, all

specimens were tabbed with Garolite G-11 using 3M DP420 adhesive. Tensile tests were again performed per ASTM D3039 and compression tests per ASTM D3410.

Material properties for the crush can coupons are compared to those from flat plaques in Table 10. Both sets used the same prepreg and molding parameters. The only difference between the sets was the molded geometry. The crush can coupon tests show significantly reduced mechanical properties. The crush can coupon tensile strength was 32% lower and the compression strength was 22% lower than the strength of the flat plaques. The cause of this reduction in strength and modulus is most likely to be distortion/wrinkling of the fabric during molding, which misaligns fibers relative to their intended orientation. The results from NDE discussed in the next section further elucidate this phenomenon.

Table 10. Comparison of mechanical performance in tension and compression for coupons cut from crush cans vs. those cut from flat plaques. The materials and processes are the same in each case, and the only differing factor is the molded part geometry.

Test	**Modulus (GPa)**	**Failure Stress (MPa)**	**Strain to Failure (%)**
Compression Testing			
Crush Can Coupons	32.1 ± 2.9	348 ± 55	1.24 ± 0.24
Flat Plaque	38.5 ± 0.2	446 ± 27	1.29 ± 0.10
Tensile Testing			
Crush Can Coupons	32.4 ± 2.9	332 ± 93	0.89 ± 0.34
Flat Plaque	37.4 ± 0.2	486 ± 20	1.31 ± 0.07

4.9 Non-Destructive Evaluation Findings Related to Manufacturing

NDE revealed several processing imperfections that were not initially apparent during molding. These issues would need to be resolved before a similar FBCC design could go into production but for the purposes of this paper are only identified.

Defects were detected initially using visual methods, and where possible, analyzed further in FBCC components using both non-destructive and destructive methods as detailed in the report section on Task 6. Non-destructive methods included radiograph, ultrasonic inspection, and computed tomography, while cross-sectioning and imaging was the main destructive method. The aim of these inspections was to identify discrepancies between the virtual part design and the actual part that was manufactured. Predictions were based on the virtual part design, and therefore, these discrepancies represent gaps between the modeling and the reality of the build and test. The primary defect in the crush can was distortions of the prepreg due to intrusion of the SMC during molding (Figure 30). The challenge of co-molding the SMC and prepreg, each of which had very different rheological and cure kinetic behaviors, resulted in significant bunching, stretching, and waviness in the prepreg section of the crush can near the flange. These distortions of the fabric are in addition to the distortion caused by draping the prepreg to form the complex shape of the crush can, in comparison to a flat plaque.

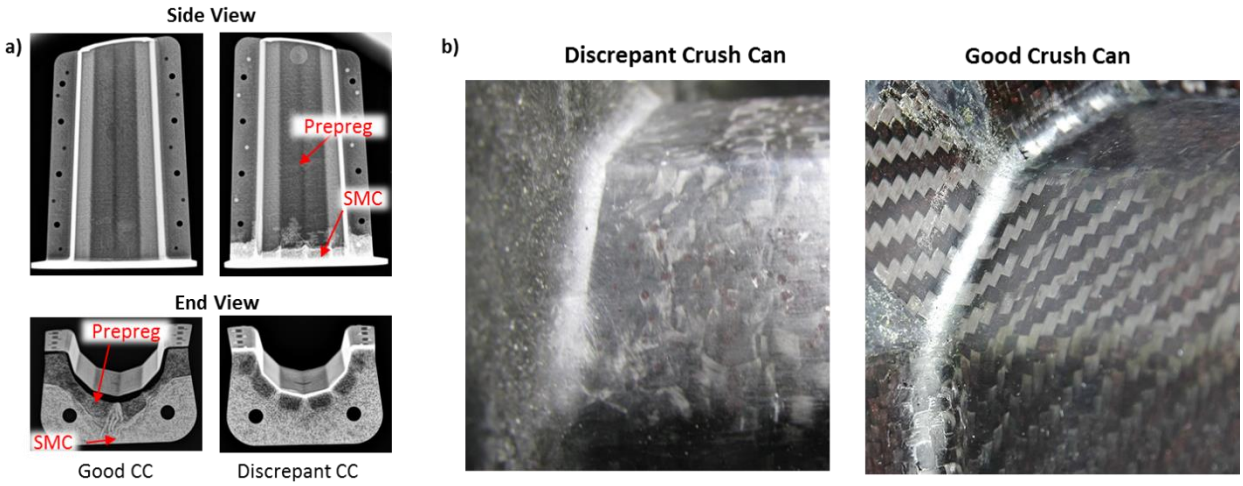

Figure 30. NDE using radiography on a crush can. (a) Radiographic images of a crush can showing the distribution of prepreg and SMC in a "good" crush can vs. a discrepant crush can, and (b) Image of the base of a crush can showing the weave pattern in a good vs a discrepant crush can.

It should be noted that the material models used for FBCC crash predictions were primarily based on flat-plaque coupon data, with tuning of the models using the hat-section data. However, this approach does not consider the effects of manufacturing on material performance. As stated, draping of the prepreg and interaction of the SMC and prepreg in the mold caused distortion of the fabric from its architecture in a flat plaque (Figure 29). To quantify the effect of these distortions, coupons were cut from a crush can and compared to the flat plaque coupon data in longitudinal compression and tension tests. Table 11 shows that the performance of the composite was significantly reduced in the crush can in terms of modulus and strength in both compression and tension.

Defects were also examined on the bumper beam (Figure31). Both, cross-sections and computed tomography showed the presence of extensive porosity in the SMC, as well as resin rich regions, and waviness in the prepreg. While the effect of these defects on material properties was not quantified, it is clear that such defects reduced bumper beam performance and may account for some discrepancies between the crash performance and CAE predictions, as noted in this report under Task 7.

Table 11. Comparison of flat plaques and crush cans tested in compression and tension. Values in red signify the percent reduction in properties.

Test	Modulus (GPa)	Failure Stress (MPa)
Compression Testing		
Flat Plaque	38.5 ± 0.2	446 ± 27
Crush Can Coupons	32.9 ± 2.8 (-14.5%)	352 ± 44 (-21.1%)
Tensile Testing		
Flat Plaque	37.4 ± 0.2	486 ± 20
Crush Can Coupons	37.0 ± 5.8 (-1.1%)	364 ± 86 (-25.1%)

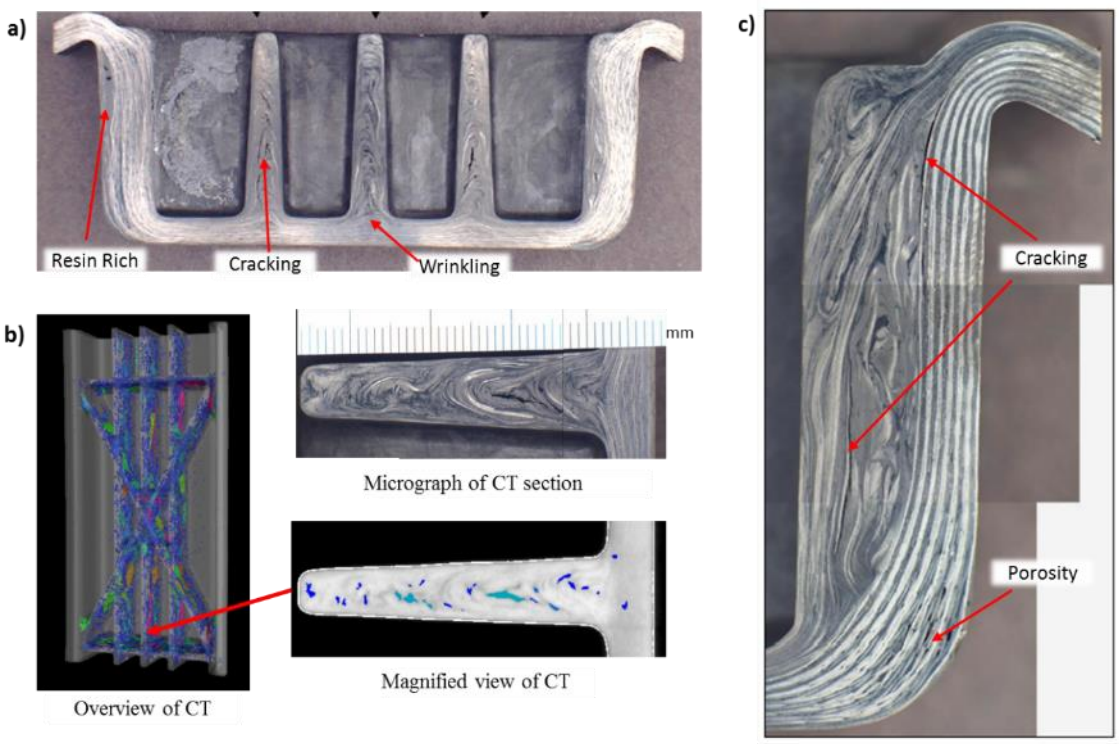

Figure 31. Images from NDE of various FBCC components. (a) Photograph of a cross-section of the bumper beam with several imperfections marked. (b) CT images and associated photograph showing porosity in the ribs of the bumper beam - Colors denote the size of porosity with blue corresponding to small pores and red to large pores. (c) Micrograph showing cracking and porosity where the SMC ribs meet the interior of the beam fabric.

4.10 Thermoplastic Materials for FBCC Components

The main objective of this portion of the project was to demonstrate predictability during a crash event when using a thermoplastic composite version of the crush can. The MPS team worked with Shape Corp., Century Tool and Gage, and Continental Structural Plastics to develop a manufacturing process for prototype runs of thermoplastic composite parts. Tooling developed for the thermoset epoxy prepreg and polyester based SMC materials along with a layup configuration and flat pattern was leveraged to fabricate and assemble the thermoplastic crush cans. Due to limited resources, the efforts were focused on producing sufficient crush cans for crash testing to evaluate an alternative material and process system to the thermoset composite that could meet the same vehicle packaging constraints as the thermoset system.

The thermoplastic effort included the initial selection of materials, and measurement of basic material properties that were then passed onto the VMM Project Design/CAE team for predicting crash performance of the crush can (using MAT_058 in LS-DYNA only). The design effort was followed by manufacturing two types of thermoplastic carbon composite crush can, and crash testing samples for direct comparison to the thermoset epoxy composite system– the first set of TP material crush cans was produced with commercially available carbon fiber/nylon PA6 TP prepreg systems, and the second involved use of Low Cost Carbon Fiber (LCCF) obtained from the ORNL Carbon Fiber Technology Facility (CFTF). These approaches are summarized below.

4.10.1 Evaluation of Commercial Thermoplastic Materials for Crush Cans

After surveying the TP material suppliers based on commercial availability and interest in offering engineering support, the VMM team determined the nylon PA6 composite materials offered by TenCate Performance Composites and BASF had the potential to meet the need of the project. The nylon PA6 was the chosen resin system based on its compatibility with carbon fiber, low processing temperature, and availability among the limited affordable options. The material supplied by Tencate was 200 gsm 2x2 twill woven carbon fabric laminated with layers of PA6 film. This material was based on a standard product, however, due to the performance and molding requirement, the laminate panels were further tailored for this project. This material was used in the crush can body to serve as an equivalent to the epoxy prepreg system used previously. Carbon fiber UD tape pre-impregnated with PA6 supplied by BASF was used to make the flanges of the crush can. This was a standard product that allows significant flexibility in processing, and was selected to mimic the characteristic of the SMC used previously in the thermoset system. Additionally, it would serve to provide some process-friendly characteristics needed for handling the charge during molding.

TP panel production was completed using a vertical stack press for lamination (done at Tencate Performance Composites division), as shown in Figure 32 below. Carbon fabric was alternated with PA6 film to achieve desired thickness and fiber wetting. Heat was cycled to 535° F and cooled to 200° F under 100 psi of pressure to produce 95 cm X 125 cm panels. Although the thermoset manufacturing used a 12-layer laminate, the thermoplastic film thickness and viscosity limited consolidation to 7 layers of carbon reinforcement. Any additional layers would exceed the design thickness, preventing direct comparison of crash performance to models and thermoset parts construction. The final panel construction was 0/±45/90/±45/90/±45/0, which came close to achieving a target panel thickness of 2.85 mm. These TP composite charges were designed for fast transfer into the mold to keep the PA6 resin at a molten state until mold close. They also required a radiant oven that would allow for steady rise to melt temperature without reaching a temperature gradient that would cause resin oxidation and further degrade the performance.

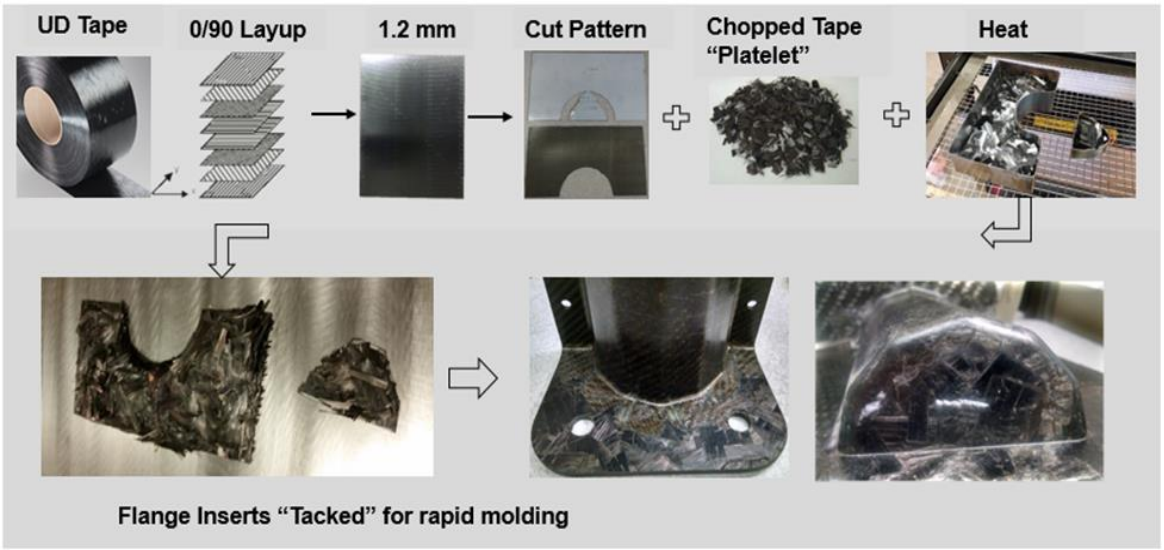

Figure 32. Thermoplastic crush can and flange preform productions steps.

The success of the molding of the crush can halves relied heavily on the composite charge design, placement accuracy, rate of transporting the charges from oven to closed mold, and uniformity of temperature in preform and oven. Placement sequence required chopped material to be inserted

prior to the can body charge. Manual transfer and manipulation of the molten charges, while not without error, allowed enough of the preform to clear the shear edges before shutoff to completely consolidate the parts. Transfer time ranged from 18-22 seconds from the point of removal of the charges to start of mold close. The aluminum tooling was heated to 150°C by steam to prevent rapid heat removal from the composite prior to compression. Once the targeted closed mold pressure was reached, the tool was held closed for 60 seconds to cool the completed part to a state of dimensional stability. This part and tool design did not require high ejection force to remove, so a demold temperature of 150°C was not a concern. Once outside the compression mold the part was cooled in open air at a nearby work station. Total cycle time from removal of charges from oven to removal of completed part from the tool was approximately 2 minutes. Once cooled, the parts were measured and shipped for trimming and joining. In total, 18 complete crush can sets were molded. Final part thickness averaged approximately 2.81 mm in the can body and 5.27 mm in the base flange. As with thermoset cans, these crush can halves were joined using the same adhesive bonding material and riveting. The mating surfaces were primed with Dow BETAPRIME 5406 and BETASEAL 43532 then bonded with BETAFORCE 2850L. Rivets and a mechanical clamping fixture held the parts in place during cure.

The process used to produce these crush cans yielded acceptable prototype parts for evaluating crash behavior of carbon fiber/ PA6 composite. There were some challenges to achieving defect free parts that may affect performance as well as predictability. With the heat source coming from radiant transfer, it was difficult to ensure a complete and equal temperature distribution of the laminate prior to transfer and compression. Many of these challenges can be overcome with production level equipment and automation to ensure proper heating, handling, transfer and placement of charge.

4.10.2 Sled-Based Crash Tests on Crush Cans

Sled tests were performed on both the thermoset- and thermoplastic- based (standard CF only, not LCCF) crush cans to compare their behavior. The impactor weighed 1145 kg and traveled at 4.85 m/s at the time of initial impact. While the materials used for the thermoset and thermoplastic crush cans were not perfect analogs, they were designed to be as similar as available materials allowed. A comparison of the materials is shown in Table 12. Figure 33 shows an image of a crush can ready for testing.

Table 12. Comparison of the epoxy-based and PA6-based composite crush cans.

Attribute	Epoxy/CF	PA6/Woven CF
Ply Count	12	7
Average Side Wall Thickness (mm)	2.95	2.82
Average Mass (kg)	0.74	0.64
Average Fiber Volume Fraction	58±1%	38±1%

Figure 33. A crush can ready to be impacted on the crash-test sled. Four load cells are used to track the force during the impact. The crush can is mounted stationary on the wall while the sled travels along rails to impact it.

The crash test results showed very similar behavior between the thermoset and thermoplastic crush cans (Figure 34). Thermoplastic crush cans had slightly less total crush length and slightly higher peak load than the thermoset crush cans. However, it is notable that the thermoplastic crush cans contained 38% carbon fiber by volume, whereas the thermoset crush cans contained 58% carbon fiber by volume While a detailed cost analysis has not been conducted on the two materials, this has the potential to reduce the cost of thermoplastic-based material compared to the thermoset-based material. Another notable difference between the behaviors of the two materials is that the thermoplastic material fractures into larger pieces and creates less dust.

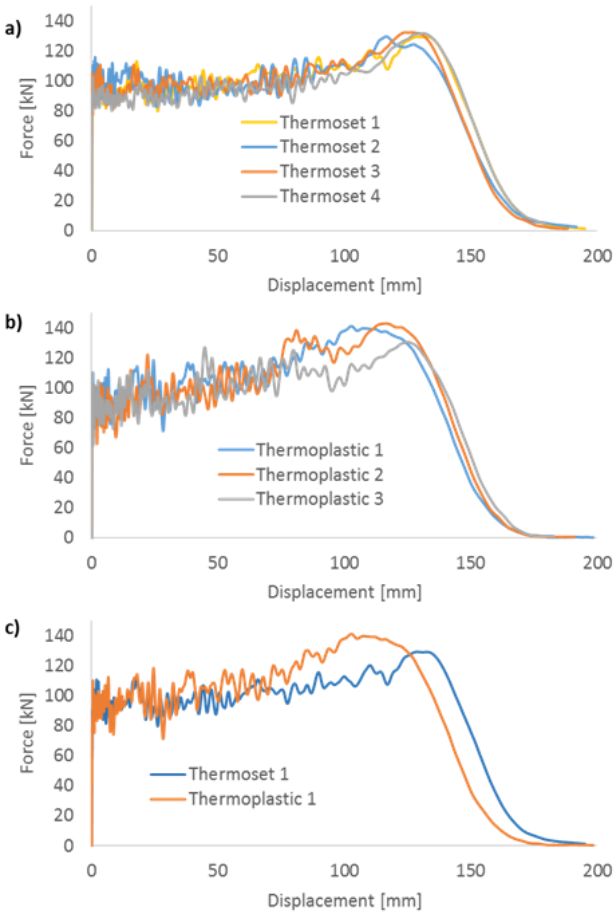

Figure 34. Force vs displacement from the crash tests of thermoset and thermoplastic crush can. (a) Results from 4 separate thermoset crush cans. (b) Results from 3 separate thermoplastic crush cans. (c) Overlay of thermoset and thermoplastic crush cans.

4.10.3 Evaluation of Prepreg from ORNL LCCF for Crush Cans

The second thermoplastic composite material intended for molding into crush cans was derived from LCCF produced from ORNL's CFTF which shipped approximately 40 kg of LCCF to Chomarat in 2016. This large tow format (457K tow) required significant time developing methods to spread and place into a 120 gsm knit for use in the automotive market. Two trials were necessary to achieve yield of fabric for a thermoplastic laminate system using the LCCF. The large tow format made it unlikely to be successfully woven, so a non-crimp fabric (NCF) was the production method of choice. Initial trials focused on evenly spreading the tow into a ±45° NCF that could be useful in many different processes and applications. These initial runs provided 20 linear meters of 120 gsm double bias fabric that were trialed with 340 gsm PA6 thermoplastic film to determine what level of fiber wetting could be achieved. In this trial, 10 layers of the double bias NCF was stacked with nylon film between each layer then consolidated using the same process used to produce the previously discussed thermoplastic panels. The layup was quasi-isotropic (0/45/90/45/0/0/45/90/45/0) with film on the outside layer and between each ply of fabric. As with the previous material, a vertical stack press was used for lamination.

Woven reinforcement is often the textile of choice for thermoplastic composites because the interlocking and crimp of the tows allows resin to flow and properly wet out the fiber while locking

the tows in a fixed orientation. In contrast, the NCF acts like a barrier to the thermoplastic resin, limiting fiber wetting and forcing resin flow along the face of the ply instead of through. This first round of consolidation trials confirmed this hypothesis and resulted in significant resin-less regions through the thickness of the composite. These layers were easily separated by hand, confirming poor fiber wetting and the need for the film to be stitched between each sub-ply. Also observed, was the absence of the polyester stitching due to the relatively lower melt temperature when compared to nylon, yet fiber remained orientated. This was likely due to the frictional interaction of the dry layers of carbon fiber within each fabric ply. This task was also complicated by the nature and viscosity of the thermoplastic Nylon 6 resin system used in the previous laminates. Special steps had to be taken to ensure proper fiber wetting and panels consolidation.

For the second round of trials, the team modified the fabric production process to stitch a layer of nylon film between the +45° and -45° sub-plies. To prove the concept was possible with the fabric production equipment, PA6 film was initially stitched to the outside of the fabric. After these promising results, the final step of stitching film in between each sub-ply was successfully completed producing 20 linear meters of material. The resulting material was 120 gsm carbon combined with 340 gsm film to produce a 460 gsm thermoplastic fabric kit. This fabric was then sent to be laminated with multiple layers of alternating film and fabric containing film to achieve the target thickness and quasi-isotropic layup.

The material produced with PA6 film stitched between each sub-ply was laminated into 8 layer panels (0/45/90/45/45/90/45/0) with film added between each layer of fabric. Fiber wetting was improved, but fiber and resin migration was a significant problem. The defect occurred due to the melt temperature of the polyester stitching being well below the melt temperature of the Nylon 6 resin. These and other processing complications resulted in a greatly reduced yield of moldable laminate with sufficient PA6 film between each sub-ply – certainly not enough to produce sufficient quantities of crush cans for crash-tests as in case of commercial TP material described in section 4.9.1. Hence, a decision was taken to maximize the use of available LCCF-based by molding the laminate into (smaller) hat sections that could be adhesively joined with flat plates to form hat section crush tubes. These tubes were suitable for limited comparison in drop-tower tests with the thermoset-based hat crush tubes.

Drop tower tests were performed by GM R&D on hat-section crush tubes (Figure 35 shows sample details) molded from carbon fiber/epoxy prepreg, woven standard carbon fiber-nylon PA6, and NCF LCCF-nylon PA6 material for comparison. The crush test results are shown in Figure 36. During the test, a 276 kg weight was dropped from a 84 cm height. The hat section samples were supported by placing them vertically approximately 1 inch into the cavity of an aluminum fixture providing approximately 1-3 mm of spacing around the edges and using hot-melt adhesive to hold the sample in place. Two bolts were added on each flange to provide additional support between the two parts of the sample.

(a) (b)

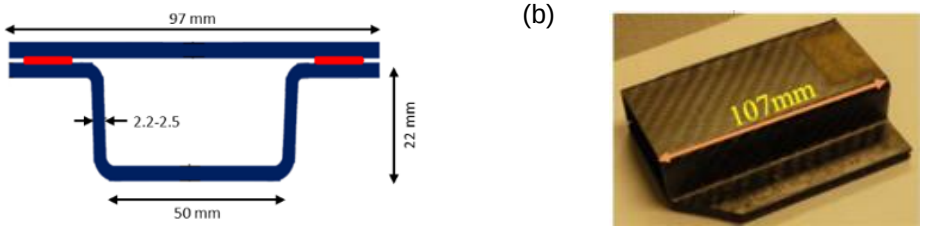

Figure 35. Drop tower test crush tube samples made from LCCF TP hat sections. (a) Schematic of the geometry of the tube sample. (b) Photograph of the sample.

Drop tower results are shown in Figure 36 for each of the three sample types. Overall, the epoxy-based samples had the highest peak load, while the woven-CF/nylon-based material performs similarly. In contrast, the LCCF/nylon material showed significantly lower loads throughout the test, likely due to the defects in the laminated fiber architecture. Additionally, the use of an NCF for this material, rather than weaving the carbon fiber, may have also contributed to these differences. The experiment was not designed with the proper controls to indicate whether the difference in NCF vs. woven, the defects in the NCF samples, or the effect of reduced fiber performance in the LCCF was a larger contributor to the poor performance of these samples.

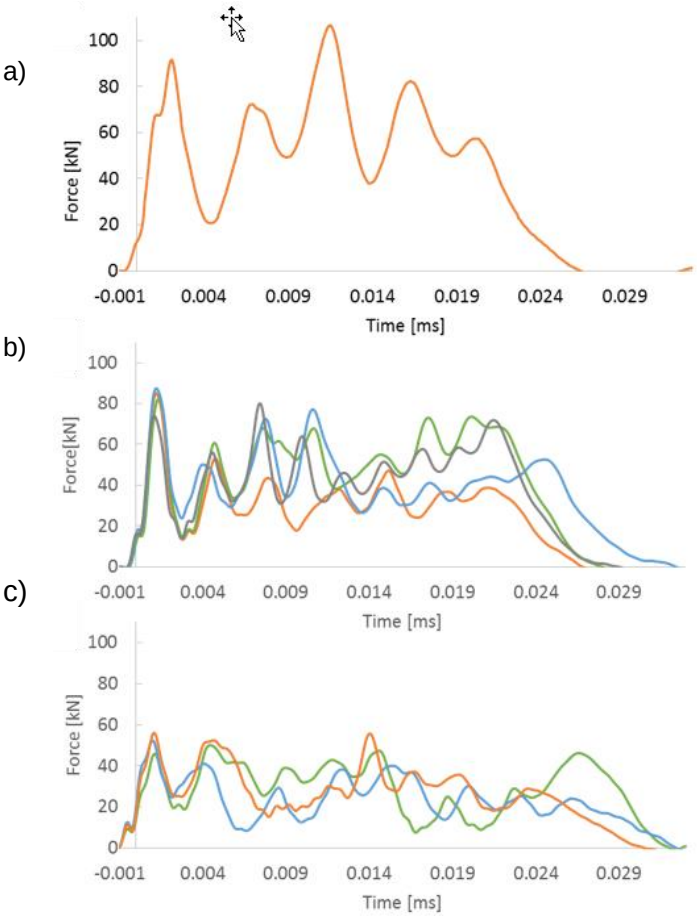

Figure 36. Drop tower test results for (a) carbon fiber/epoxy prepreg, (b) woven standard carbon fiber and nylon, and (c) NCF LCCF material. Each curve represents the results from one test. Note that only one test was run for the epoxy-based material under these conditions.

It can be concluded that challenges in processing the TP materials likely resulted in imperfect parts. Yet, comparison of these two thermoplastics resin systems with the thermoset test showed significant energy absorption potential in crush can applications. If low cost carbon fiber reaches large scale production, the automotive industry has an opportunity to benefit with more integration of carbon fiber composites at lower cost. With further development, thermoplastic composites could make a positive impact to lightweighting in higher volume applications.

5.0 Crash Testing of Composite FBCCs

The principal objectives of Task 5 were to utilize the sled system/fixture resulting from Task 2 (with minor modifications if necessary), to physically crash-test FBCCs in the same six crash modes of various impact velocities, and thereby to obtain objective and useful data to quantify and compare how good commercial CAE crash codes are at predicting carbon fiber behavior. Task 5 began at Wayne State University (WSU) in the fourth quarter of FY 2015 and ended in the fourth quarter of FY 2016.

5.1 Summary of Task Objectives and Milestones

- Adapt a sled fixture from steel tests to test composite FBCCs under several modes.
- Test all load cases and provide reliable, valuable data to team to provide boundary conditions for simulations
- Complete all six load cases
- Provide CAE predictions of composite tests.
- Analytically compare CAE predictions to composite tests

Milestones for Task 5:

Milestone	Title	Description	Metrics	Status
M13	Crash Test Fixtures for Composite FBCC Complete	Determine the need for design and fabrication of six different FBCC test fixtures for composite system testing (for all load cases). If needed, design and complete the fabrication.	Completion of fixtures for 6 load cases.	Completed
M14	Crash Testing of Composite FBCC Complete	The composite FBCC will be physically crash tested for each of the load cases, and the experimental results compared with the CAE predictive results. Sufficient crash test repetitions will be done to establish reproducibility, and determine part-to-part variability.	Report on crash test results and comparison to CAE. OEM-approved correlation metric to quantify a goodness-of-fit of the CAE predictions to the physical test performance.	Completed

5.2 Crash Sled Fixture and Test Protocol

Major sled modifications or fixturing changes were not needed to the scale originally required in the steel FBCC crash testing under Task 2. Only minor changes and reinforcements to the sled were needed (e.g., adding approximately 3.0 kg to the sled for the frontal offset, angular and low-speed quarter). This was a time-save and cost-save as the carbon fiber FBCC was designed in a manner to use the same mounting and fixturing footprint as the steel system as discussed in the Task 2 report. High-powered vacuums were added for collecting carbon fiber debris expected in all crash modes. The same test protocol was initially followed as detailed in Task 2, however, during practice runs for each load case, it was observed that the energy absorption capabilities differed significantly from the steel FBCC. This was especially true for the frontal offset, pole and angular tests. Therefore, impact velocities were reduced to obtain meaningful data. The NCAP and low-speed frontal and quarter maintained roughly the same impact velocities.

5.3 FBCC Crash Testing and Data Collection

Testing of the baseline steel and composite FBCCs was conducted by WSU for the six crash modes shown in Figure 37, including four-high speed and two low-speed modes. Five repeat tests were planned for each mode, requiring at least 30 assembled FBCCs. The high-speed modes were aimed at simulating vehicle crashes where the FBCC would need to absorb energy through progressive crush to protect the occupants. The low speed modes simulated low-energy events where, ideally, no permanent damage would occur to the FBCC system, such as a parking lot fender-bender or impact from a loaded shopping cart. Crash testing of the baseline steel FBCC system was conducted in these same modes to develop test protocols and determine performance benchmarks used to evaluate the carbon fiber FBCC system.

For all test modes, the same sled-on-sled setup was employed (Figure 38). Data acquisition and measurements included accelerations using accelerometers, force using the accelerometers and load cells, overall system displacement using high-speed video analysis and accelerometers, and crush-can deformation using potentiometers and high-speed video analysis. As in Task 2, all redundant instrumentation and measures for velocity, force and displacement showed excellent correlation. Due to some of the manufacturing variations discussed in Task 4, the repeatability of test results within each test mode showed marked increase in variability for the composite FBCCs.

Data from multiple repetitions in each mode were averaged using a straight-forward time-wise averaging. Because the impact velocity varied little within each crash mode, this method of averaging was deemed suitable. Overall, the test-to-test variation in force, displacement, and acceleration were all found to be minimal. However, the only test at the correct velocity was conducted in the angular test mode and, therefore, predictions were compared to only the results from that test.

The angular crash test mode was also the most challenging to perform and acquire meaningful data, as the crush can consistently failed prematurely at the base of the sled fixture upon impact, and hence, no measurable progressive crush was achieved and testing was discontinued after three FBCCs. Challenges were encountered in stabilizing FBCC components and several precautionary safety measures were required such as barricading the test area and tying the bumper to a rigid connection at the celling. The inability of the FBCC to handle asymmetric loading may indicate design issues, as well as weaknesses in the fabrication and joining.

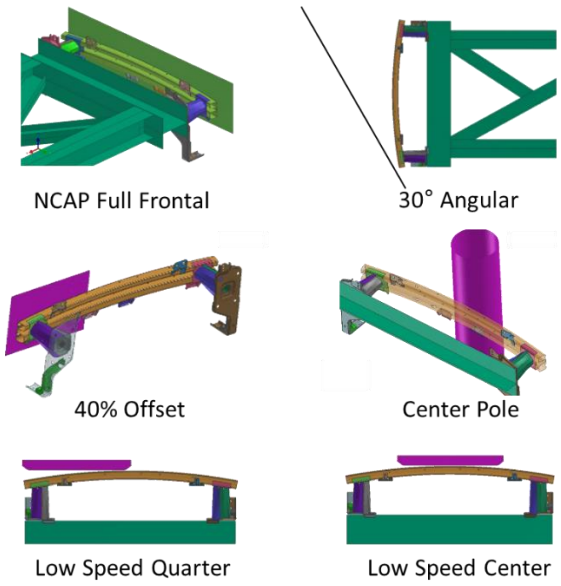

Figure 37. Diagrams of the six crash modes used for FBCC crash and CAE evaluation.

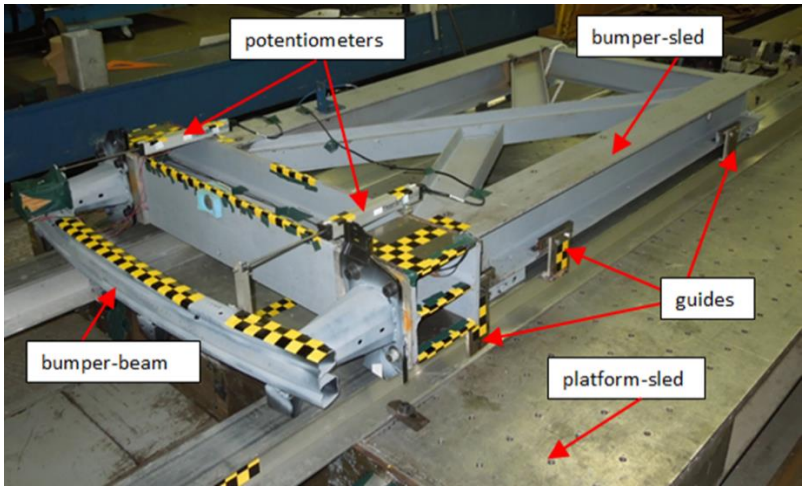

Figure 38. Set-up of sled-on-sled system used for all high-speed test modes.

5.4 Crash Test Results

Table 13 shows the results from testing that were used in subsequent analysis and comparison to CAE predictions from vendors (discussed under Task 7), the boundary conditions provided to ESI and standard deviations in Impact Velocity and Energy absorbed. Note that the angular data is represented as one test, as the angular test setup did not permit further crash tests that yielded progressive crush of the composite. This was due to the instability of the part during impact, and possibly due to premature adhesive failure of the crush can-bumper joint. The crush can would detach from the bumper within 10 ms of impact and the bumper became a projectile.

Table 13. Summary of all crash test modes and experimental results. (Values are given as means and standard deviations are shown in parentheses).

Crash Mode	Number of Tests Analyzed	Mass (kg)	Impact Velocity (m/s) [S.D.]	Energy (kJ) [S.D.]
NCAP	4	300.00	15.30 [0.24]	33.17 [1.54]
Offset	4	323.00	9.16 [1.98]	13.10 [4.50]
Pole	4	306.00	2.54 [0.16]	1.06 [0.17]
Angular	1	323.00	5.19	4.11
Low-Speed Midpoint	2	302.30	4.56 [0.02]	3.15 [0.04]
Low-Speed Quarter	2	326.40	4.21 [0.26]	2.42 [0.23]

Figures 39 and 40 show the force vs. time raw data (individual tests and average curve) collected by WSU for high speed modes and low speed modes, respectively. These data were further signal-processed for comparison to predictions in the Task 7 effort. Data from several multiple repetitions in each mode was averaged using a straight-forward time-wise averaging. Because the impact velocity varied little within each crash mode, this method of averaging was deemed suitable. Overall, the test-to-test variation in force, displacement, and acceleration were all found to be minimal. However, the only test at the correct velocity was conducted in the angular test mode and, therefore, predictions were compared to only the results from that test. The angular crash test mode was also the most difficult to perform, as the crush can consistently failed prematurely at the base of the sled fixture upon impact, and hence, no measurable progressive crush was achieved– the inability of the FBCC to handle asymmetric loading appeared to indicate weaknesses in the fabrication and joining.

Although only force vs. time data is presented here for the six crash load cases, displacement and acceleration were also considered when comparing predictions to tests. The zero-time point shown in each plot corresponds to the time of impact and the end time was chosen to best match with the time-window over which the predictions were made.

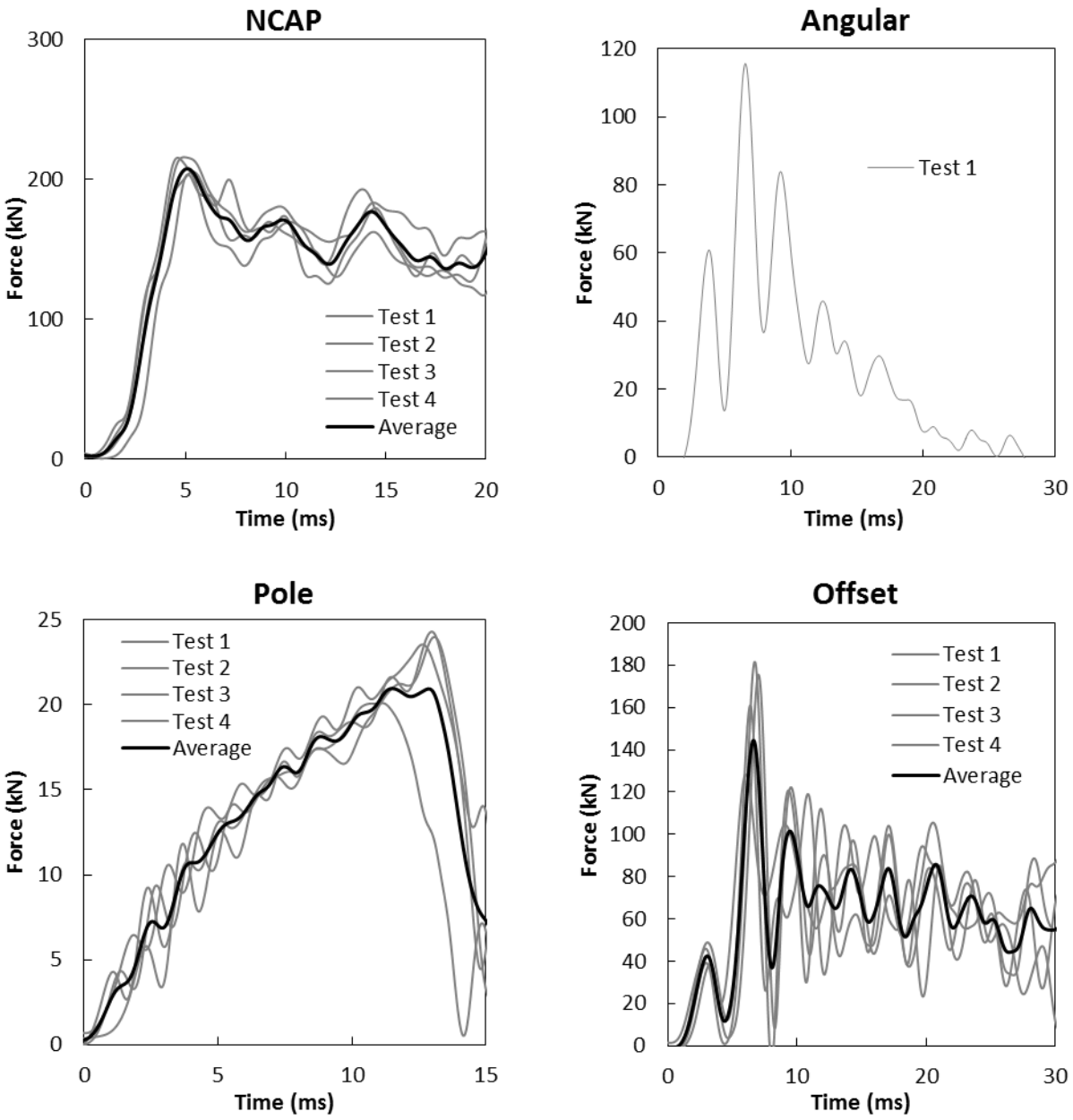

Figure 39. Force vs time data for the high-speed modes, showing the data from each test and the average. Note that for the angular case, only two crash experiments were conducted, of which only one complete dataset was collected.

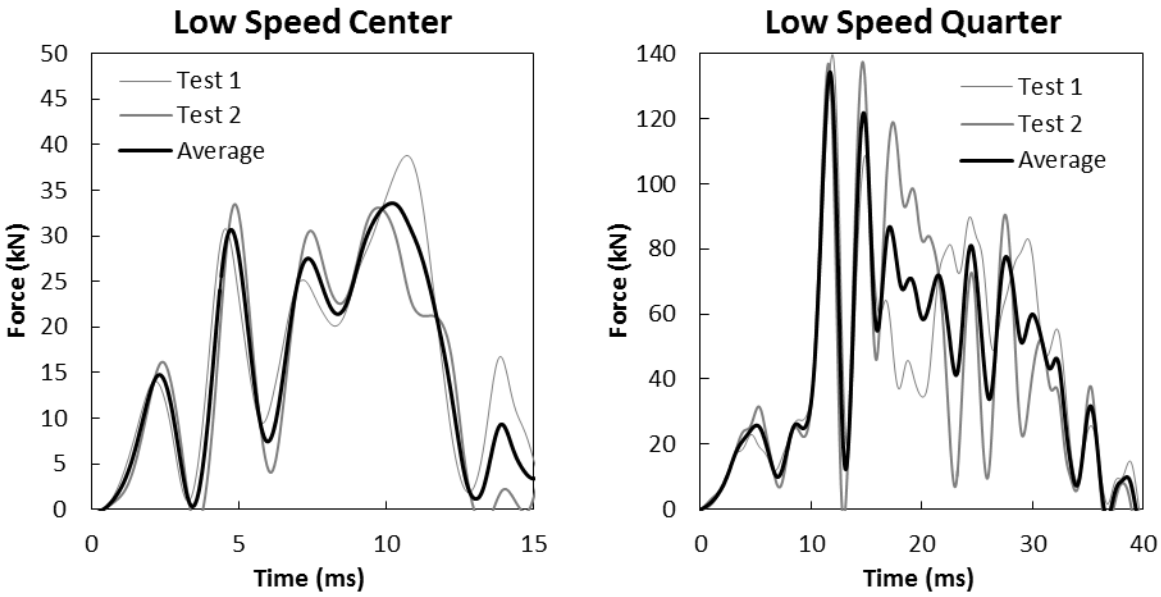

Figure 40. Force vs time data for the low-speed modes showing the data from each test and the average.

5.5 Task Conclusions

While the repeatability with each physical test with thermoset composite FBCCs was good, there were component and system failures that were unanticipated. Some test conditions impact velocities had to be reduced for safety and acquisition of valid data. Additionally, the behavior of some of the tests, such as the pole and low-speed center had undesigned failures which were not seen in the models. While the gaps for the performance can be traceable to the design limitations and manufacturing/assembly processes undertaken to adapt the FBCC for sled testing, it appears the majority of crash testing of the composite FBCC assemblies was successful in that progressive crush was achieved for both, high-speed and low-speed test cases.

6.0 Non-Destructive Evaluations and Structural Health Monitoring

6.1 Task Objectives and Milestones

Task 6 had three milestones as described below, integrated within the overall VMM Project.

#	Objective	Description	Status	Output
M15	Methodology for NDE of FBCC Composite Structures and Joints	Various NDE techniques tested on coupon samples. These trials provide the methodology for NDE of the FBCC composites and joints.	Completed	Report with results from flat plaques and flat adhesive bond samples and comparison to destructive tests
M16	NDE of FBCC Composite Structures and Joints	NDE testing of both pre- and post-crash FBCC samples. This data will be provided to test analysis activities.	Completed	Report evaluating FBCC samples before and after crash
M17	Health Monitoring Feasibility Analysis	Methods will be evaluated for in-service monitoring of the composite structure.	Completed	Report with analysis of alternative in-service monitoring methods.

6.2 Summary of NDE Task Progress

Task 6 (NDE and SHM) began work in the Spring of 2013. An NDE inspection program was defined which would use methods that are well established in the automotive sector and which have wide capabilities for detecting the most common carbon composite discrepancies. The primary methods were X-ray radiography testing (RT), X-ray computed tomography (CT), and ultrasonic testing (UT). These were selected from among other methods evaluated previously on both carbon and glass fiber composites. Ultrasonic and radiographic inspections can be used to rapidly qualify carbon composites in the automotive production environments as well as detect in-service damage.

The performance of these methods was demonstrated beginning in August 2013 when Round 1 flat plaques were made using a thermoset (epoxy) matrix and molding in a shear mold with high pressures. These plaques covered a wide range of materials (unidirectional plies, 2x2 twill woven plies, chopped tows) in several layups (0°, 0°/90°, and quasi-isotropic). Several plaques were also built with thin inserts to serve as “phantom discrepancies.” These samples were used by the MPS Team to determine the porosity and the mechanical properties that would be used for the finite element modeling. The NDE Team sectioned these for SEM inspection to determine the micro-structure. The NDE Team’s ultrasonic and radiographic inspections confirmed the high quality of the material, finding no delaminations, porosity, or foreign matter. The inserts were detected by ultrasonic and radiographic inspections.

These ultrasonic inspections were performed with high resolution, single-element transducer raster scanners. The resulting 3-d datasets demonstrated that individual tows and plies could be imaged in these thin (2.4-mm, 8-ply) materials. A custom Matlab® routine was written to analyze the ply by ply orientation and the ply thickness variations. In flat patches, as small as 50x50 mm, the ply orientation could be measured to ±0.5°.

In the Spring of 2014, the Round 2 flat plaques were made. These were larger panels that would be used for additional mechanical property testing. The NDE Team used this round for two major activities: (1) several plaques were built with two types of thin inserts at all the inter-plies to more systematically evaluate the performance of the NDE methods. (2) Several of the plaques were used for compression-after-impact (CAI) testing. The NDE Team also determined the locations of the inserts needed for the G1 and G2 shear test coupons for the Northwestern University team.

The CAI testing was used to quantify the size of discrepancies which would significantly affect the strength of materials. The CAI testing lasted from mid-2014 to completion in early 2015. CAI testing begins with impact testing, followed by ultrasonic and visual measurements of the impact damage, and concludes with compression testing. The compression testing of these thin plaques (<3mm) was problematic. Using the standard ASTM D7137 compression fixture, the samples tended to buckle at the top rather than through the impact damage. This issue was resolved by bonding tabs on both sides of the top and bottom of the impacted coupons to reduce the gauge length from 6-inches to 2-inches. The impacts were found to have a very small effect on the strength of woven composites with a quasi-isotropic layup. The ultrasonic scans provided detailed 3-d images of the impact cone. The maximum allowable discrepancy was set to 6-mm diam. These are readily resolved by the inspection methods used in this work, all of which have sub-millimeter resolution.

During the Autumn of 2014, simple hat-section parts were molded. Several of these, again, had thin film inserts to verify the NDE performance. In addition, some of these samples were subjected to 4-point bending tests. The damage zones were evaluated with both ultrasonic and radiographic inspections, as shown in Figure 41. The NDE showed a marked difference between unidirectional materials (large delamination zones) and woven materials (very localized damage). Some of the hat sections were also bonded to flat plates to make tubular assemblies. The adhesive bonds were nondestructively evaluated helping to improve the adhesive application. This included CT inspections. The tubes were also subjected to end-crush testing followed by NDE of the damage zones. In total, three types of damage were imaged: impact, flex, and crush damage.

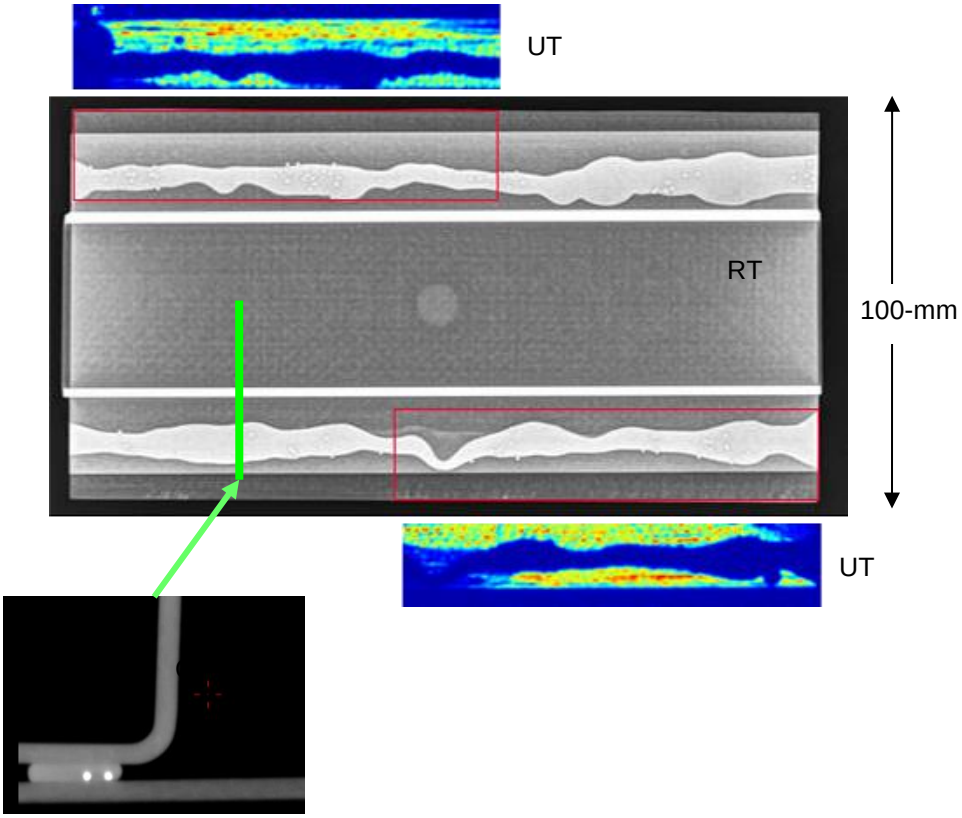

Figure 41. Ultrasonic inspection of a hat section crudely adhesively bonded to a flat plate. The upper BW image is the radiograph (RT) while the color inserts show the ultrasonic reflectivity from the bottom surface (UT). The CT is a cross-section through the flange area showing the adhesive bond with the glass beads used to control the bond thickness.

From late 2014 to mid-2015, the NDE task focus was on the final FBCC design released for production. The NDE Team guided the design of the crush cans to have a polyhedral form with flat planar facets rather than a cylindrical cone. This allows better nondestructive inspections, especially ultrasonic where the inspection transducer needs to be normal to the part's surface. This period was also used for evaluation of an ultrasonic phased array for the FBCC inspections. This provides a focused beam that is electronically scanned along the axis of the linear array. The ultrasonic inspection plans were then finalized: they would be performed in a large water bath with an ultrasonic phased array be mounted on a small surface-riding fixture. The array would be manually scanned over the flat surfaces of the components with a string encoder to measure the location. Separate jigs would be assembled to hold each component with the scanned surface horizontally, to hold a guide bar to control the orientation of the array, and to mount the string encoder. The crush can jig had two sub-sections: one allowed the can to be rotated to inspect the six polyhedral facets and two side flanges and a second section to inspect the back of the rear flange. Radiography and CT would be used to inspect the adhesive bonds, the bumper rib structure and the transition filet at the rear flange of the can. The design was frozen in mid-2015.

There was only a few-month window between when the FBCC design was finalized and components were being made. To confirm the ability of the CT scans to resolve features, especially the adhesive bond, a prototype model of the crush cans and one side of the front bumper beam were 3-D printed in nylon. These models were also useful for the final design, construction, and testing of the ultrasonic jig.

The FBCC components were molded in four separate stages from the Fall of 2015 through the Spring of 2016. Four different processing configurations were tried on the crush can sections to resolve material strength issues. In addition to the previously used UT, RT, and CT methods, optical surface scans were performed to measure the thickness over the entire bumper and crush can surfaces, and to measure part distortion from the CAD model. The external dimensions of the parts were excellent with negligible part distortion. However, major discrepancies were found inside the parts. In the bumper, porosity throughout the rib structure was first detected by CT scans (see Figures 42, 43 and 44). In the crush can sections, the infiltration of SMC from the rear flange into the filet area was first measured by radiography. While processing improvements helped, these discrepancies had a major impact on the strength of the bumper beam and cans.

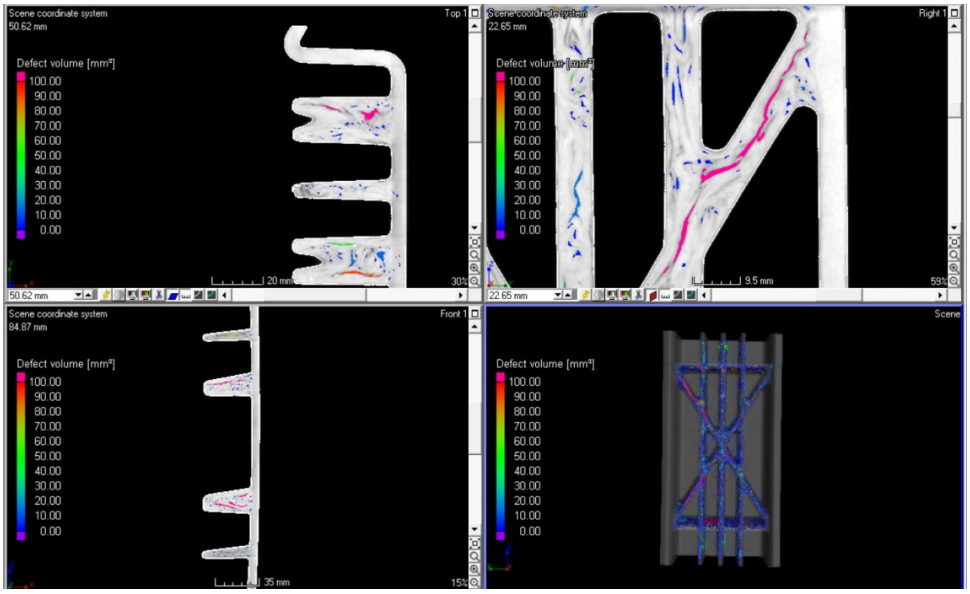

Figure 42. CT of FB section showing perspective view (lower right) and three orthogonal slices. These are composite images of the density (in gray) overlaid by a porosity analysis. The color of the porosity indicates the volume of the pore/crack.

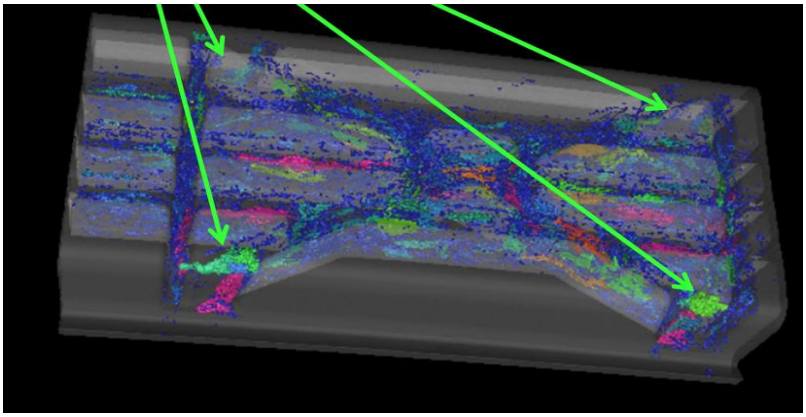

Figure 43. Magnified view of the CT image with porosity analysis. The areas of delamination within the side fabric of the FB are highlighted.

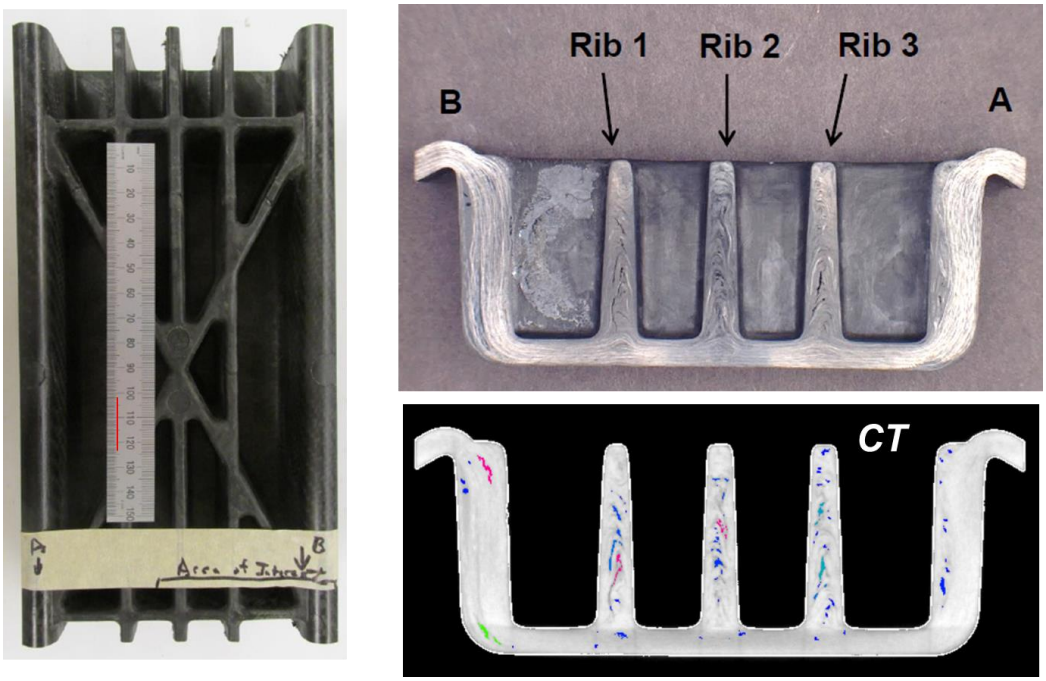

Figure 44. Detailed view of the FB porosity showing a comparison of a CT section and a physical slice through the same area.

In the Spring of 2016, there were two unplanned initiatives to understand and possibly improve the strength of the crush cans. Specimens were cut from the can facets by the MPS Team. Before tensile and compression testing these, the NDE Team ultrasonically scanned them. Only minor discrepancies attributed to fabric waviness were detected. The strengths of these were reduced by roughly 30% from the flat plaques. In addition, the NDE Team provided visual inspection of all the crush cans made beginning March 2016. All of these showed SMC intrusion to various degrees, along with fabric distortion in the rear flange fillet.

The visible failure locations of the crash components were tabulated. The crush cans primarily failed at the rear flange fillet especially in crashes with a side force component (shear). The bumper beam primarily failed through the vertical rib closest to the highest stress location. From these crashed parts, two front bumpers with low-speed damage were CT-scanned at the failure area. The CT shows that the bumper failed at both, the vertical and horizontal ribs and also at various delaminations between the SMC and woven materials.

6.3 Structural Health Monitoring

In the Spring of 2013, after a review of previous approaches, an alternative strategy for structural health monitoring (SHM) was developed. This would use very low-cost MEMS accelerometers that would be bonded to the interior of the composites and could autonomously and wirelessly record the maximum stresses experienced by the panel. Molded-in sensors were incompatible with the high compression forces and shear-edge molds to be used. During the Fall of 2013, two low-cost accelerometers and accessory electronics were acquired.

During much of 2014 planning and evaluation was undertaken to identify a strain gauge sensor system to compare to the accelerometer sensors. After identifying optical fiber Bragg grating (FBG) sensors as the target method, both outside partners and potential vendors were evaluated. A plan for a three strain-gauge evaluation of the FBCC was proposed. Preliminary finite element

analysis was performed to predict the needed frequency response. This was augmented by measurements of the acoustic emission from tap tests on the hat sections.

During the early part of 2015 a pendulum impact stand was built that would allow the response of various sensors to be tested using flat plaques or other components. A commercial FBG was identified and an PO was issued. Due to uncertainty in the level of resources required to fabricate and join the FBCC components for crash testing, the USAMP VMM leaders elected to conclude this sub-task as a proposal evaluation only without direct measurements of the sensors.

6.4 Conclusions and Gap Analysis

The VMM project task 6 has successfully accomplished its overall goals of delivering and testing an inspection protocol for automotive carbon composites for structural applications. This includes: (1) a strength criterion for needed spatial resolution, (2) a method to test the NDE method sensitivity throughout the molded component, (3) the importance of having a suite of NDE methods for development projects, (4) evaluation of NDE performance of UT, RT, and CT on highly 3-dimensional parts with both thin and thick sections and with adhesive bonding.

There were several gaps in the project methodology and in the available NDE methods: (1) the NDE needed to be resourced to perform 100% inspection as is generally needed for structural parts; (2) more destructive testing of the earliest parts is essential including both sectioning and strength tests; (3) better NDE methods for areas with a tight radius such as the crush-can rear-flange filet; and (4) methods to measure the fabric stretching, bunching and twisting in addition to ply rotation.

Extensive work on structural health monitoring was performed. This resulted in a recommendation to evaluate very low cost sensors (cellphone type accelerometers) and to compare them to a high-performance strain gauge (optical fiber Bragg grating). However, no experimental evaluation was performed. SHM methods that meet the cost, simplicity, and manufacturing requirements of automotive applications is still an open question.

6.5 Recommendations for Future Research

The NDE Team recommends two areas to be addressed in future composites projects:

1. NDE methods that can better resolve fabric distortion in regions with tight radii. While ultrasonic inspections provided the only information of fabric distortion in this project (on flat regions), it is difficult to perform in radius areas. Future ultrasonic work should include surface-following methods and signal processing work to resolve tow-level structure. Alternatively, CT work is needed with very large detectors that can both, resolve the tows and span a component.

2. Development work on a low-cost SHM sensor.

7.0 Comparison and Correlation of Predictions and Experiments

7.1 Quantitative Comparison Methodology for Composite FBCC Crash

The discussions in this section only apply to the data analysis for the thermoset FBCC crash tests versus CAE. For the composite crash predictions, ESI continued its contractual role as the main vendor to provide simulations for VPS/PAM-CRASH (done internally), while simulations in LS-DYNA, RADIOSS, and Abaqus were provided by subcontracted vendors. Additionally, LSTC, Altair and AlphaSTAR were separately contracted by USAMP to lend their expertise as code developers in providing simulations with the same boundary conditions using LS-DYNA and RADIOSS; AlphaSTAR was engaged to demonstrate its multi-scale modeling approach, while using the LS-DYNA solver. In all, the USAMP received three LS-DYNA simulations, two with RADIOSS, one with Abaqus and one simulation with VPS/PAM-CRASH for comparison with crash test results.

Once again, the ISO/TR 16250: “Road vehicles: Objective rating metrics for dynamic systems,” or CORA process – was used to assess the accuracy of the vendor predictions to the physical tests. As in Task 2, the individual CAE codes and corresponding vendors are not identified for discretionary purposes.

Previously, to compare two non-ambiguous time history signals in passive safety, such as force or displacement, between a numerical simulation and a physical test, a rather subjective method was in place. The two signals would be overlaid and given a weighted score based on how good the two fit within a corridor (usually +/- standard deviation). Only recently, has a more quantifiable approach been proposed. The ISO/TR Standard 16250 (that has been proposed) gives a score from zero to one on how well the two signals correlate. The proposal constitutes two primary drivers: the first, the corridor method where the signals are compared using constant width or sigma based widths and having a weight factor of 40%. The second driver is the cross-correlation method that looks at the differences between the two signals with respect to phase shift, amplitude, and slope. Each one of these carries a weight of 20%.

The method described in ISO/TR Standard 16250 was applied to objectively compare the predictions to the physical crash tests. Physical relevance of the scores is described below:

- Excellent: ISO Score > 0.94
  - The characteristics of the reference signal are captured almost perfectly.
- Good: 0.80< ISO Score ≤ 0.94
  - The characteristics of the reference signals are captured well, but there are noticeable differences between both signals.
- Fair: 0.58< ISO Score ≤0.80
  - The characteristics of the reference signal are basically captured, but there are significant differences between both signals.
- Poor: ISO Score ≤ 0.58
  - There is almost no correlation between both signals.

An example of one test condition and one metric using all seven codes are provided in Figure 45. Only one example plot of acceleration versus time is given for brevity, as a total of eighteen similarly formatted comparison curves were generated by the Task 7 team for the six crash test load cases. The zero-time point shown in each plot corresponds to the time of impact, and the end time was chosen to best match with the time-window over which predictions were made.

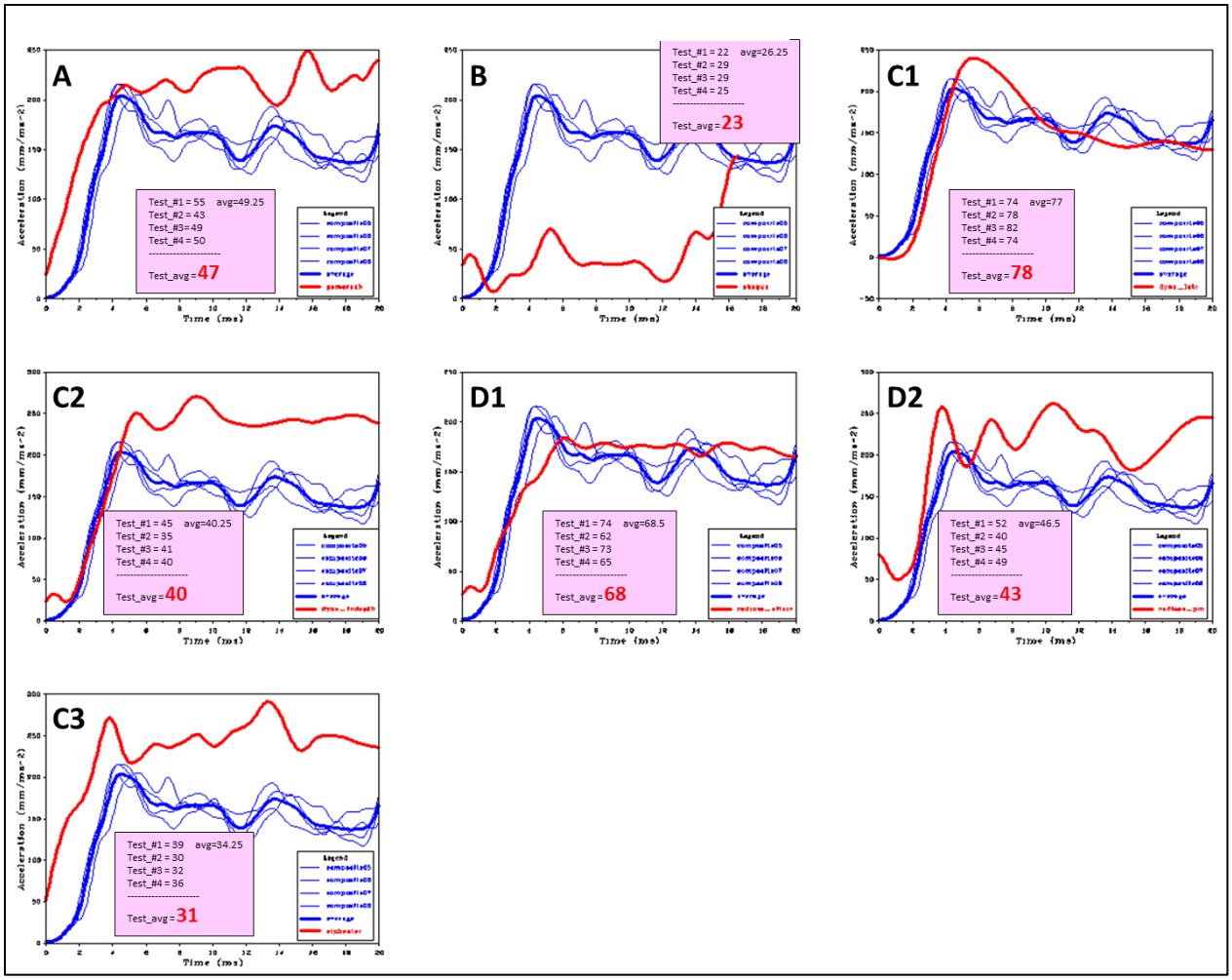

Figure 45: Sample of acceleration-time history comparisons of physical tests, average of those tests and the simulation and the corresponding CORA scores for each crash code. The red curve represents the simulation, the light blue curves represent an individual test and the dark blue curves represent the average of the tests.

7.2 Correlation of Composite Crash Tests to Simulations

Seven sets of simulations using VPS/PAM-CRASH, LS-DYNA, RADIOSS, Abaqus and GENOA-MCQ were compared to all experimental crash testing results. Figure 46 illustrates the bar graph summary CORA results of each crash code and crash mode. Unlike the steel FBCC analysis where there was no obvious superior code, the carbon fiber FBCC CAE analysis yielded greater variability between codes, both within a given crash mode as well as across the six crash modes.

The results from the CORA analysis yielded new insights into CAE code variability not seen on the steel analysis. Accounting for the wide variation of a given code between crash modes is complex - several factors may be interacting including, but not limited to: meso-scaling, joint modeling, bumper stiffness and method of element deletion as carbon fiber is destroyed during the loading process. Steel fails by buckling and folds with no material loss, just deformation.

The VMM OEM team provided detailed individualized feedback to each CAE vendor to spur potential improvements, as well as solicited responses from each vendor; selected highlights are discussed in the Technological Gap Analysis.

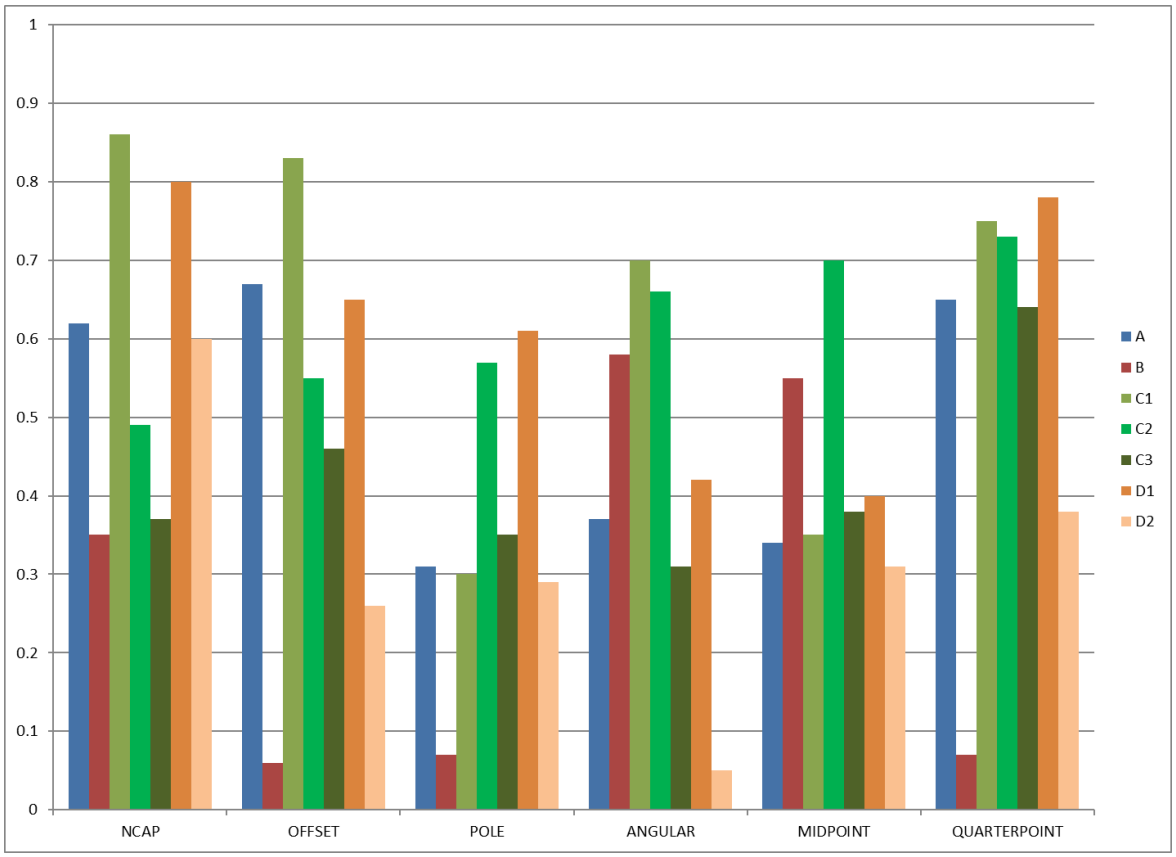

Figure 46. CORA results for all crash modes using each commercial crash code. (Includes VPS/PAM-CRASH, LS-DYNA, RADIOSS, Abaqus and GENOA-MCQ). The 7 sets of predictive results were obtained from 6 vendors running 5 CAE codes - all codes are left unidentified.

7.3 Correlation Results of Commercial CAE versus Test

A ‘heat-map’ of numerical results using ISO 16250 is provided in Figure 47 and visual comparisons for each crash mode with corresponding vendor-delivered CAE predictions are shown in Figures 48-53. Comparison results indicate that, overall, CAE predictions in any code were neither consistent nor reliable in accurately predicting the composite crash behavior. In terms of average ISO 16250 score, the best predictions came from Software C – Supplier 1, while the worst were from Software B. However, looking closely at the scores for each set of predictions shows that Software C – Supplier 1 had scores as low as 30 and 35, while Software B had scores as high as 55 and 58. Overall, while some software and suppliers had higher average scores than others, the variation for any given set of predictions was large. Even for the same software, predictions varied greatly from one supplier to the next. Comparing both, Software C and Software D indicated that there were large differences in accuracy of the predictions when comparing one supplier to the other for the same crash mode. For example, for Software C, Supplier 1 scored 86 in NCAP and 35 in LS-Center, while Supplier 2 scored 49 for NCAP and 70 for LS-Center. Variation in prediction accuracy is also observed from mode-to-mode, with the highest scores on average observed for NCAP and the lowest for Angular. The highest scores were generally achieved for modes that were crush can-dominated, including NCAP, IIHS, and LS-Quarter. The lowest scores were generally observed for those where the response was bumper beam dominated, including Angular, Pole, and LS-Center.

Examining the force vs. time and displacement vs. time curves for each mode shows that most predictions did capture the general shape of the crash test responses, but simulations generally predicted a stronger composite FBCC than was observed during the test. Force predictions were higher than the forces generated during the crash tests and displacement at any given time was generally lower than the predicted displacement. For example, simulations predicted NCAP forces greater than 200 kN, whereas the actual test response showed forces below 200 kN (Figure 48.48). The main exception to the ability of the simulations to capture the correct shape of the response was Software B, which did not show similar behavior in terms of shape or magnitude to the actual crash response.

Crash Mode	Software A	Software B	Software C		Software D		Software E	Average
			Supplier 1	Supplier 2	Supplier 1	Supplier 2		
NCAP	62	35	86	49	80	60	37	58
IIHS	67	6	83	55	65	26	46	50
Angular	31	7	30	57	61	29	35	36
Pole	37	58	70	66	42	5	31	44
LS Center	34	55	35	70	40	31	38	43
LS Quarter	65	7	75	73	78	38	64	57
Average	49	28	63	61	61	31	42	

0-20 21-40 41-60 61-80 81-100

Figure 47. ISO 16250 results for each prediction load case and CAE code tabulated as a heat map. A higher score indicates a better correlation between prediction and experiment.

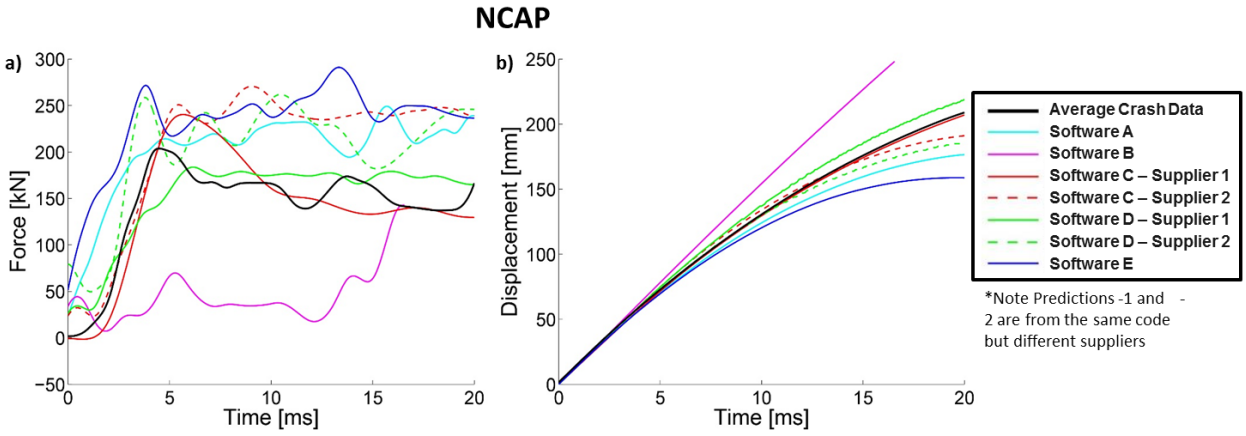

Figure 48. Comparison of each prediction to average crash data for the NCAP mode. Results are shown in terms of (a) force vs time and (b) displacement vs. time.

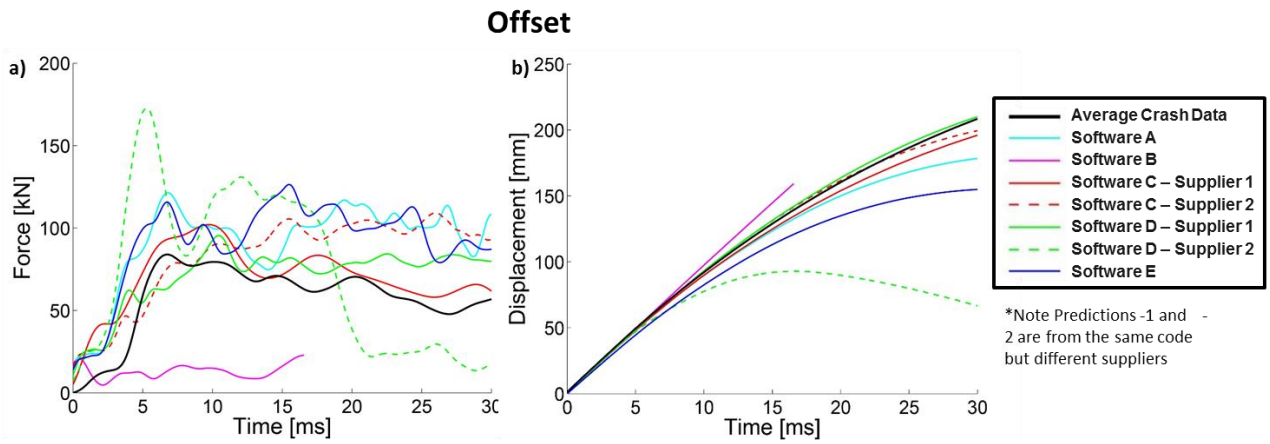

Figure 49. Comparison of each prediction to average crash data for Offset mode. Results are in terms of (a) force vs time and (b) displacement vs. time for the offset mode. Note that the crash data was filtered differently here, accounting for the different appearance.

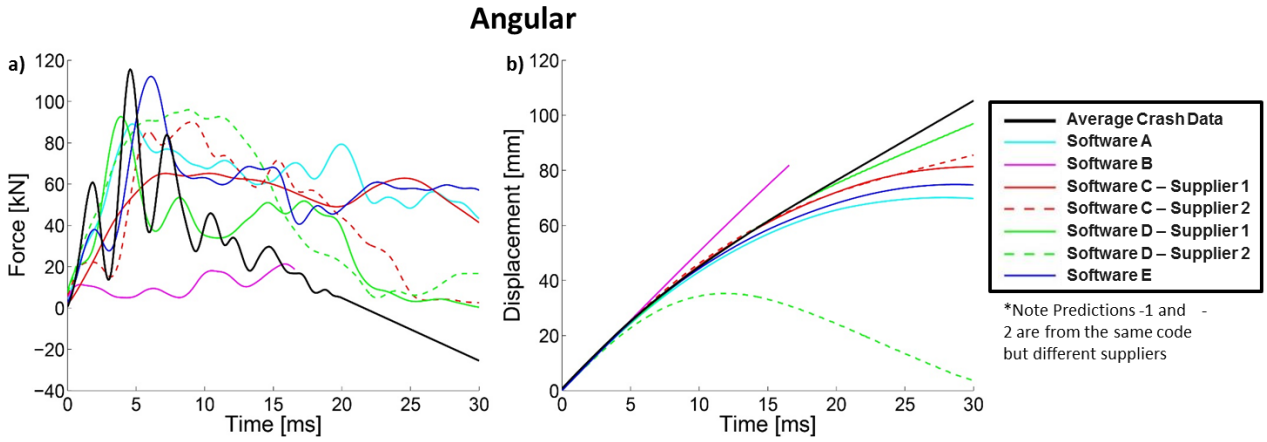

Figure 50. Comparison of each prediction to average crash data for the Angular mode. Results are in terms of (a) force vs time and (b) displacement vs. time for the angular mode.

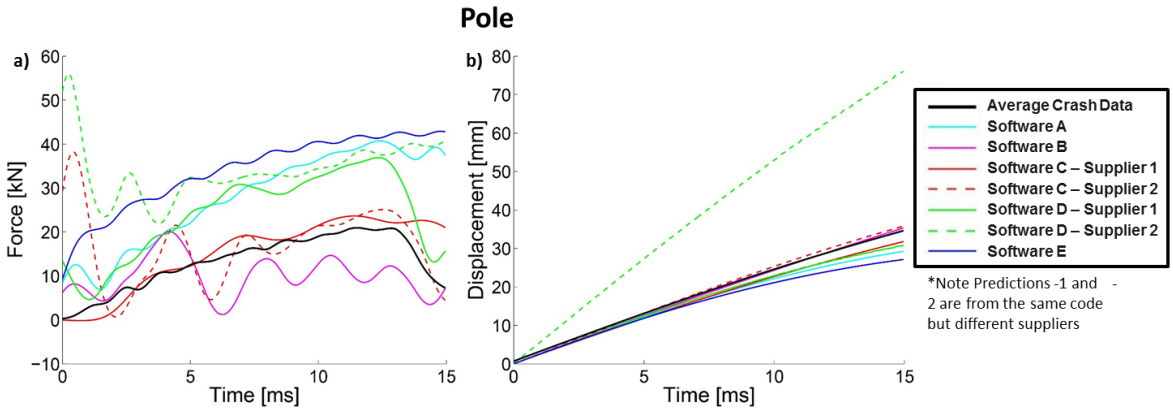

Figure 51. Comparison of each prediction to average crash data for the Center Pole mode. Results are in terms of (a) force vs time and (b) displacement vs. time for the pole mode.

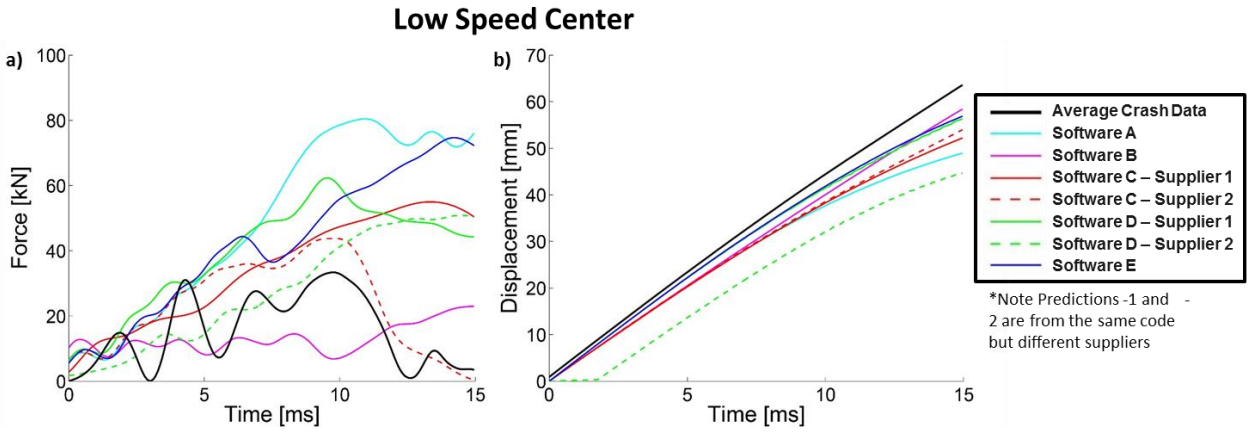

Figure 352. Comparison of each prediction to average crash data for the Low-speed Center mode. Results are in terms of (a) force vs time and (b) displacement vs. time for the low-speed center mode.

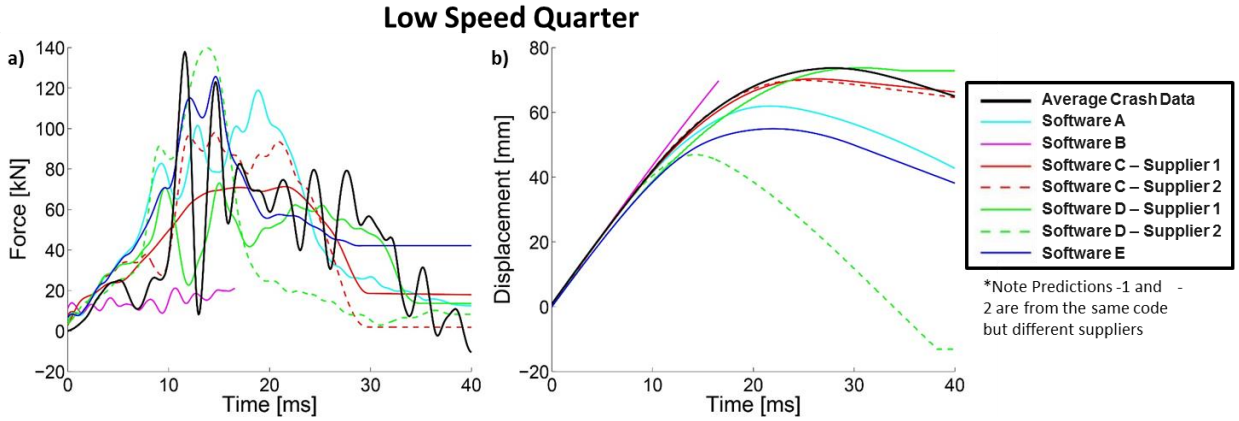

Figure 53. Comparison of each prediction to average crash data for the Low-speed Quarter mode. Results are in terms of (a) force vs time and (b) displacement vs. time for the low-speed quarter mode.

7.4 Assessment of FBCC Failure Modes

The ISO 16250 analysis discussed in the previous section compared the predictions to crash tests based on the FBCC's response in terms of displacement, force, and acceleration. However, this analysis does not examine how well the predictions captured the failure modes and overall physics of the FBCC's crash response. Figure 54 shows a comparison between the failure during an angular crash mode test to simulations in Software C from each of the two suppliers. Comparison between the prediction and experiment resulted in an ISO 16250 score of 30 for Supplier 1 and 57 for Supplier 2. While both suppliers showed average force responses of similar magnitude early in the test, Supplier 2 more accurately captured the drop in force near the end of the test. Examining the videos from the crash shows that the FBCC experienced premature, catastrophic failures at the base of the crush can where it meets the flange, as well as at the joint between the crush can and the bumper beam. These failures happen nearly at the same time and correspond with the drop in force that was measured during the test. Interestingly, when examining the failure locations in each prediction, Supplier 1 captures both the failure at the flange

and at the joint, whereas Supplier 2 predicted a split down the crush can that never happened and missed capturing the failure at the flange. In this way, Supplier 1 more accurately captured the physical behavior of the FBCC during the test, and it was largely coincidental that Supplier 2 more closely matched the force vs. time response.

The ISO 16250 analysis alone does not fully capture the accuracy of the predictions. To truly call a prediction 'accurate' requires that the physical behavior is captured such as failure mode and global deformation, in addition to the force, displacement, and acceleration responses. Unfortunately, as noted here, the accuracy of the predictions is further brought into question because a prediction that matched the experiment well in terms of force vs. time did not capture the corresponding material failure mode, while a prediction that appeared less accurate captured the failure mode quite closely.

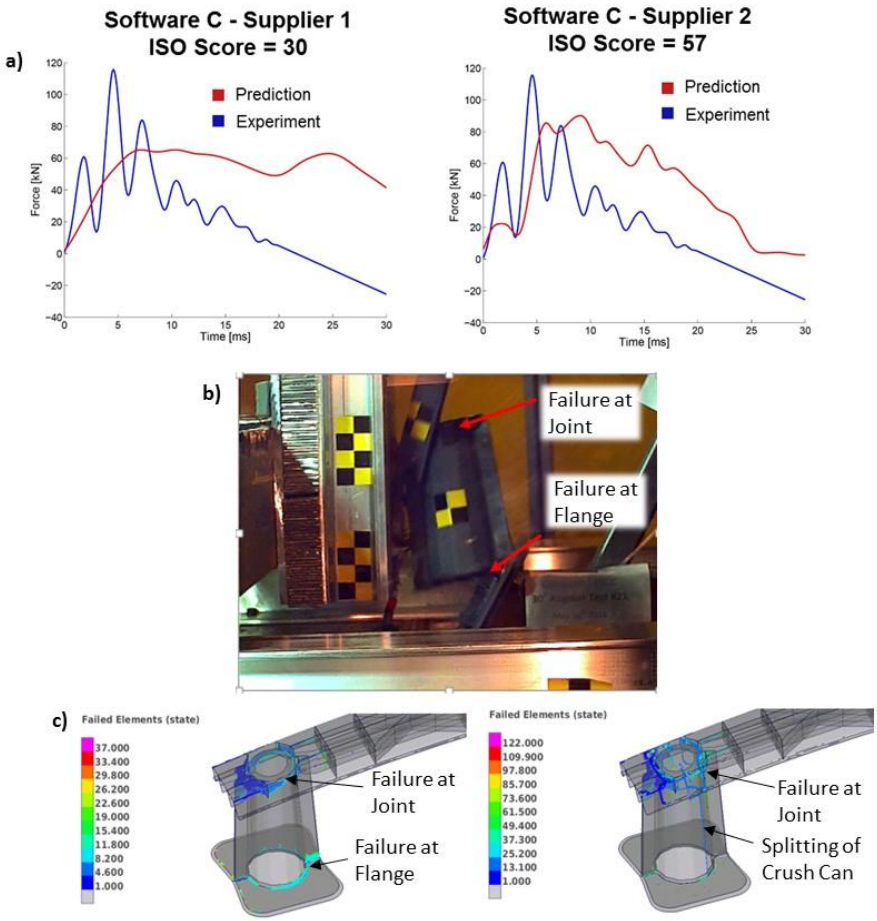

Figure 54. Comparison of crash results from the angular test mode on the composite FBCC to predictions in software C by two suppliers. (a) Force vs. time curves comparing each predictions from each supplier. (b) Image showing the FBCC during the crash highlighting the failure at the base of the crush can. (c) CAE predictions showing failed elements at the end of the test. The color scale indicates the time at which the element failed.

7.5 Comparison of Steel vs. Composite FBCC Performance

The target for the composite FBCC was to achieve equivalent structural performance at a 30-35 % mass reduction compared to the steel baseline design. A comparison of the two is shown in Figure 55 and Table 14. The composite FBCC showed a notable reduction in energy absorption,

peak load, and average crush load compared to the steel design. However, the composite FBCC was significantly lower in mass, with a 45% reduction compared to the steel FBCC. It should also be noted that no significant optimization effort was expended by the VMM team on improving the performance of the composite FBCC – optimization was not in the scope of the project, but rather, the objective was to ensure that progressive crush was achievable, so that CAE models could be validated. The composite FBCC is able to use the entire crush can length for energy absorption because there is no “crumple zone” (as in metallic structures), accounting for the longer displacement shown for the composite FBCC despite the same packaging space. This resulted in the composite crush cans absorbing only 23% less energy despite a 35% reduction in average crush load. Ultimately, it is most advantageous to the vehicle and occupants’ safety to absorb energy at a lower load and with no high peaks, making the flatter load displacement curve of the composite FBCC favorable. Adding mass (i.e. thickness) to the crush cans would result in equivalent energy absorption, while still maintaining lower mass than the steel design.

This ‘head-to-head’ performance comparison of steel with composite was only possible in the NCAP mode because the composite FBCC had to be run at lower impact velocities than the steel FBCC in the other modes, where the lower performance of the composite FBCC necessitated reduced impact velocities for more relevant comparisons or progressive crush with predictions.

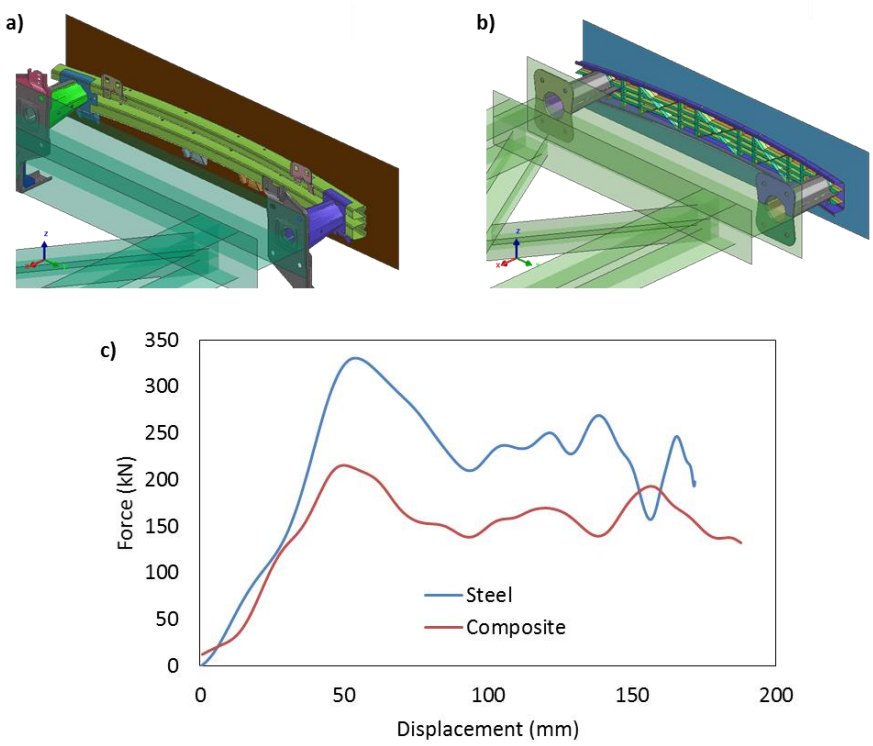

Figure 55. Comparison of the steel FBCC vs. the composite FBCC crash performance in the NCAP mode. Illustration shows (a) CAD model of the steel FBCC at the time of impact with the wall, (b) CAD model of the composite FBCC at the time of impact with the wall, (c) Force vs displacement curves from one representative test for each FBCC type. The data is trimmed at the end at the time in which the crush cans no longer absorbed more energy.

Table 14. Comparison of crash performance in NCAP of the steel FBCC vs. the composite FBCC. (The plateau region is defined as the portion of the test between the first peak in load and the end of the curves shown in Figure 55 above).

	Steel FBCC	Composite FBCC	Percent Change
Mass	**10.7 kg**	**5.8 kg**	**-45 %**
Impact Velocity	**15.6 m/s**	**15.3 m/s**	**-**
Impact Energy	**35.9 kJ**	**33.2 kJ**	**-**
Average Crush Load During Plateau	**330 kN**	**215 kN**	**-35 %**
Peak Crush Load	**236 kN**	**164 kN**	**-30 %**
Energy Dissipated During Plateau	**30 kJ**	**23 kJ**	**-23 %**
Percentage of Impact Energy Absorbed During Plateau	**83 %**	**69%**	**-**

7.6 Comparison of Academic Codes with Experiments

The objective of this sub-task was to evaluate academic crash codes, specifically from Northwestern University and the University of Michigan. The Northwestern University micro-plane code modeled only the carbon fiber crush can to predict energy absorption and peak loads; the bumper beam was not considered. A series of sled tests on individual molded thermoset CF crush cans were conducted in 2016 at the General Motors Sled Laboratory to obtain force and deflection data to quantify the goodness of fit from the two CAE conditions NWU ran (i.e., SSMM[7] Perfect Bonding and MTM[8] Perfect Bonding as described in the Task 3 report). Graphs illustrating Displacement vs Time and Force vs Time are provided below (see Figures 56 and 57), and once again, ISO/TR Standard 16250 was used to quantitatively assess the goodness of the CAE predictions to the physical crash data collected in the sled test (shown in green).

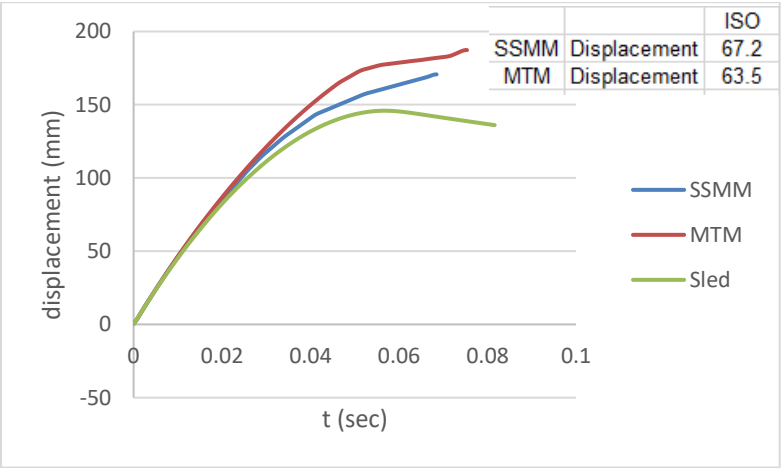

Figure 56. Displacement-time histories between SSMM and MTM to crash data. The ISO scores are provided.

[7] *Spectral Stiffness Microplane Model*
[8] *Microplane Triad Model*

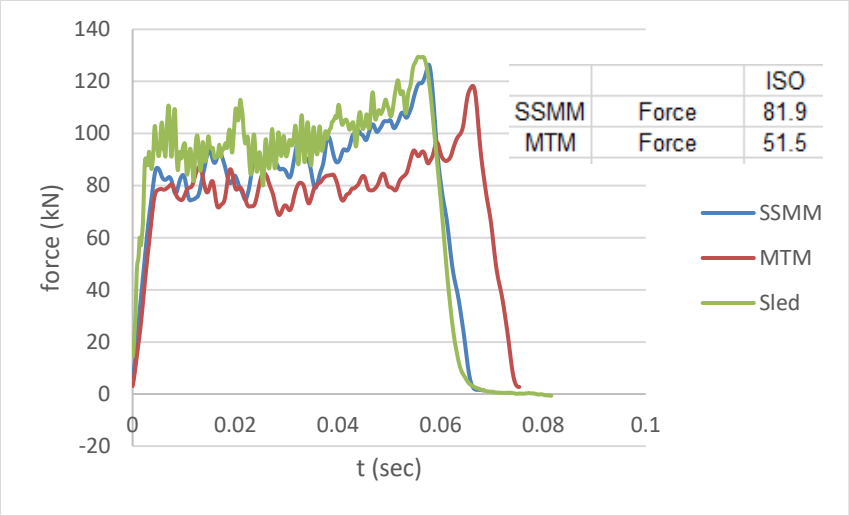

Figure 57. Force-time histories between SSMM and MTM to crash data. The ISO scores are provided.

Once again, 60% of the scoring is derived from amplitude, phase and rate. From Figure 55, it is clear that the amplitude and phase differences caused the score to be 51.5 compared to the SSMM and score of 81.9. Another caveat to the use of this ISO/TR Standard is the limitation in data analysis. For example, in Figure 54, the smallest array is the SSMM simulation, therefore, the physical test data array requires truncation. When comparing two signals, not only do they have to be the same size, but also within the same frequency domain. Several times, during our comparisons of the academic code simulations and the commercial code simulations to physical crash results, sizes and sample frequencies differed in nearly all instances. This was due to unexpected failures in some of the more aggressive test modes including the pole and angular modes, while if element deletion occurred too early compared to a physical test that continued to collect data, the resulting quantification comparison arose from truncated data. This situation was more evident in the UM data.

The UM's simulations consisted of two conditions: potential contact and perfect bonding. Additionally, whether the data should be filtered or not filtered was raised and options were analyzed. UM predicted behavior at all six high-speed crash modes (NCAP, Offset, Angular, Center pole, Low-speed Center and Low-speed Quarter) and measured displacement and force, bringing the total data set to be approximately 64 data files. For brevity, a few example overlays with respective CORA scores are provided. Figure 58 illustrates the crash data and the four CAE simulations: Potential contact filtered and unfiltered, and Perfect Bond filtered and unfiltered.

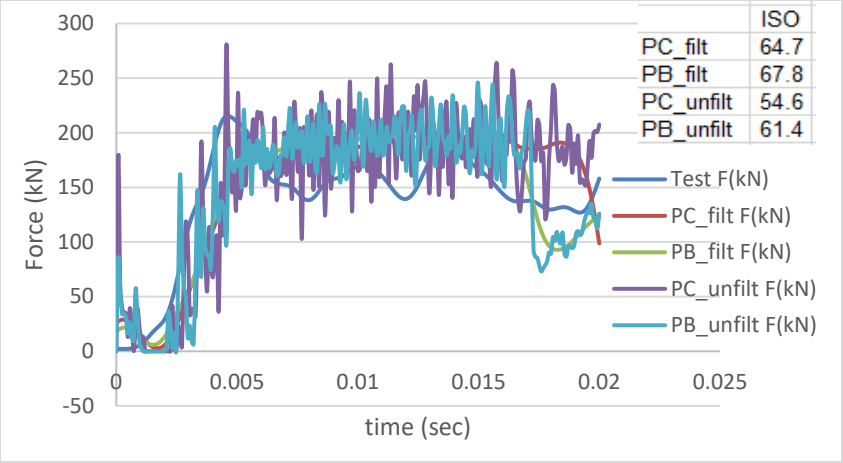

Figure 58. Force time overlays between for CAE simulations and physical test. Note that the unfiltered data scored less.

As mentioned before, truncation plays a role in what data is actually being compared. The following Figure 59 demonstrates the overall time domain from the test shown as Figure 58.

The overall UM results are displayed in Table 15 below.

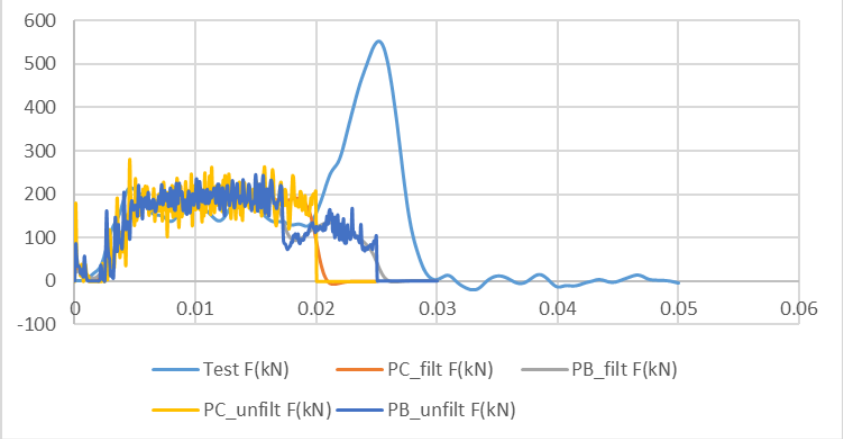

Figure 59. Example of a truncation discrepancy. Due to the simulations ending approximately at 20 ms, the large force spike in the physical test was not compared.

Table 15. Summary of CORA results for the UM datasets.

	ISO_combined		ISO_combined
Angular_disp_PBfilt	0.366	LSDC_disp_PBfilt	0.967
Angular_disp_PCfilt	0.356	LSDC_disp_PCfilt	0.832
Angular_force_PBfilt	0.452	LSDC_force_PBfilt	0.365
Angular_force_PBunfilt	0.399	LSDC_force_PBunfilt	0.318
Angular_force_PCfilt	0.593	LSDC_force_PCfilt	0.365
Angular_force_PCunfilt	0.587	LSDC_force_PCunfilt	0.233
	ISO_combined		ISO_combined
LSDQ_disp_PBfilt	0.99	NCAP_disp_PBfilt	0.491
LSDQ_disp_PCfilt	0.671	NCAP_disp_PCfilt	0.499
LSDQ_force_PBfilt	0.514	NCAP_force_PBfilt	0.678
LSDQ_force_PBunfilt	0.501	NCAP_force_PBunfilt	0.614
LSDQ_force_PCfilt	0.635	NCAP_force_PCfilt	0.647
LSDQ_force_PCunfilt	0.597	NCAP_force_PCunfilt	0.546
	ISO_combined		ISO_combined
Offset_disp_PBfilt	0.796	Pole_disp_PBfilt	0.751
Offset_disp_PCfilt	0.793	Pole_disp_PCfilt	0.751
Offset_force_PBfilt	0.63	Pole_force_PBfilt	0.101
Offset_force_PBunfilt	0.648	Pole_force_PBunfilt	0.19
Offset_force_PCfilt	0.624	Pole_force_PCfilt	0.291
Offset_force_PCunfilt	0.609	Pole_force_PCunfilt	0.19

Notice that all unfiltered values scored lower than their corresponding filtered metric. Currently, to objectively rate and quantifiably assess CAE simulations to physical tests, the field is limited to this ISO/TR Standard 16250: Road Vehicles – Objective Rating Metrics for Dynamics Systems. Data being compared are limited to actual test length of time. If a part is not built to design and fails quickly but the corresponding simulation doesn't factor in that deviation, to quantify how good the CAE is, it's limited to the finite amount of time that can be compared. This is true for a simulation that ends too quickly. The Standard is a useful tool in comparing data, but additional factors should be considered such as the value of the data being compared due to truncation, possibly looking outside of the time domain, say force-deflection as well as labeling scoring ranges with "good" assignments. Perhaps, the value ranges are adjusted for differing dynamic systems, for instance an actual dummy occupant in a sled test or barrier test compared to the simulation.

7.7 Task Conclusions

As discussed above, the composite CAE models did not show the same level of predictive accuracy as was observed with the steel FBCC models in Task 2. For the same FEA-based crash simulation software, such as C and D, the composite CAE predictions were provided by different code suppliers – C1, C2, C3 and D1, D2. The results from each supplier are very different, and the CORA analysis indicates that the current CAE modeling method or best practice for carbon fiber composites has not achieved standardization, and its accuracy is highly reliant on the experience of its users. Section 8 provides further discussions of the differences in commercial CAE codes, and the USAMP's efforts to engage CAE vendors in meaningful dialog.

8.0 Technological Gaps Identified and Remaining Challenges

The main objectives of this project were to quantify the accuracy of the CAE predictive tools as was performed in Task 7, and to assess the technological gaps that exist between the industry's current approach to predicting crash response of composite automotive structures and the physics of reality. The discussion in this chapter is provided as a framework for future technical developments needed to accelerate the industrialization of carbon fiber and composite materials for high-volume applications in the automotive industry.

8.1 Approach Used for Gap Analysis

The process to develop a consensus technological gap summary for this task began with the USAMP OEM team first formulating key areas of technological gaps based on Task 7 findings, and later engaging the simulation vendors that had supported the project as well as other experts from the USCAR OEM side who had provided technical input. From engineering observations discussed above, we summarize the main CAE modeling technology gaps in current commercial CAE software codes into four categories:

A. Inaccurate material properties

- Matrix compression strength obtained from compression coupon test appeared low. The observed matrix compression failure in coupon tests is not the same as which was observed in component tests.
- Fiber compression strength obtained from compression coupon tests appeared low. The observed fiber compression failure in coupon test is not the same as which was observed in component tests.
- There are two sets of shear properties from two different tests – i.e., 45-degree test and notch test. The values of stiffness and strength from two different sets of shear tests are very different, and can thus, yield very different simulation results.
- Overall, coupon test data is generally not fully representative of the performance of the material in the FBCC system

B. Insufficient material models

- No accurate failure criterion to predict laminate delamination.
- No proper failure treatment for laminate delamination.
- No proper damage model to describe the intermediate step between the initiation of matrix compression cracking (matrix still can transfer load through contact) and the dusting (pulverization) collapse of matrix material (i.e., no material left to carry load).

C. Improper treatment of brittle failure

- Element deletion is not a good practice to simulation of CF composite brittle failure
- The element deletion in brittle failure can lead to simulation instability

D. ***Insufficient shell formulation***

- Current CAE shell formulation does not reflect the fact that the shifting of shell neutral axis is due to the failure of lamina's failure.
- It leads to over-estimation of the bending stiffness in a damaged CF shell.

The USAMP's initial gap assessment was augmented by a poll of the seven CAE prediction suppliers whereby the USAMP OEM team asked each supplier the following questions:

1. How close do you feel your tool's prediction was to the reality of the test?
2. What do you believe may be the cause(s) of any inaccuracies?

3. What approaches would you suggest to improve these predictions?

4. Do you feel that the material models chosen are sufficient to predict performance of this type of structure?

The feedback from vendors was collected once final predictions were submitted and the physical tests were completed. The vendors were provided the physical test results and asked the questions above regarding the accuracy of their predictions and possible causes of inaccuracy or poor correlation to physical tests, steps that could be taken to rectify this inaccuracy, and the current state of their material models to generate good predictions. The commercial vendors generally responded in a similar way for causes of inaccuracy, citing poor assumptions in the adhesive bonding, as well as part defects due to the manufacturing process that were not captured in the model as the primary causes of low simulation accuracy. Some vendors identified an instability in the bending behavior of the shell element model, which is expanded further in the section, below.

Steps recommended by CAE vendors to improve prediction accuracy unanimously aligned around areas such as:

(a) Improving material property characterization including for the SMC and adhesive,

(b) Adding a step to capture and include manufacturing defects in the model,

(c) Developing an improved contact model that would mitigate the unrealistic effects of element deletion as part of the failure mode, and

(d) Running additional component tests (such as a test to characterize the crush can to bumper beam joint) to improve material model tuning on a component level.

The request from the supply base to add additional component testing signifies a confidence gap in the ability to translate flat coupon test data to a more complicate manufactured part, with the primary difference being the effects of additional geometrical form, resin flow and fiber orientation changes induced by the manufacturing process, and the resulting changes in post-yield behavior and fracture characterization of the brittle matrix.

8.2 Material, Design and Manufacturing Technology Gaps

A central principle of formulating CAE predictions is that if one puts bad data into a model, then one can only expect bad data out. The current approach to material modeling of composites involves characterizing the material in coupons, then inputting this coupon data into the material models. This method is generally used because flat plaques are easy to mold and the tests are well standardized by ASTM, ISO, and other trade/industry groups. A major drawback of such testing is that it doesn't account for variations in material properties resulting from the manufacturing process, and the defects that may arise. These interacting factors and variations warrant better characterization of the composite materials and fiber orientations, to better correlate the effects of manufacturing with performance, and to characterize the joining of the components. The material models themselves were, by common consensus, found to be less limiting to accuracy than these inputs used to populate the data for the material cards.

Although significant effort was applied to the calibration of the single element, coupon and component models, there remain some inherent shortcomings in the accurate digitization and characterization of composite materials for virtual simulation as described below.

Firstly, material properties are somewhat inaccurate. The laminate compression strength obtained from the compression coupon test seems low; it is not the same as observed in a larger scale component test. The fiber compression strength obtained from compression coupon test also seems low and is not equivalent to that observed in the component test. Characterizing the shear properties of the material can be performed in two different ways – the 45 degree shear test and the notch test. The values of stiffness and strength from these two different shear tests are very different which can therefore yield very different simulation results.

For manufacturing the FBCC design, significant draping of the prepreg was required when molding the dodecagonal crush cans. This draping realigned the fibers from their original orientation in the flat stack of prepreg layers. In addition, molding pressures on the SMC ribs and backing were found by NDE to cause bunching and stretching of the fabric near the flanges, which weakened the base of the crush cans. Tests on coupons cut from the crush cans were found to have significantly lower strength and stiffness relative to coupons obtained from flat plaques. This was likely the leading cause for the vendor simulations generally predicting the FBCC to have higher structural performance than was observed during crash tests. Therefore, in the VMM project, hat section crush tube tests were conducted using an intermediate representative component to help refine and tune the material models further than was possible with coupon data alone. However, in retrospect, the hat sections did not fully capture all the intricacies of the FBCC manufacturing process, including the actual draping angles, or the interaction of the SMC and prepreg during molding.

Incorporating accurate material data into a CAE model requires a robust framework to tie together predictions of the materials properties and the manufacturing process across length scales. Many modeling tools now exist for predicting manufacturing effects such as draping, resin flow, and cure kinetics. However, bringing all of this data together, with verification by NDE techniques, and using it to predict the effect of manufacturing on material properties is far from trivial. This challenge is addressed by the Integrated Computational Materials Engineering (ICME) approach. ICME ties together design, material selection, manufacturing, and performance predictions. Importantly, both, the effect of processing on material structure, and the effect of material structures on material properties is considered.

While composites are often able to achieve part-consolidation compared to a metal design, most complex structures still require multiple components, due in part to the lack of reliable design guidelines, and non-optimal manufacturing processes. Joining of composite materials and parts in a reliable and effective manner is an area of active research. Methods such as adhesive joining, riveting/bolting, or thermal/ultrasonic welding (in the case of thermoplastics only) are commonly employed. However, the capability for characterization and design of these joints utilizing CAE tools is far from mature, and is complicated by the requirement to not only characterize the material doing the joining, such as the adhesive or the rivet, but also the substrate and the interface between each component. This often means that testing conducted for an adhesive on one substrate is not relevant to its performance with a different substrate, even if the substrates are the same material with different thicknesses. In the VMM project, this challenge of characterizing and designing the joints became apparent through the results of FBCC crash testing for the angular and pole modes. Unfortunately, this happened too late in the project sequence to permit further iteration in the joining process. In these modes, the premature failure of the joint between the crush cans and the front bumper led to greatly reduced FBCC performance compared to design intent. Nearly all of the predictions assumed a perfect bond at these joints due to the challenge and complexity of modeling the joint more accurately, which led to the models greatly over-predicting FBCC crash performance in these modes. While much of the knowledge gap here is in development of the modeling methods, a separate research effort

focused on accurate and efficient experimental characterization of these joints would greatly aid in improving these predictions in future.

8.3 Gaps in Material Models and Analytical Methods

In examining the post-linear behavior of matrix composites, the team found that the material models used in this project have some deficits in their definition and ability to capture delamination and to accurately define a failure criterion to predict laminate delamination or treatment of the element stiffness and strength following the onset of delamination. This observation is made even without considering local voids, fiber waviness of other manufacturing defects which instigate laminate delamination on their own.

The damage material model also fails to describe the intermediate step between the initiation of matrix compression cracking (where matrix is still able to transfer load through the contact of adjacent fibers) and the dusting collapse of matrix material (where no material is left to carry load). The characterization of brittle failure was also found to have significant shortcomings. Element deletion, which is often used and provides a relatively accurate characterization of the stress-strain curve on simple models becomes less ideal and realistic when considering the brittle failure components and larger systems. This creates a geometric inaccuracy as small “chunks” of the model are sometimes not eliminated or deleted from the physical property, but may remain somehow attached to the primary structure and can shunt load or tether other particles to the structure during collapse. Further, the rapid change in energy transfer through the model may also cause simulation and numerical instability in the model, bringing the predictions into question.

Finally, the shell element, which has been the back-bone of finite element modeling of thin-walled structures, is exposed to some limitations when it comes to describing the behavior of thin-walled membranes made from multiple layers of thin-walled membranes. Notably, the current shell element formulation assumes a constant neutral axis based on the input properties of the laminate, and cannot reflect the shifting of the shell neutral axis due to the failure of laminate layers. This, therefore, leads to an over-estimation of the bending stiffness in a damaged laminate discretized by shell elements. The UM team attempted to overcome this issue by running a crush can model with shell and solid elements, and the results showed that the solid model exhibited generally softer behavior than the shell model. While the solid element may capture the softening effect not captured in the shell element, it has other drawbacks in characterizing the behavior of thin-walled structures, due to reasons such as the high number of elements required to discretize the structure, the low aspect ratio of these elements, and increased solution times. This reduces the industrialization potential of these elements due to the large computing effort. It was concluded that in addition to improvements in the material model for the handling of compressive loads and brittle failure, a more efficient finite element model is required to properly handle the bending behavior and laminar property changes due to laminate damage and delamination during crash.

Adding to the characterization challenge in this project was the application of random chopped fiber for the SMC ribs of the bumper beam. These fibers pose challenges to the CAE model on two fronts: the effect of the random orientation of the fibers on material properties, and the flow of the random chopped fibers during the injection molding process. While carbon fiber structures made from tape or woven sheet vary their orientation and local resin density considerably with certain geometries, they are somewhat held together and their orientation is somewhat predictable. However, the random chopped fibers require further investigation to realize the local, in situ material properties following the molding process.

The CAE-related technology gaps can therefore be summarized into the following four areas:

1. Finite element characterization of laminates
2. Modeling of brittle failure mechanisms
3. Modelling of delamination mechanisms and post-damage behavior
4. Unique characterization of areas in the crush can subject to property variation due to manufacturing processes

8.4 Carbon Fiber Composite Assembly Technology-Level Gaps

While the focus of the design was on the ability of commercial and academic simulation codes to predict composite performance, the bigger picture is to gain confidence in the application of carbon fiber parts for strength and energy absorbing applications in an automotive structure. There is currently a lack of production examples in industry where composite panels have been integrated into automotive structures on a large scale, and there are several challenges to this beyond cost or predictability of carbon fiber materials. The mitigation of mixed-material corrosion under automotive duty cycles, mixed material joining and the understanding of design fundamentals for carbon fiber parts, are all challenges that must be addressed to build industry confidence for the most efficient industrialization of this technology on a larger scale.

Current automotive production examples that are deployed in impact areas for the purpose of energy absorption or strength improvement emphasize adhesive joining, sometimes with mechanical connections. This supports both, corrosion isolation of the composite material from the adjacent aluminum or steel structural panel, and compensates for some differential in thermal expansion coefficient. The adhesive presents a new modeling challenge, as the adhesive failure mechanisms and behavior must also be captured, and this effort is not trivial. The intent of the applying rivets with adhesive were to mitigate any adhesive failure, so that the failure would be limited to the composite, and the project would remain a composite material modeling investigation, and not deviate into an adhesive modeling study. However, this topic would need to be fully addressed and risks mitigated for a production program where adequate adhesive strength may not be practical or feasible to achieve. Finally, in other applications of carbon fiber integrated as part of a mixed material strategy for automotive body structures, an inert boundary layer (such as glass mat) may be used with a bolted mechanical connection to provide the strength to the joint. As mentioned above, this was the approach used in the FBCC design so that the carbon fiber crush can could be joined to the steel sled fixture without concern of corrosion. The characterization of the bolted connection and the effect this has on local fiber properties subject to the clamping load is also not trivial. While much is understood in the aerospace industry about such joints, these learnings still need to be adapted across the automotive industry. Engineers responsible for design of composite automotive structures must anticipate and address how their individual composite parts will interact with surrounding components.

Finally, regarding the industry knowledge of designing composite structures, the learnings derived from this VMM Project imply that simple composite geometries offer the best chance for meaningful virtual predictions of performance. When surfaces are bent, tapered or flared from the nominal axes, there is a strong chance of re-aligning fibers off axis, and reducing the strength of the physical part from the virtual model. This can be addressed in new developments of commercial draping simulation software that captures fiber orientation changes subsequent to tool design and the molding process. The geometric design should also mitigate any opportunities for resin pooling or dry areas which will locally change the strength of the component. Without detailed flow analysis, this aspect is difficult to capture in a CAE model, and current alternatives that offer some application to the concept iteration phase are limited to computationally expensive

sensitivity studies that apply varying material strength properties in areas of concern to assess the stability of the design and robustness against resin-rich or resin-poor areas.

While further discussion on this topic was provided in greater depth in the Task 4 and Task 6 reports, the inability to easily and accurately characterize the local material properties of a production design composite part is a key gap that needs to be addressed for the industrialization of composite components for large scale automotive production.

9.0 Conclusions

Modeling methods for simulating behavior of carbon fiber composites during crash are continuously improving, but still have a long way to go before they can be considered truly predictive and reliable. Accurate modeling requires a combination of robust best practices, and a strong level of user expertise and experience with the software packages and material models. Overall, it was observed that the CAE suppliers that had a proven track record with the software package they were using generated more accuracy predictions than those that did not. This arises from the fact that developing the material cards for finite-element analysis and selection of computational routines still requires a large amount of subjective tuning to best match failure modes and element deletion criteria with the available material test data, as well as a sound perspective on how that material will perform during the actual test. No set of predictions from a supplier were found to be universally accurate among all the six crash modes, with the best performer having an average ISO 16250 score of 63, but also a wide CORA score range with a low of 30 and high of 86. Most software packages had the tools available to provide reasonable predictions, except for Software B. Yet still, there was much variation in the average ISO 16250 scores from code to code and because the results varied with supplier, it is impossible to fully assess what differences can be attributed to the software versus what could be attributed to the expertise of the CAE practitioner, without undertaking further expansive studies on this aspect. Crash modes that were most dependent on the properties of the prepreg were more accurate than those that were heavily dependent on the behavior of the joints and SMC.

The CORA analysis indicates that the current CAE modeling methods or best practices for carbon fiber composites have not achieved standardization, and the accuracy of CAE is highly reliant on the experience of the users. Much of the unreliability of the predictions can be attributed to shortcomings in our ability to mathematically link the effects of manufacturing and material variability into the material models. Coupon tests alone are not sufficient to develop an accurate material model and it is necessary to bridge the gap between the coupon data and the actual structure with a series of subcomponent level tests. The selection of these subcomponent tests and the application of their results to tuning the material models is, again, heavily dependent on the expertise of the modeler. ICME techniques show promise for creating a framework to take manufacturing and material microstructure simulations and apply them to structural predictions, but the tools are still under development and not yet industry standard.

The following lists summarize the initial technological impact of the DOE-USAMP VMM Project:

9.1 Innovations Enabled by the USAMP VMM Project

1. Unique (US Patent 9,598,033 B1) Design of the Thermoset Composite Front Bumper Beam and Crush Can (FBCC) System was developed by the USAMP VMM Composites project team that combines the benefits of part consolidation with joint strength and manufacturability - The ribs could be configured to provide a pocket for locating and bonding the crush can.

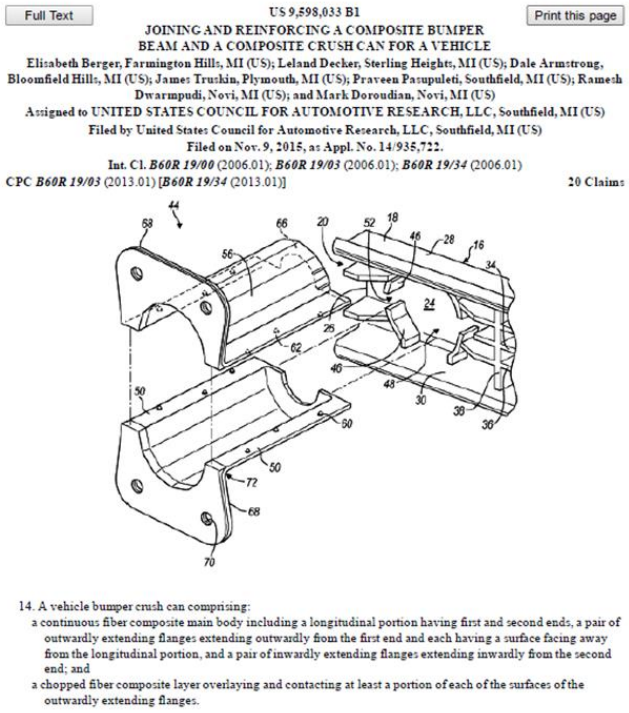

Full Text

US 9,598,033 B1

Print this page

JOINING AND REINFORCING A COMPOSITE BUMPER BEAM AND A COMPOSITE CRUSH CAN FOR A VEHICLE

Elisabeth Berger, Farmington Hills, MI (US); Leland Decker, Sterling Heights, MI (US); Dale Armstrong, Bloomfield Hills, MI (US); James Truskin, Plymouth, MI (US); Praveen Pasupuleti, Southfield, MI (US); Ramesh Dwarmpudi, Novi, MI (US); and Mark Doroudian, Novi, MI (US)

Assigned to UNITED STATES COUNCIL FOR AUTOMOTIVE RESEARCH, LLC, Southfield, MI (US)

Filed by United States Council for Automotive Research, LLC, Southfield, MI (US)

Filed on Nov. 9, 2015, as Appl. No. 14/935,722.

Int. Cl. *B60R 19/00* (2006.01); *B60R 19/03* (2006.01); *B60R 19/34* (2006.01)

CPC *B60R 19/03* (2013.01) [*B60R 19/34* (2013.01)]

20 Claims

14. A vehicle bumper crush can comprising:

a continuous fiber composite main body including a longitudinal portion having first and second ends, a pair of outwardly extending flanges extending outwardly from the first end and each having a surface facing away from the longitudinal portion, and a pair of inwardly extending flanges extending inwardly from the second end; and

a chopped fiber composite layer overlaying and contacting at least a portion of each of the surfaces of the outwardly extending flanges.

Figure 60. Image of the USCAR's patent.

2. The VMM Project is the only automotive industry-led project that evaluated the LCCF product from ORNL-CFTF by applying the processed stitched LCCF fabric form (via efforts by Chomarat, Shape Corp and TenCate) to fabricate and test an equivalent thermoplastic composite hat crush tube system.
3. The VMM Project has adapted and successfully applied an ISO-Proposal methodology known as CORA (Comparison and Correlation Analysis) for the quantification of the CAE code predictions to the physical crash tests, to draw key conclusions from the analysis. Nearly 2000 time-history data curves were generated during the VMM project data analysis, based on which the final conclusions were formulated in Task 7.

9.2 Impact to U.S. Industry and CAE Technology Advancement

1. The VMM Composites Project (over its 5-year duration) has elevated the importance of accurate CAE codes and helped establish best practices in FEA-driven crash modeling across the North American automotive industry, to demonstrate methodologies that are viable for higher volume manufacturing, assembly and NDE/inspection of crashworthy composite structures.
2. Besides the design/CAE step (which was the VMM's main focus), the project has also identified challenges and technology gaps in other downstream steps that are critical for the successful application of composite structures in automotive applications – design for manufacturability, CF product forms, preforming, molding/fabrication, joining, NDE, and crash testing/analysis.
3. The VMM Project has engaged over 30 organizations (3 OEMs, 3 academia, 3 design houses, 5 crash code developers, 7 material suppliers, 5 NDE and test laboratories, 3 molding shops, 1 finish machining shop, and 2 chemical corporations, and load/sensor suppliers, and specialized analysis vendors) from all parts of the CF composite supply

chain, thereby spurring new collaborative product and process development opportunities for lightweighting future vehicles.

4. Many of these participating organizations (about 10 suppliers) have also contributed in-kind cost share to augment the OEM cost share, thereby exceeding the DOE investment matching funds. This is indicative of broad interest and urgency in the composite industry for development of new CAE technology.
5. Total number of students, post-doctoral fellows, engineering staff and technicians involved with the VMM project is estimated to be over 100 persons across all of these organizations.
6. By engaging FEA crash code developers with academia-based material scientists, the project has facilitated the evaluation and technology transfer with new material models into new commercial applications – for example, ESI has implemented the Waas-Pineda Material Model into its PAM-CRASH code during the VMM project.
7. Over 30 conference publications and journal papers (including two doctoral theses) have resulted from the project's research tasks, with several more in progress, as well as four DOE-Annual Merit Review (AMR) Presentations made by USAMP VMM Co-PIs to disseminate progress to the industry at-large during 2014-17.

Appendix

Project Acknowledgements

The USAMP team gratefully acknowledges the U.S. DOE Vehicle Technologies Office Program Managers and NETL Program Manager and contracting staff who provided valuable guidance throughout the project.

The VMM Project was a five-year collaboration involving 33 organizations and over 100 researchers - at least 30 technical staff were from the three USAMP OEMs - FCA USA LLC, Ford Motor Company and General Motors - and over 60 from academic subrecipients and project vendors/suppliers. The authors would like to thank each of the following organizations, and the individuals who participated in this project.

USAMP VMM Project Collaborating Organizations

1. USCAR/USAMP LLC
2. Accutek Laboratories
3. AlphaSTAR Corp.
4. Altair Engineering
5. BASF
6. Bucciero and Associates LLC
7. Century Tool and Gage Corp.
8. Chomarat North America
9. Continental Structural Plastics
10. Datapoint Labs
11. Dow Automotive Systems
12. Element/Delsen Test Laboratory
13. ES3 Inc.
14. ESI North America Inc.
15. Future Tool and Machine Inc.
16. Highwood Technology LLC
17. InDepth Engineering Solutions
18. Jesse Garant and Associates
19. Livermore Software Technology Corp.
20. M-Tech International LLC
21. National Center for Manufacturing Sciences
22. Northwestern University
23. Oak Ridge National Laboratory-Carbon Fiber Technology Facility
24. PCB Load and Torque Inc.
25. Pratt & Miller Engineering
26. Shape Corp.
27. Siemens/Fibersim
28. Solvay Composite Materials
29. Specialty Extrusions
30. TenCate Performance Composites
31. University of Alabama Birmingham
32. University of Michigan
33. Wayne State University

List of Publications Generated

1. Wu Xu, A. Waas, “Crush Analysis and Energy Absorption of Woven Textile Composite Tubes,” Proceedings of 17th U.S. National Congress on Theoretical and Applied Mechanics, East Lansing, MI, 2014.
2. C. J. Dasch, G. J. Harmon, M. H. Jones, “Ultrasonic and X-ray Inspection of a High-Performance Carbon Fiber Composite for Automotive Applications,” American Society for Composites, 2015 Technical Conference, East Lansing, MI, September, 2015.
3. L. Berger, O. Faruque, M. Mehta, “Validation of Material Models for Crash of Carbon Fiber Composites: Setting Targets and Initial Design,” Society for the Advancement of Material and Process Engineering, Spring Technical Conference, Baltimore, MD, May, 2015.
4. Z. Bazant, M. Salviato, K. Kirane, “Microplane-Triad Model for Elastic and Fracturing Behavior of Woven Composites,” Journal of the Mechanics and Physics of Solids., February 2015.
5. A. Seyed Yaghoubi, et al, “Frontal Impact Responses of Generic Steel Front Bumper Crush Can Assemblies”. SAE Paper #2014-01-0550.
6. A. Seyed Yaghoubi, et al, “Force-Time History Assessment of a Generic Steel Vehicle Front Bumper and Crush Can Subjected to a Rigid Center Pole Impact”. 2014 Society of Experimental Mechanics.
7. A. Seyed Yaghoubi, et al, “Rigid Angular Impact Responses of a Generic Steel Vehicle Front Bumper and Crush Can: Correlation of Two Velocity-Measurement Techniques.” 2014 Society of Experimental Mechanics.
8. O. Faruque, et al, “Validation of Crash Models for Carbon Fiber Composites: A Project Overview,” 17th U.S. National Congress on Theoretical and Applied Mechanics, 2014.
9. K. Kirane, et al, “A Multi-Scale Microplane Model for Fracturing Damage of Woven Composites,” 17th U.S. National Congress on Theoretical and Applied Mechanics, 2014.
10. W. Xu, et al. “Crush Analysis and Energy Absorption of Woven Textile Composite Tubes,” 17th U.S. National Congress on Theoretical and Applied Mechanics, 2014.
11. M. Salviato, K. Kirane, S.E. Ashari, Z.P. Bažant, G. Cusatis, “Experimental and numerical investigation of intra-laminar energy dissipation and size effect in two-dimensional textile composites,” Composites Science and Technology 135, 67-75.
12. M. Salviato, S.E. Ashari, G. Cusatis, “Spectral stiffness micro-plane model for damage and fracture of textile composites,” Composite Structures 137, 170-184.
13. K. Kirane, M. Salviato, Z.P. Bažant, “Micro-plane-Triad Model for Elastic and Fracturing Behavior of Woven Composites,” Journal of Applied Mechanics 83 (4), 041006.
14. K. Kirane, M. Salviato, Z.P. Bažant, “Microplane triad model for simple and accurate prediction of orthotropic elastic constants of woven fabric composites,” Journal of Composite Materials 50 (9), 1247-1260.
15. K. Kirane, “Fatigue, fracture and size effect in particulate and fabric composites: constitutive modeling, theory and experiments,” Doctoral Dissertation, Northwestern University, 2015.

16. M. Salviato, S. Esna Ashari, R. Rezakhani, G. Cusatis, Z. Bazant, "A Spectral Stiffness Micro-plane Model for Fracturing Behavior of Woven Composites," Engineering Mechanics Conference (EMI), Ontario, Canada, August 2014.
17. K. Kirane, M. Salviato, Z. Bazant, G. Cusatis, "Experimental and numerical analysis of intra- and inter-laminar size effect in composite materials," Engineering Mechanics Conference (EMI), San Francisco, US, June 2015.
18. L. Berger, O. Faruque, M. Mehta, "Validation of Material Models for Crash of Carbon Fiber Composites: Setting Targets and Initial Design," Society for the Advancement of Material and Process Engineering, Spring Technical Conference, Baltimore, MD, May, 2015.
19. V. Virupaksha, "Validation of Material Models for Crash Simulation of Automotive Carbon Fiber Composite Structures, Proceedings of Global Automotive Lightweight Materials Conference, Detroit, MI, August 23-25, 2016.
20. O. Faruque, A. Coppola, D. Board, J. Truskin, M. Jones, M. Mehta, "Validation of Material Models for Crash Testing of Carbon Fiber Composites," in Proceedings of SPE-Automotive Composites Conference and Exposition, September 7-9, 2016, Novi, MI.
21. P. Pasupuleti, M. Doroudian, R. Dwarampudi, A. Coppola, E. Berger, O. Faruque, J. Truskin, M. Mehta, "Design of a Composite Bumper and Assessment of Current Composite Crash Simulation Capabilities," in Proceedings of SPE-Automotive Composites Conference and Exposition, September 7-9, 2016, Novi, MI.
22. D. Board, Y. Chen, O. Faruque, G. Newaz, P. Begeman, A. S. Yaghoubi, Y. Dixit, "Physical Crash Testing of Composite Bumper Beams," in Proceedings of SPE-Automotive Composites Conference and Exposition, September 7-9, 2016, Novi, MI.
23. A. Coppola, E. Berger, G. Smith, D. Armstrong, C. Dasch, "Thermoset Composite Materials and Processing for a Composite Bumper Beam System," in Proceedings of SPE-Automotive Composites Conference and Exposition, September 7-9, 2016, Novi, MI.
24. A. Cawley, H. Stevens, J. Truskin, A. Coppola, M. Mehta), "Joining and Assembly System for Thermoset and Thermoplastic Composite Materials," in Proceedings of SPE-Automotive Composites Conference and Exposition, September 7-9, 2016, Novi, MI.
25. X. Jin, P. Pasupuleti, H. Yu, M. Doroudian, D. Armstrong, A. Coppola, E. Berger, O. Faruque, J. Truskin, "Composite Fabric Manufacturing Studies by Simulation and Experiment," in Proceedings of SPE-Automotive Composites Conference and Exposition, September 7-9, 2016, Novi, MI.
26. J. McHenry, J. Tao, "Development of Carbon Fiber Reinforced Thermoplastic Composites," in Proceedings of SPE-Automotive Composites Conference and Exposition, September 7-9, 2016, Novi, MI.
27. C. Dasch, M. Jones, G. Harmon, "Non-Destructive Testing Throughout the Development of a Carbon Fiber Composite Automotive Crash Structure," in Proceedings of SPE-Automotive Composites Conference and Exposition, September 7-9, 2016, Novi, MI.
28. P. Pasupuleti, M. Doroudian, R. Dwarampudi, A. Tramecon, A. Coppola, O. Faruque, J. Truskin, M. Mehta, "Validation of Material Models: Design and Analysis of Composite Front Bumper Crush-Can System," Paper ID# 17-0436 for presentation at 25th International Technical Conference on the Enhanced Safety of Vehicles, June 5-8, 2017, Detroit, Michigan.

29. J. McHenry, J. Tao, A. Coppola, G. Smith, M. Mehta, “Validation of Material Models: Fabrication and Crush Testing of Carbon Fiber Reinforced Thermoplastic Composites for Automotive Energy Absorption Applications,” Accepted for Proceedings of SPE-Automotive Composites Conference and Exposition, September 6-8, 2017, Novi, MI.
30. A. Coppola, O. Faruque, D. Board, M. Jones, J. Tao, J. Truskin, YJ Chen and M. Mehta, “Validation of Material Models for Crash Simulation of Automotive Carbon Fiber Composite Structures: Project Conclusions and Key Learnings,” Accepted for Proceedings of SPE-Automotive Composites Conference and Exposition, September 6-8, 2017, Novi, MI.
31. Y. Dixit, P. Begeman, GS Dhaliwal, G. Newaz, D. Board, Y. Chen, O. Faruque, “Full Frontal Crashworthiness of Carbon Fiber Composite Front Bumper Brush-Can (FBCC) Structures,” Accepted for Proceedings of the ASME 2017 International Mechanical Engineering Congress & Exposition, IMECE2017, November 3-9, 2017, Tampa, Florida, USA.
32. Y. Dixit, P. Begeman, GS Dhaliwal, G. Newaz, D. Board, Y. Chen, O. Faruque, Crashworthiness Performance of Carbon Fiber Composite (CFC) Vehicle Front Bumper Crush Can (FBCC) Assemblies Subjected to High-Speed 40% Offset Frontal Impact, Accepted for Proceedings of the ASME 2017 International Mechanical Engineering Congress & Exposition, IMECE2017, November 3-9, 2017, Tampa, Florida, USA.